COLLECTED PAPERS

ON

COHERENT OPTO-ELECTRONICS

Volume 2

June 1985—July 1987

Associate Professor

Motoichi OHTSU

TOKYO INSTITUTE OF TECHNOLOGY

THE GRADUATE SCHOOL AT NAGATSUTA

4259 Nagatsuta, Midori-ku, Yokohama,

Kanagawa 227, JAPAN

PREFACE

This is a research review on coherent opto-electronics by Assoc. Prof. M. Ohtsu, Tokyo Institute of Technology. It contains copies of technical papers published in June 1985 - July 1987. M. Ohtsu thanks Assoc. Prof. Y. Teramachi of Institute of Vocational Training for his cooperation of research.

MEMBERS

Associate Professor

Motoichi OHTSU	(Dr. Eng.)

Graduate Students (Doctor Candidates)

Katsuhiko KUBOKI	(M. Eng.)
Minoru HASHIMOTO	(M. Eng.)

Graduate Students (Master Course)

Satohiko ARAKI	(B. Eng.)[a]	(-1968.3)
Noboru TABUCHI	(B. Eng.)[b]	(-1987.3)
Tetsuya MIYAZAKI	(B. Eng.)[c]	(-1987.3)
Toru KATO	(B. Eng.)	
Hiroyuki FURUTA	(B. Eng.)	
Kaoru YOKOTANI	(B. Eng.)	

Morihiro MURATA (B. Eng.)

Undergraduate Students

Toshihiko OUCHI[d)]	(-1986.4)
Masahiro SEGAMI[d)]	(-1986.4)
Yasuji NAKAMURA[e)]	(-1987.3)
Isamu YAGYU[f)]	(-1987.3)
Toshio NAKAHARA	
Yosuke NISHIJO	

Visiting Researchers

Toru IMAI[f)]	(1986.4-)
Chul Ho SHIN[g)]	(1987.4-)

a) Presently with the Graduate School, Nagoya University.

b) Presently with NTT.

c) Presently with KDD.

d) Presently with the Graduate School, Tokyo Institute of Technology.

e) Presently with Matsushita Tsushin Industry Co..

f) Permanent Address : Tokyo Aircraft Instrument Co. Ltd., Tokyo, Japan

g) Mokpo Merchant Marine College, Mokpo, Korea

LIST OF PAPERS

[I] IMPROVEMENTS IN COHERENCE OF LASERS

(a) Journal Papers

(b) International Conferences

lasers", Conference on Lasers and Electro-Optics (CLEO'86), June 1986, San Francisco, CA, WB4, p. 154 (Invited Paper) [p. 26]

[2] K. Kuboki, M. Ohtsu, N. Tabuchi and T. Ouchi, "Electrical feedback for attaining ultrahigh coherence in semiconductor lasers", Proceedings of SPIE The International Society for Optical Engineering, Vol.723, Progress in Semiconductor Lasers, September 1986, Cambridge, MA, pp. 73 - 80 [pp. 27 - 34]

[3] M. Ohtsu, K. Kuboki and N. Tabuchi, "Ultrahigh coherence in semiconductor lasers", Sixth International Conference on Integrated Optics and Optical Fiber Communication (OFC/IOOC'87), January 1987, Reno, Nevada, TUC5 (Invited paper) [p. 35]

[4] M. Ohtsu, K. Kuboki and M. Hashimoto, "Ultrahigh Coherent Semiconductor Lasers And Their Applications To Rb Atomic Clock", US - Japan Seminar, Quantum Mechanical Aspects of Quantum Electronics, July 1987, Monterey, CA, Session III, Paper number 4 [pp. 36 - 37]

[II] ANALYSES OF LASER DYNAMICS

(a) Journal Papers

[1] M. Ohtsu, Y. Teramachi, Y. Otsuka and Osaki, "Analyses of Mode-Hopping Phenomena in an AlGaAs Laser", IEEE J. Quantum Electron., Vol. QE-22, No. 4, April 1986, pp. 535 - 543 [pp. 38 - 46]

Vol. 26, No. 3, February 1987, pp. 464 - 470

[pp. 64 - 70]

(b) International Conferences

[1] M. Hashimoto and M. Ohtsu, "Semiconductor laser-pumped rubidium atomic clocks and attainment of 20-Hz double-resonance linewidth", XIV International Quantum Electronics Conference (IQEC'86), June 1986, San Francisco, CA, THFF2, pp. 164 - 165 (Invited Paper) [pp. 71 - 72]

[2] M. Ohtsu, M. Hashimoto and H. Furuta, "Ultrahigh sensitive frequency discrimination in diode laser pumped ^{87}Rb atomic clocks", A Workshop on Fundamental Measurements on Optically Prepared Atoms, September 1986, Gaithersburg, MD, D5

[p. 73]

[3] M. Hashimoto, M. Ohtsu and H. Furuta, "Ultra-sensitive Frequency Discrimination in a Diode Laser Pumped ^{87}Rb Atomic Clock", Proceedings of the 41st Annual Frequency Control Symposium, June 1987, Philadelphia, PA, Session B3, Paper number 3 [pp. 74 - 84]

[IV] ORAL PRESENTATIONS IN DOMESTIC CONFERENCES

[1] Nat. Conv. Rec. of Jpn. Appl. Phys. 20 papers

[2] IECE Japan, Tech. Group Meeting, OQE 15 papers

[3] Lidar Symposium 2 papers

[V] Books

[1] "Lasers and Atomic Clocks" (Ohm-sha, 1986, in Japanese)

[2] Light Emitting Devices and Photodetectors for Optical Sensing (Chapter 3 of "Optical Fiber Sensors", Ed. by T. Okoshi, Ohm-sha, 1986, in Japanese)

[3] Frequency Noise, Spectral Width of Semiconductor Lasers and Their Control (Chapter 2 of "Fundamentals of Semiconductor Lasers", Ed. by H. Takuma, Ohm-sha, 1987, in Japanese)

Linewidth Reduction of a Semiconductor Laser by Electrical Feedback

MOTOICHI OHTSU AND SHINICHI KOTAJIMA

Abstract—**An electrical feedback technique was proposed to stably reduce the linewidth of a semiconductor laser without changing its cavity structure. Calculations and experiments were carried out to reduce the linewidth of a 1.5 μm InGaAsP laser (DFB type) according to the following procedure. A compact Fabry-Perot interferometer was used as a freqeuncy discriminator. The minimum attainable linewidth, limited by the detector noise, was estimated as being narrower than 1 kHz when the reflectance of the interferometer used was higher than 0.9. The minimum linewidth obtained in the experiment was 330 kHz, which was 15 times as narrow as in the case of a free-running laser. The improvements of this experimental result can be expected by simultaneously reducing the AM noise of the laser.**

I. Introduction

THE spectral properties of semiconductor lasers have been recently improved as a result of the demands of the optical communication industry. When they are used for coherent optical communication or coherent optical measurements, their frequency stabilities should be sufficiently high. For these purposes, these stabilities have been already improved to values as high as 1×10^{-12} by using absorption spectral lines of stable atoms or molecules as frequency references [1]. Furthermore, the spectral linewidth of these lasers should also be reduced. A linewidth narrower than 4 MHz, for example, is essential to reduce the bit error rate as low as 10^{-9} in PSK heterodyne optical communication system of 1 Gbit/s bit rate [2]. Several techniques have been proposed to reduce the linewidth for these applications. One of them is to increase the cavity Q factor by using an external mirror or an optical fiber. This has been called an optical feedback technique [3]–[5], and it makes use of the injection of reflected light into the laser from an external mirror or an optical fiber. By using an external mirror, the linewidth of an InGaAsP laser has been reduced to a value as narrow as 1 kHz [5]. However, this technique presents several problems. One of them is that the linewidth can be temporally affected by phase fluctuations of the reflected light induced by the mechanical vibration of the external mirror or the thermal extension of the optical fiber. This fluctuation can also induce chaotic instabilities in laser oscillations [6]. To avoid these instabilities, extra servo-control circuits are required to stabilize the mirror position or fiber length, making the system more complex and the cavity size of the system larger. Even when these extra circuits are not used, it is essentially required to considerably increase the size of the laser cavity to reduce the linewidth by this technique. But this sacrifices an advantageous property of the semiconductor laser, its small size. Furthermore, one more essential difficulty is that the direct modulation index by the injection current is decreased.

To overcome these difficulties, we have proposed a simpler and more stable technique, i.e., an electrical feedback to reduce the linewidth of a 1.5 μm InGaAsP laser by controlling the injection current. A linewidth of 2 MHz has already been realized, which is more than five times as narrow as that of a free-running laser [7]. This technique utilizes a popular phenomenon, that a wide-band direct frequency modulation for semiconductor laser is possible through the injection current. Therefore, the cavity size does not have to be increased. Furthermore, since the feedback applied to the laser is negative, a high temporal stability of the center frequency and a narrow linewidth of its oscillation spectrum can be obtained. Quite recently, Saito *et al.* [8] have also reported that the electrical feedback of a 0.8 μm AlGaAs laser can reduce its linewidth to a value smaller than the one given by the modified Schawlow–Townes formula [9]. This makes the electrical feedback a more promising technique to realize a stable and ultranarrow linewidth laser.

In this study, the minimum attainable linewidth through application of electrical feedback is estimated and experimentally tested.

II. Estimation of the Minimum Attainable Linewidth

A. Bandwidth Required for Electrical Feedback

The electrical field of the single longitudinal mode laser is expressed as

$$E(t) = E_0 \exp\left[i2\pi\nu_0 t + i\varphi(t)\right] + \text{c.c.} \qquad (1)$$

where E_0 is the amplitude, ν_0 is the optical frequency, and c.c. represents the complex conjugate. $\delta\nu(t)$ $(= d\varphi(t)/dt\ 2\pi)$ is the frequency fluctuation, which corresponds to the FM noise. In Fig. 1, an experiment for FM noise and linewidth reduction is shown. A Fabry–Perot interferometer is used as a frequency discriminator for the FM noise detection, and the output signal from the detector is negatively fed back to the laser in order to control the injection current.

Manuscript received May 2, 1985; revised July 8, 1985.

The authors are with the International Cooperation Center for Science and Technology, Tokyo Institute of Technology, Tokyo 152, Japan, on leave at the Graduate School at Nagatsuta, Tokyo Institute of Technology, Yokohama, Kanagawa 227, Japan.

0018-9197/85/1200-1905$01.00 © 1985 IEEE

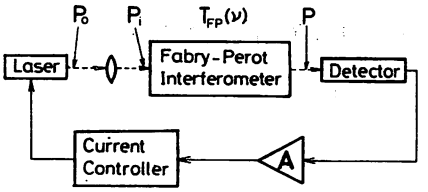

Fig. 1. Block diagram of the electrical feedback. P_0, P_i, and P represent the single-ended output power of the laser, and the powers incident into the Fabry–Perot interferometer and into the detector, respectively. $T_{FP}(\nu)$ represents the transmittance of the Fabry–Perot interferometer.

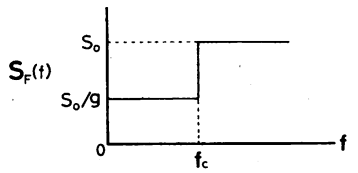

Fig. 2. Schematic explanation of the FM noise reduction by feedback. The power spectral density $S_F(f)$ of the FM noise at $f < f_c$ is assumed to be reduced g times by the feedback.

As shown in Fig. 2, it is supposed that the feedback will reduce the power spectral density of the FM noise g times that as compared to the case of the free-running laser for a Fourier frequency range lower than f_c:

$$S_F(f) = \begin{cases} S_0/g & (f \leqq f_c) \\ S_0 & (f > f_c) \end{cases} \tag{2}$$

where S_0 represents the value of $S_F(f)$ for the free-running laser. Here, the FM noise of the free-running laser is assumed to be white noise because the cutoff frequency f_c required for the linewidth reduction is about 100 MHz at most (as will be explained later in reference to Fig. 3), which is far lower than the relaxation oscillation frequency of about 1 GHz [10]. For (2), the corresponding value of the Allan variance $\sigma_F^2(\tau)$ [11], which is an alternative measure for the FM noise generally used to evaluate the frequency stability, is expressed as

$$\sigma_F^2(\tau) = \begin{cases} (S_0/2g) \cdot \tau^{-1} & (\tau \geqq 1/\pi f_c) \\ (S_0/2) \cdot \tau^{-1} & (\tau < 1/\pi f_c) \end{cases} \tag{3}$$

where τ represents the integration time of FM noise measurements. By using the Allan variance, the autocorrelation function of the electric field of (1) is expressed as [1], [11], [12]

$$\begin{aligned} R_E(\tau) &= \langle E(t)\, E^*(t+\tau)\rangle / \langle |E(t)|^2 \rangle \\ &= \exp\left[i2\pi\nu_0\tau - 2(\pi\tau)^2 \cdot \sigma_F^2(\tau)\right] \end{aligned} \tag{4}$$

where $\langle\ \rangle$ and * represent the time average and complex conjugate, respectively. Then, the spectral line shape of the laser oscillation is derived from the Fourier transform of (4), which is given by

$$I(\nu) = \int_0^\infty R_E(\tau) \cdot \exp(-i2\pi\nu\tau)\, d\tau + \text{c.c.} \tag{5}$$

Substitution of (3) and (4) into (5) gives

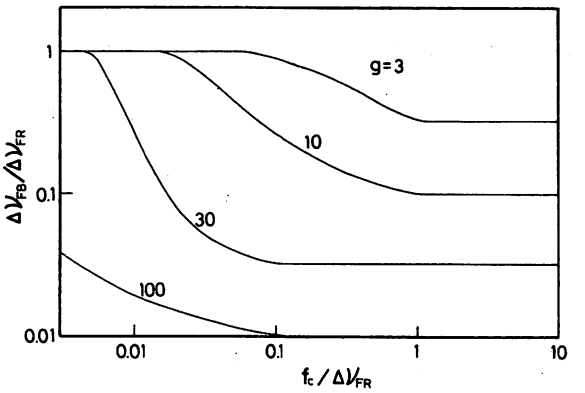

Fig. 3. Relation between the linewidth $\Delta\nu_{FB}$ under the feedback condition and the cutoff frequency f_c derived from (6). $\Delta\nu_{FR}$ is the linewidth of a free-running laser. $1/g$ is the FM noise reduction factor appearing in Fig. 2 and (2).

$$\begin{aligned} I(\nu) = {} & \frac{1}{\pi \cdot \Delta\nu_{FR}} \\ & \cdot \left[\frac{1}{x^2+1}\left\{1 - e^{-1/a}\left(\cos\left(\frac{x}{a}\right) - x \cdot \sin\left(\frac{x}{a}\right)\right)\right\}\right. \\ & \left. + \frac{1}{x^2 + 1/g^2} \cdot e^{-1/ag}\left\{\cos\left(\frac{x}{a}\right) - x \cdot \sin\left(\frac{x}{a}\right)\right\}\right] \end{aligned} \tag{6}$$

where $\Delta\nu_{FR}$ is the linewidth (FWHM; full width at half-maximum) of the free-running laser, which is given by

$$\Delta\nu_{FR} = \pi S_0. \tag{7}$$

x and a in (6) are defined as

$$\begin{aligned} x &= 2(\nu - \nu_0)/\Delta\nu_{FR} \\ a &= f_c/\Delta\nu_{FR}. \end{aligned} \tag{8}$$

The factor $1/(x^2 + 1)$ in (6) represents the Lorentzian spectral line shape under the free-running condition, and the factor $1/(x^2 + 1/g^2)$ is the line shape obtained if the bandwidth of the feedback is infinite. The other factors, i.e., $\exp(-1/a)$, $\exp(-1/ag)$, $\cos(x/a)$, and $\sin(x/a)$, appear because of the fact that the actual bandwidth of the feedback is not infinite but limited to f_c. Fig. 3 shows the linewidth $\Delta\nu_{FB}$ (FWHM) under the feedback condition derived from $I(\nu)$ of (6). It is seen that $\Delta\nu_{FB}$ approaches the following constant value if $f_c > \Delta\nu_{FR}$:

$$\Delta\nu_{FB} = \Delta\nu_{FR}/g \tag{9}$$

which means that the cutoff frequency f_c required for linewidth reduction is approximately equal to $\Delta\nu_{FR}$. Since it has been reported that $\Delta\nu_{FR}$ of the single longitudinal mode laser is between several megahertz and several tens of megahertz [10], [13], a bandwidth of several tens of megahertz is sufficient for the feedback. It means that a wide-band amplifier, e.g., one with a bandwidth larger than 100 MHz, is not necessarily required for the linewidth reduction. Instead, it is more essential to increase the feedback gain in order to obtain a narrower linewidth, because the value of g in (9) is proportional to this gain.

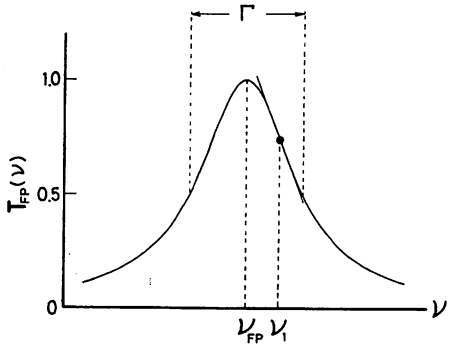

Fig. 4. Transmittance curve $T_{FP}(\nu)$ of the Fabry-Perot interferometer used as a frequency discriminator. ν_{FP} is the resonant frequency of the interferometer. ν_1 is the frequency of the maximum slope of this curve, at which the laser frequency is locked by the feedback.

Since the feedback is required only for the low Fourier frequency range of $f < f_c$ (< 100 MHz), the direct modulation index is not decreased when this laser is modulated by a modulation frequency larger than f_c. This makes a fast direct modulation still possible while keeping the linewidth as narrow as expressed in (9). This cannot be done by the optical feedback technique. In the next subsection, the minimum attainable linewidth is estimated in the case where a sufficiently wide bandwidth is provided, i.e., $f_c > \Delta\nu_{FR}$.

B. The Detector Noise Limited Linewidth

Quite recently, Saito *et al.* [8] have reported that electrical feedback may control the quantum FM noise of 0.8 μm AlGaAs lasers without changing any macroscopic properties of oscillation, and reduce the FM noise to a value less than that limited by spontaneous emission. This result was obtained through an analysis based on a quantum mechanical Langevin equation. They have also pointed out that the linewidth can be reduced to a value limited by the noise of the feedback loop, which is less than the value given by the modified Schawlow-Townes formula. In [8], an optical heterodyne was employed for FM noise detection, while a Fabry-Perot interferometer was used in the present study. Although FM noise detection configurations are different each other, an electrical feedback was commonly employed to reduce the quantum FM noises in both cases. Therefore, it can also be concluded in the present case that the linewidth is ultimately reduced to a value limited by the noise of the feedback loop, i.e., the noise of the detector which is installed at the initial stage of the feedback loop.

The injection current is controlled so that the laser frequency is locked at the frequency ν_1 of the maximum negative slope of the transmittance curve of the Fabry-Perot interferometer used for frequency discrimination (see Fig. 4). If the laser power P_i incident into the interferometer is assumed to be constant, the fluctuation of the power δP incident into the detector is due to the residual frequency fluctuations $\delta\nu(t)$ under the feedback condition. This is given by

$$\delta P = P_i \cdot \delta T_{FP}(\nu) \tag{10}$$

where $\delta T_{FP}(\nu)$ is the fluctuation of the transmittance of the Fabry-Perot interferometer induced by $\delta\nu(t)$. If the transmittance curve $T_{FP}(\nu)$ is approximated to be the Lorentzian, $\delta T_{FP}(\nu)$ at $\nu = \nu_1$ is given by

$$\delta T_{FP} = \frac{3\sqrt{3}}{4} \cdot \frac{1}{\Gamma} \cdot \delta\nu \tag{11}$$

where Γ is the linewidth (FWHM) of T_{FP} which is given by the refractive index n_{FP}, the length L_{FP} of the interferometer, and the reflectance R_{FP} of its mirrors [14]. By using (11), δP of (10) is transformed into the following form:

$$\delta P = \frac{3\sqrt{3}\,\pi}{2} \cdot \frac{n_{FP}L_{FP}}{c} \cdot \frac{\sqrt{R_{FP}}}{1 - R_{FP}} \cdot P_i \cdot \delta\nu \tag{12}$$

where c is the speed of light.

On the other hand, it has been known that the minimum detectable change in the laser power by a photoelectric or photoconductive detector is expressed as [15]

$$\delta P_{min} = \sqrt{16\left(Fk_BT + \frac{h\nu_0}{\eta} M^x\right) B\{P_i \cdot T_{FP}(\nu_1)\}} \tag{13}$$

where B is the bandwidth of the detection, k_B the Boltzmann's constant, T the temperature, h the Planck's constant, F the noise figure, η the quantum efficiency, and M^x the excess noise factor. In general, $M^x > 1$ (for an avalanche photodiode or APD), $M^x = 1$ (for a p-i-n photodiode), $F > 1$, and $\eta < 1$. According to a study of the sensitivity of laser spectrometers [16], the signal-to-noise ratio of the FM noise detection is obtained from (12) and (13)

$$S/N = \delta P/\delta P_{min}. \tag{14}$$

Therefore, the minimum detectable frequency fluctuation $\delta\nu_{min}$ is estimated by setting $S/N = 1$. Since the square of $\delta\nu_{min}$ corresponds to the magnitude of the Allan variance for the minimum detectable FM noise [15], it is given by (12)-(14) as

$$\sigma_F^2(\tau) = (\delta\nu_{min})^2 = \frac{4}{9\pi^2}\left(\frac{c}{n_{FP}L_{FP}}\right)^2 \frac{(1 - R_{FP})^2}{R_{FP}} \frac{Fk_BT + \frac{h\nu_0}{\eta} M^x}{P_i} \tau^{-1} \tag{15}$$

where the relation (15)

$$B = \tfrac{1}{4}\tau \tag{16}$$

was used.

Substitution of (15) into (4) and (5) gives the Lorentzian spectral line shape of $I(\nu)$, and its linewidth $\Delta\nu_{FBm}$ (FWHM) is obtained as

$$\Delta\nu_{FBm} = \frac{8}{9\pi}\left(\frac{c}{n_{FP}L_{FP}}\right)^2 \frac{(1 - R_{FP})^2}{R_{FP}} \frac{Fk_BT + \frac{h\nu_0}{\eta} M^x}{P_i}. \tag{17}$$

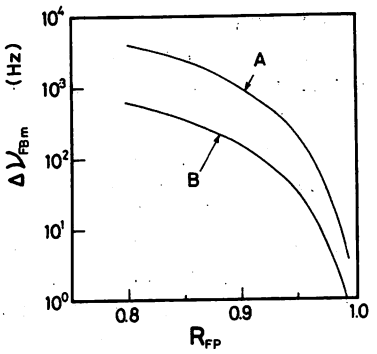

Fig. 5. Relation between the minimum attainable linewidth $\Delta\nu_{FBm}$ and the reflectance R_{FP} of the Fabry-Perot interferometer. The curves *A* and *B* represent the results when a Ge-APD and Ge-p-i-n photodiode, respectively, were used as detector in the feedback loop.

This equation represents the minimum attainable linewidth in case of electrical feedback, where the only limiting factor is the detector noise. Fig. 5 shows the relation between $\Delta\nu_{FBm}$ and R_{FP} derived from (17). Typical numerical values for the 1.5 μm InGaAsP laser were used:

$$\left.\begin{aligned} &T = 293\ \text{K}, \quad \nu_0 = 2 \times 10^{14}\ \text{Hz}, \\ &P_i = 3\ \text{mW}, \quad n_{FP} = 1.4, \\ &L_{FP} = 10\ \text{mm}, \\ &F = 25, \quad \eta = 0.73, \\ &M^x = 9(\text{APD}),\ 1(\text{p-i-n photodiode}). \end{aligned}\right\} \tag{18}$$

It is seen from Fig. 5 that the linewidth can be ultimately reduced to a value less than 1 kHz when $L_{FP} = 10$ mm and $R_{FP} > 0.9$. This makes the electrical feedback a quite promising technique to realize an ultranarrow linewidth.

III. Experimental Apparatus

A distributed feedback (DFB)-type InGaAsP laser of 1.5 μm wavelength [17] was used in the present study. The lengths of the diffraction grating and the window region were 445 μm and 50 μm, respectively, corresponding to a total length of 495 μm. The threshold current I_{th} was 30.2 mA at the heat sink temperature T_h of 293 K. The laser was used within an injection current range of less than 100 mA. It was confirmed by using a conventional grating monochromator that it showed a single longitudinal mode oscillation within this range.

Fig. 6 shows the experimental apparatus used for the present study. The laser was fixed on a heat sink, which was composed of a copper block and a Peltier element. The temperature T_h of the heat sink was controlled so that $T_h = 293 \pm 0.05$ K. The laser beam was collimated by a small AR-coated Gran-Thompson prism and a YIG crystal in a dc magnetic field. The resulting isolation ws 36.5 dB. By careful optical alignments of the optical components used in this apparatus, the power of the light reflected back into the laser cavity was reduced to less than -50 dB with respect to the single-ended output power P_0 from the laser cavity.

Two Fabry-Perot interferometers, made of cylindrical

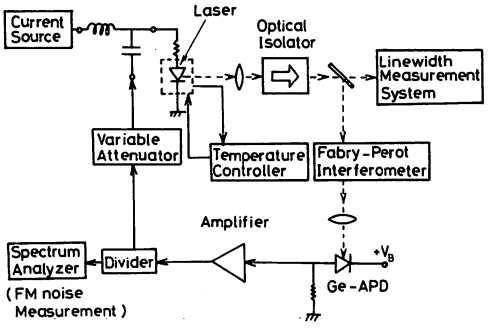

Fig. 6. Experimental apparatus used for the linewidth reduction by electrical feedback. The linewidth measurement system itself was composed of apparatus for the delayed self-heterodyne technique [18].

rods of fuzed silica 10 mm thick, were used for frequency discrimination. Dielectric multilayers were coated on both ends of the rods to obtain reflectances R_{FP} of 0.9 for one interferometer, and 0.95 for the other. The optical axis of the interferometer was tilted about 1.5° with respect to that of the laser beam propagation. The injection of the reflected light from the mirror surface of the interferometer into the laser was suppressed by this optical misalignment.

The laser power transmitted through the interferometer was detected by a Ge-avalanche photodiode (APD). The output power from the APD was negatively fed back to the laser after being amplified by a low noise amplifier with 30 dB gain. The bandwidth of this amplifier was 100 MHz, which should be wide enough, as has been demonstrated in Section III. The feedback loop was kept as short as possible, and the resultant time delay around the feedback loop was 13 ns. The electrical components in the feedback loop were carefully shielded to reduce electromagnetically induced noise. The total gain of the feedback was adjusted by the bias voltage of the APD and the variable attenuator.

The spectral line shape was observed by means of the delayed self-heterodyne technique [18] using a single mode optical fiber with a cutoff wavelength of 1.2 μm. The fiber length was 1.5 km, which corresponds to a resolution of 125 kHz for the linewidth measurement [18]. An acoustooptical modulator was used as a frequency shifter for the delayed self-heterodyning, and the frequency shift of the laser beam provided by this modulator was 80 MHz.

IV. Experimental Results and Discussions

Fig. 7 shows the relation between the linewidth $\Delta\nu_{FR}$ of the free-running laser and the inverse of the normalized injection current $(I/I_{th} - 1)^{-1}$. P_0 represents the single-ended output power. The slope of this curve gradually increased with increasing injection current, and the fitted folded line shows a kink at $(I/I_{th} - 1)^{-1} = 0.85$. The linewidth $\Delta\nu_{FR}$ can be expressed as follows:

$$\begin{aligned} \Delta\nu_{FR} &= 12.5(I/I_{th} - 1)^{-1} \\ &= 50.1P_0^{-1} \quad (\text{MHz}) \\ &\qquad \text{for } (I/I_{th} - 1)^{-1} < 0.85 \end{aligned} \tag{19a}$$

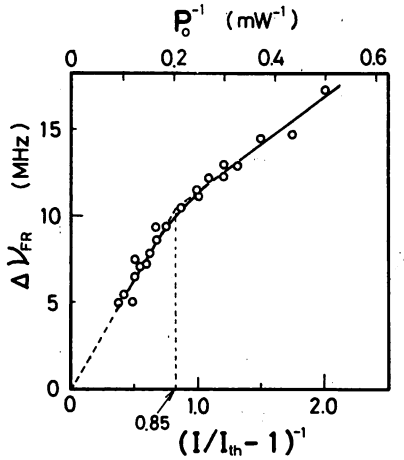

Fig. 7. Experimental result of the relation between the linewidth $\Delta\nu_{FR}$ of the free-running laser and the inverse of the normalized injection current $(I/I_{th} - 1)^{-1}$

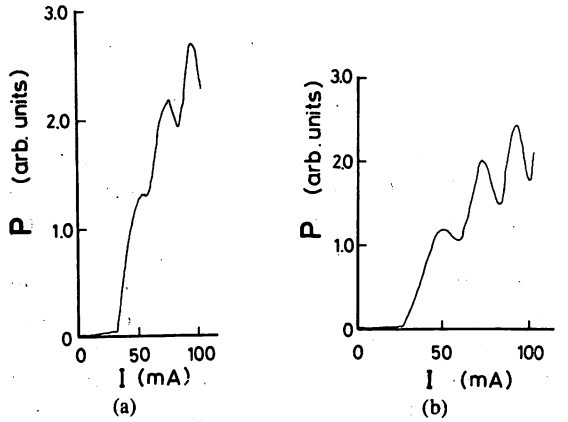

Fig. 8. Relation between the laser power transmitted through the Fabry-Perot interferometer and the injection current. (a) $R_{FP} = 0.9$. (b) $R_{FP} = 0.95$.

$$\Delta\nu_{FR} = 5.7 + 5.4(I/I_{th} - 1)^{-1}$$
$$= 5.7 + 21.6P_0^{-1} \quad \text{(MHz)}$$
$$\text{for } 0.85 < (I/I_{th} - 1)^{-1} < 2.0 \quad (19b)$$

where P_0 is expressed in milliwatts. For $(I/I_{th} - 1)^{-1} < 0.85$, $\Delta\nu_{FR}$ approaches zero with increasing current, which means that $\Delta\nu_{FR}$ follows the modified Schawlow-Townes formula, and that this laser does not have a power-independent linewidth [13].

The experiments related to linewidth reduction were carried out for $(I/I_{th} - 1)^{-1} < 0.85$. Fig. 8 shows the relation between the laser power transmitted through the Fabry-Perot interferometer and the injection current. The finesse of the Fabry-Perot interferometer estimated from these curves are much lower than those of the theoretically expected values [30 in Fig. 8(a) and 60 in Fig. 8(b)]. This is because the optical axis of the Fabry-Perot interferometer was tilted, the wavefront and intensity profile of the laser beam were not uniform, the laser frequency was drifted by residual temperature fluctuations, and so on.

The parts of the curve of Fig. 8 with negative slope were used for frequency discrimination. It was essential to use a negative slope for negative feedback because a noninverting amplifier was used in the feedback loop of the present experiment.

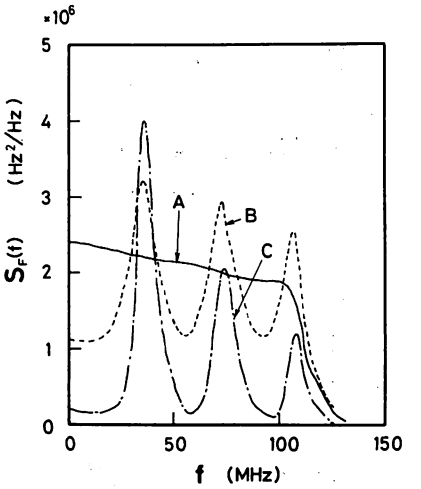

Fig. 9. Power spectral density of the FM noise, where $(I/I_{th} - 1)^{-1} = 0.51$ and $R_{FP} = 0.95$, respectively. Curve A is the result for the free-running laser. Curves B and C are the results under feedback condition, where the attenuation of the variable attenuator in the feedback loop was fixed at -20 dB and 0 dB, respectively. The decreases of $S_F(f)$ at $f > 100$ MHz are due to the bandwidth of the FM noise measurement.

Fig. 9 shows the relation between the power spectral density of the FM noise and the attenuation of the variable attenuator in the feedback loop. It is seen that resonant peaks appeared in the power spectral density by decreasing the attenuation, i.e., by increasing the feedback gain. This is because the feedback is positive rather than negative at these Fourier frequencies, due to the 13 ns delay time and the phase delay inherent in direct frequency modulation. Except for these resonant peaks, however, the power spectral density decreased with increasing feedback gain. A minimum was observed when the variable attenuator was fixed at 0 dB, where the limiting factor was the noise from the Ge-APD. The linewidth measurements were carried out under this feedback condition. Fig. 10 shows the power spectra of the outputs from the delayed self-heterodyne system. They represent spectral line shapes of the laser output, i.e., the optical carrier spectrum. But it should be pointed out that the observed line widths are double that of the actual laser linewidth [18]. As is shown in this figure, the linewidth of the free-running laser $\Delta\nu_{FR}$ was 5 MHz, whereas under the feedback condition, this linewidth $\Delta\nu_{FB}$ was reduced to a value as narrow as 330 kHz. This is the minimum value we were able to obtain in the present experiment. The spectral line shape showed none of the temporal fluctuations which have sometimes been observed in the feedback technique [3]-[5].

FM sidebands appeared at 38 MHz distance from the optical carrier spectrum of Fig. 10(b), which were caused by the resonant peaks of the power spectral density $S_F(f)$ of Fig. 9. However, since their peak values were about 20 dB less than that of the optical carrier spectrum, they did not interfere with the linewidth measurements. These sidebands can be removed farther away from the optical carrier spectrum by reducing the length of the feedback loop. It may be successfully carried out if the detector and amplifier are integrated together with the laser diode. This

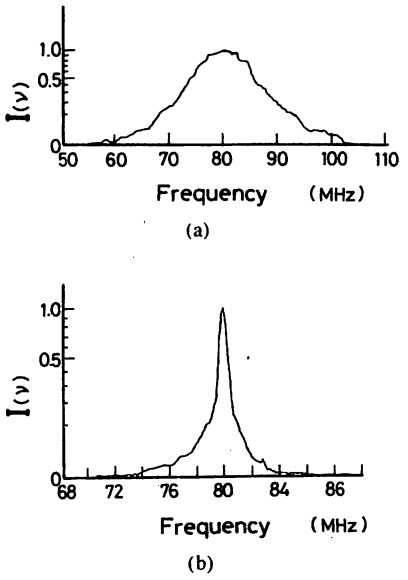

Fig. 10. Power spectra of the outputs from the delayed self-heterodyne system, where $(I/I_{th} - 1)^{-1} = 0.41$ and $R_{FP} = 0.9$. Center frequencies of these spectra correspond to the frequency of the oscillator for the acoustooptic modulator. (a) The result for the free-running laser, from which the linewidth $\Delta\nu_{FR}$ was derived as being 5 MHz. (b) The result under feedback condition, from which the linewidth $\Delta\nu_{FB}$ was derived as being 330 kHz.

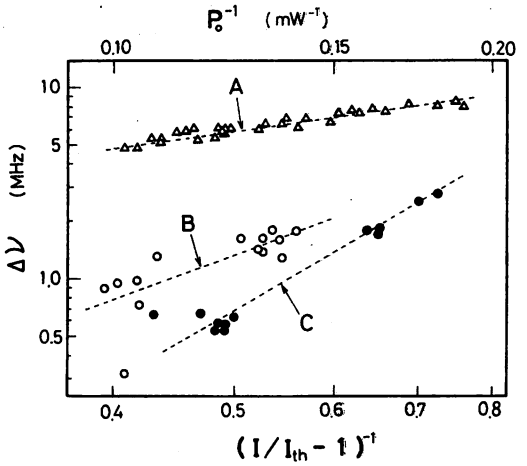

Fig. 11. Relation between the linewidth and the inverse of the normalized injection current. *A*: The linewidth $\Delta\nu_{FR}$ of free-running laser. *B*: The linewidth $\Delta\nu_{FB}$ under feedback condition, where $R_{FP} = 0.9$. *C*: The linewidth $\Delta\nu_{FB}$ under feedback condition, where $R_{FP} = 0.95$.

integration will also bring about an effective reduction on the noise from the feedback loop, which will improve the performance of the ultranarrow linewidth laser.

Fig. 11 shows the relation between the linewidth $\Delta\nu_{FB}$, the single-ended output power P_0, and the injection current I normalized to its threshold value I_{th}. A linewidth narrower than 1 MHz was obtained by feedback, and the minimum was 330 kHz, as shown in Fig. 10(b). The value of $\Delta\nu_{FB}$ can be expressed as

$$\Delta\nu_{FB} = 7.2(I/I_{th} - 1)^{-2.5} = 2.16 \times 10^2 P_0^{-2.5} \quad \text{(MHz)} \quad \text{for } R_{FP} = 0.9 \tag{20}$$

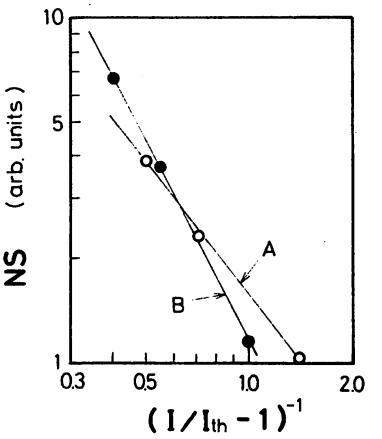

Fig. 12. Relation between the values of the negative slope NS of the curves in Fig. 8 and $(I/I_{th} - 1)^{-1}$. *A*: $R_{FP} = 0.9$. *B*: $R_{FP} = 0.95$.

$$\Delta\nu_{FB} = 8.5(I/I_{th} - 1)^{-3.6} = 1.22 \times 10^3 P_0^{-3.6} \quad \text{(MHz)} \quad \text{for } R_{FP} = 0.95 \tag{21}$$

where P_0 is expressed in milliwatts. These are given by broken lines *B* and *C* in Fig. 11. Some experimental values in this figure deviate from these lines. One of the possible reasons is that the reproducibility of the locked frequency ν_l of the laser on the slope of the transmittance curve of the Fabry–Perot interferometer was not high enough, due to the residual temperature fluctuations of the heat sink. A comparison between (19)–(21) shows that the dependence of $\Delta\nu_{FB}$ of the injection current is different from that of $\Delta\nu_{FR}$. This is because the value of the negative slope NS of the curves in Fig. 8 increases with increasing injection current. Fig. 12 shows the relation between the negative slope NS and $(I/I_{th} - 1)^{-1}$, which are expressed as

$$\text{NS} \propto \begin{cases} (I/I_{th} - 1)^{1.3} & \text{for } R_{FP} = 0.9 \\ (I/I_{th} - 1)^{1.9} & \text{for } R_{FP} = 0.95. \end{cases} \tag{22}$$

A relation between $\Delta\nu_{FB}$ and $(I/I_{th} - 1)^{-1}$ can now be derived in the following way.

Using (10) and (13), S/N of (14) can be expressed as

$$S/N \propto P_i^{1/2} \delta T_{FP}(\nu) \propto P_i^{1/2} \cdot \text{NS} \tag{23}$$

where the right-hand side of this equation was derived because $\delta T_{FP}(\nu)$ is proportional to NS of (22). Furthermore, the value of g in (2) or (3) is proportional to the feedback gain and, therefore, is given by

$$g \propto S/N. \tag{24}$$

Then, the value of $\Delta\nu_{FB}$ given by (9) can be expressed as

$$\Delta\nu_{FB} \propto \begin{cases} (I/I_{th} - 1)^{-2.8} & \text{for } R_{FP} = 0.9 \\ (I/I_{th} - 1)^{-3.4} & \text{for } R_{FP} = 0.95 \end{cases} \tag{25}$$

where we make use of (9), (19a), (23), and (24). Equation (25) agrees well with (20) and (21). From these equations,

it can be concluded that a larger reduction of the linewidth can be obtained at a higher value of the injection current.

The minimum of $\Delta\nu_{FB}$, i.e., 330 kHz, obtained in the present experiment satisfies the condition required to reduce the bit error rate to a value as low as 10^{-9} in a PSK heterodyne optical communication system with bit rate of 1 Gbit/s. However, this experimentally obtained value is still larger than the theoretical limit of (17) and Fig. 5. The possible reasons are: the actual noise of the Ge-APD employed was larger than that given by (13), noises from other electrical components in the feedback loop were not negligible, the finesse of the Fabry–Perot interferometer realized in the experiments was lower than that of the theoretically expected value, and the fluctuations of the laser power incident into the Fabry–Perot interferometer were not negligible. For further linewidth reductions and approach to the minimum attainable linewidth, these noises should be reduced and the finesse of the interferometer should be improved by careful optical alignment, because they limit the sensitivity of the actual FM noise detection.

For example, there are several possibilities of reducing fluctuations of the laser power as required above. One of them is to use an external modulator as an automatic power controller. However, the use of such a modulator will have disadvantages because the AM noise inside the laser cavity cannot be reduced. The AM noise inside the laser cavity at the low Fourier frequency range may be increased when the FM noise is sufficiently reduced to the ultimate level by controlling only the injection current. This is a consequence of the uncertainty principle governing the simultaneous measurement of the photon number and phase [19]. If an increase in AM noise occurs, the minimum attainable value of the linewidth is increased by an increase in the level of the unresolved AM sidebands located close to the optical carrier frequency, and therefore, some modification of (17) should be considered. This increase in the AM noise cannot be avoided as long as only the injection current is controlled. However, if a laser with segmented electrodes will be used, FM and AM noise can be reduced simultaneously by independently controlling the currents injected into each electrode. Since such a laser with segmented electrodes has already been developed and wavelength tuning has also been demonstrated [20], realization of an ultranarrow linewidth can be expected in the future by applying the present technique to this kind of laser.

Designs of appropriate lasers for realizing ultranarrow linewidths are now in progress by the authors, and will be published elsewhere.

V. Summary

Calculations and experiments were carried out to investigate the linewidth reduction of a 1.5 μm InGaAsP laser by an electrical feedback technique. A compact Fabry–Perot interferometer was used as a frequency discriminator. The minimum attainable linewidth, being limited only by the detector noise, was estimated. According to this estimation, a linewidth less than 1 kHz can be realized when the reflectance of the Fabry–Perot interferometer is higher than 0.9. As a result of experiments, a linewidth as narrow as 330 kHz was obtained, which is 15 times as narrow as that in the case of the free-running laser. It was pointed out that further reduction of the experimentally obtained linewidth and approach to the minimum attainable linewidth can be expected by simultaneously reducing the AM noise of the laser.

From these results, we may conclude that electrical feedback is a promising technique to realize an ultranarrow linewidth laser.

Acknowledgment

The authors would like to express their thanks to Dr. T. Yamamoto and Dr. S. Akiba of KDD Research and Development Laboratories, and Dr. Y. Yamamoto of NTT for their valuable discussions. They also wish to thank Prof. Y. Suematsu of their institute for his encouragements during this work.

References

[1] M. Ohtsu, H. Fukada, T. Tako, and H. Tsuchida, "Estimation of the ultimate frequency stability of semiconductor lasers," *Japan. J. Appl. Phys.*, vol. 22, pp. 1157–1166, 1983.

[2] K. Kikuchi, T. Okoshi, M. Nagamatsu, and N. Henmi, "Bit-error rate of PSK heterodyne optical communication system and its degradation due to spectral spread of transmitter and local oscillator," *Electron. Lett.*, vol. 19, pp. 417–418, 1983.

[3] S. Saito and Y. Yamamoto, "Direct observation of Lorentzian lineshape of semiconductor laser and linewidth reduction with external grating feedback," *Electron. Lett.*, vol. 17, pp. 325–327, 1981.

[4] F. Favre, D. Le Guen, and J. C. Simon, "Optical feedback effects upon laser diode oscillation field spectrum," *IEEE J. Quantum Electron.*, vol. QE-18, pp. 1712–1717, 1982.

[5] R. Wyatt, "Line-narrowed lasers for coherent optical fiber systems," in *Proc. Conf. Opt. Fiber Commun.*, San Diego, CA, Feb. 11–13, 1985.

[6] R. Lang and K. Kobayashi, "External optical feedback effects on semiconductor injection laser properties," *IEEE J. Quantum Electron.*, vol. QE-16, pp. 347–355, 1980.

[7] M. Ohtsu and S. Kotajima, "Linewidth reduction of a 1.5 μm InGaAsP laser by electrical feedback," *Japan. J. Appl. Phys.*, vol. 24, pp. L256–L258, 1985.

[8] S. Saito, O. Nilsson, and Y. Yamamoto, "Frequency modulation noise and linewidth reduction in a semiconductor laser by means of negative frequency feedback technique," *Appl. Phys. Lett.*, vol. 46, pp. 3–5, 1985.

[9] C. H. Henry, "Theory of the linewidth of semiconductor lasers," *IEEE J. Quantum Electron.*, vol. QE-18, pp. 259–264, 1982.

[10] Y. Yamamoto, S. Saito, and T. Mukai, "AM and FM quantum noise in semiconductor lasers–Part II: Comparison of theoretical and experimental results for AlGaAs lasers," *IEEE J. Quantum Electron.*, vol. QE-19, pp. 47–57, 1983.

[11] D. W. Allan, "Statistics of atomic frequency standards," *Proc. IEEE*, vol. 54, pp. 221–230, 1966.

[12] M. Ohtsu and S. Kotajima, "Derivation of the spectral width of a 0.8 μm AlGaAs laser considering $1/f$ noise," *Japan. J. Appl. Phys.*, vol. 23, pp. 760–764, 1984.

[13] D. Welford and A. Mooradian, "Observation of linewidth broadening in (GaAl)As diode lasers due to electron number fluctuations," *Appl. Phys. Lett.*, vol. 40, pp. 560–562, 1982.

[14] M. Born and E. Wolf, *Principle of Optics*, 4th ed. Oxford, England: Pergamon, 1970.

[15] K. Shimoda, "Ultimate stability of methane-stabilized lasers," *Japan. J. Appl. Phys.*, vol. 12, pp. 1222–1226, 1973.

[16] ——, "Limits of sensitivity of laser spectrometers," *Appl. Phys.*, vol. 1, pp. 77–86, 1973.

[17] S. Akiba, K. Utaka, K. Sakai, and Y. Matsushima, "Distributed feedback InGaAsP/InP lasers with window region emitting at 1.5 μm range," *IEEE J. Quantum Electron.*, vol. QE-19, pp. 1052–1056, 1983.

[18] T. Okoshi, K. Kikuchi, and A. Nakayama, "Novel method for high

resolution measurement of laser output spectrum," *Electron. Lett.*, vol. 16, pp. 630-631, 1980.
[19] D. Marcuse, *Engineering Quantum Electrodynamics*. New York: Harcourt, 1970.
[20] Y. Tohmori, Y. Suematsu, H. Tsushima, and S. Arai, "Wavelength tuning of GaInAsP/InP integrated laser with butt-jointed built-in distributed Bragg reflector," *Electron. Lett.*, vol. 19, pp. 656-657, 1983.

Motoichi Ohtsu was born in Kanagawa, Japan, on October 5, 1950. He received the B.S., M.S. and Ph.D. degrees in electronics engineering from the Tokyo Institute of Technology, Tokyo, Japan, in 1973, 1975, and 1978, respectively.

He is an Associate Professor in the Graduate School at Nagatsuta, Tokyo Institute of Technology. He is interested in frequency control of lasers and its applications to coherent optical measurements and optical communications.

Dr. Ohtsu is a member of the Institute of Electronics and Communication Engineers of Japan, the Institute of Electrical Engineers of Japan, the Japan Society of Applied Physics, and the Optical Society of America. He was awarded a prize from the Japan Society of Applied Physics in 1982. He was also awarded the Issac Koga Gold Metal from the International Union of Radio Science in 1984.

Shinichi Kotajima was born in Niigata, Japan, in 1960. He received the B.S. and M.S. degrees in electronics engineering from the Tokyo Institute of Technology, Tokyo, Japan, in 1983 and 1985, respectively.

In 1985 he joined the NEC Corporation, Kanagawa, Japan.

Mr. Kotajima is a member of the Institute of Electronics and Communication Engineers of Japan and the Japan Society of Applied Physics.

Frequency Offset Locking of AlGaAs Semiconductor Lasers

KATSUHIKO KUBOKI AND MOTOICHI OHTSU

Abstract—**Frequency offset locking was proposed as a reliable electrical negative feedback technique for tracking and sweeping of a semiconductor laser frequency. A frequency stabilized laser was used as a master laser, whose residual frequency fluctuations were 140 (kHz) at the integration time (τ) of 100 ms $\leqq \tau \leqq$ 100 s. A digital phase comparator of a large dynamic range of $2\pi \times 2^{11}$ (rad) was employed in the feedback loop to reduce the phase fluctuations of the beat signal between the master and slave lasers. Performances of frequency tracking and sweeping of the slave laser were quantitatively evaluated, and the results are: residual frequency fluctuations of the beat signal were reduced as low as 11 (Hz) at τ = 100 s, which meant that the residual frequency fluctuations of the slave laser were almost equal to those of the master laser, i.e., the slave laser frequency tracked accurately to the master laser frequency. Both the capture range and lock range of the beat frequency were 1.22 GHz. Frequency tunable range of the slave laser was 36.6 GHz under the condition of frequency offset locking, in which the slave laser frequency fluctuations were maintained as low as the one given above.**

I. Introduction

ATTEMPTS at improving temporal coherence in semiconductor lasers have been made in recent years for coherent optical measurements, coherent optical communications [1], and so on.

It can be deduced from well-developed techniques for coherent microwave oscillators [2] (H masers, Cs or Rb atomic clocks) and gas lasers [3] that at least four subjects should be simultaneously carried out for this improvement, which are 1) stabilization of center frequency of field spectrum, 2) linewidth reduction of the field spectrum, 3) frequency tracking to the other highly coherent laser, and 4) stable and wide-band frequency sweep.

Ohtsu has proposed that electrical negative feedback can be used as a promising technique to carry out these four subjects simultaneously, and has tried an experimental work on subject 1) to improve the frequency stability of a 0.8 μm AlGaAs laser as high as 1.4×10^{-12} at the integration time of 100 s [4]. Theoretical analyses, based on semiclassical Langevin's equation of motion, have shown that this stability is as high as the one limited by quantum noise sources of the laser [5]. Frequency stability of a 1.5 μm InGaAsP laser has been also improved to as high as 6.7×10^{-11} at the integration time of 20 s [6].

With respect to subject 2), the linewidth of a 1.5 μm InGaAsP laser has been reduced to 330 kHz by electrical negative feedback, and the theoretical limit has been estimated as being about several hundred hertz [7].

In the present study, subjects 3) and 4) were carried out. A technique of electrical negative feedback was commonly used also for these subjects in order to combine these servo control systems with those for subjects 1) and 2). By this combination, it can be expected that a synthesized technique is established for realizing ultrahigh coherence in the future.

Aside from establishments of such a synthesized technique, a technique for frequency tracking [subject 3)] itself would be useful for applications to heterodyne optical measurements and communications, and so on. A nonlinear phenomenon of injection locking can be used for this purpose [8], and preliminary experiments on electrical negative feedback have been carried out for FSK heterodyne optical communications [9], [10]. However, any accurate experiments and quantitative evaluations of their performances have not yet been fully documented. The authors propose here a technique of frequency offset locking for semiconductor lasers to improve the performances of frequency tracking, which has never been successfully employed for gas lasers [11], [12]. Several experiments were carried out to evaluate the performances of this technique quantitatively.

Frequency offset locking can be also used for subject 4), i.e., stable and wide-band frequency sweep. The technique for wide-band frequency sweep would be useful to realize a tunable coherent light source for high resolution laser spectroscopy, frequency multiplexing in coherent optical communications, and so on.

II. Experimental Setup

Fig. 1 shows an experimental setup. Two 0.8 μm CSP-type AlGaAs lasers (Hitachi, HL8311E) were used as master and slave lasers, and the slave laser was frequency offset locked to the master laser. The powers of these lasers were about 0.5 mW at the position of the detector Si-APD2 of Fig. 1. Temperatures of their heat sinks were controlled to reduce their temperature fluctuations as low as 1×10^{-4} K. For this purpose, the temperature fluctuations of a small copper block used as a heat sink were

Manuscript received June 12, 1986; revised October 22, 1986. This work was supported in part by a Grant-in-Aid for Scientific Research from the Ministry of Education, Science, and Culture of Japan, and by the Funds for International Communication Research from the KDD Engineering and Consulting Foundation.

The authors are with the Graduate School at Nagatsuta, Tokyo Institute of Technology, Yokohama, Kanagawa 227, Japan.

IEEE Log Number 8612645.

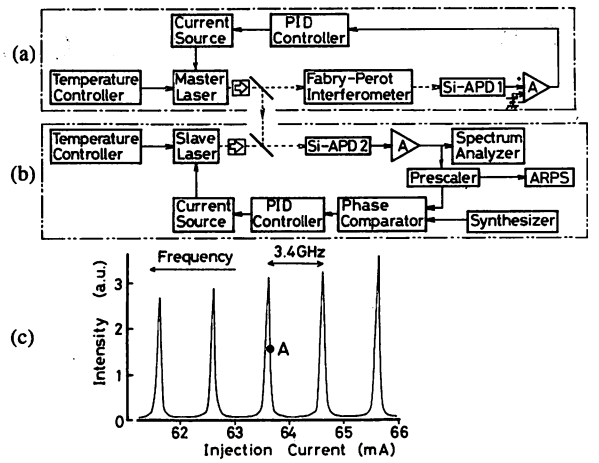

Fig. 1. Experimental setup. (a) Feedback loop for the master laser. (b) Feedback loop of the frequency offset locking for the slave laser. ARPS: computerized Allan variance real-time processing system. (c) Transmission spectral lineshapes of the Fabry–Perot interferometer of (a). *A*: The point at which the master laser frequency was locked.

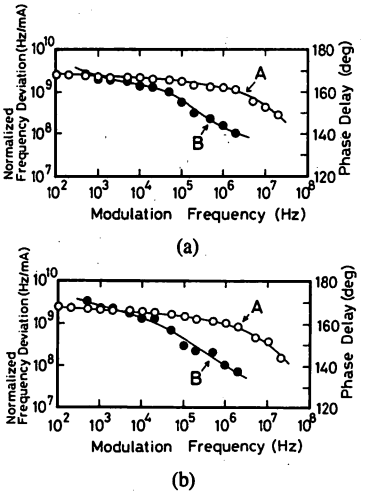

Fig. 2. Characteristics of direct frequency modulation of the master (a) and slave (b) lasers. *A*: Normalized frequency deviation. *B*: Phase delay.

detected by a thermistor bridge and was controlled by a peltier element. Frequency drifts of the free-running lasers were reduced to as low as about 20 MHz/h by this temperature control.

Fig. 2(a) and (b) shows the characteristics of direct frequency modulation of these lasers, which were measured by employing a technique using a Michelson interferometer [13]. These characteristics are consistent with ones which have been already reported [14], [15].

The experimental setup of Fig. 1 was composed of two parts. One part is a feedback loop for the frequency stabilization of the master laser [Fig. 1(a)]. A Fabry–Perot interferometer used for its frequency reference was made of a rigid cylindrical rod of fused silica with multilayered films coated on both ends, and had a free spectral range of 3.4 GHz with reflectivities of 90 percent. A linear part of the slope of the transmission spectral lineshape was used as a frequency discriminator. The output signal from a Si-APD behind the interferometer was negatively fed-

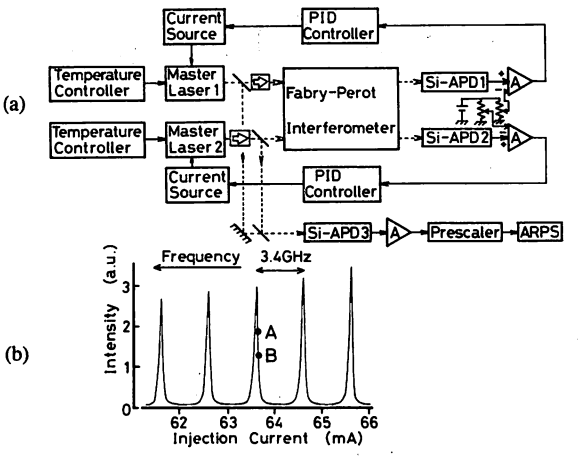

Fig. 3. (a) Experimental setup to evaluate the frequency stability of the master laser, for which one more laser was used as the second master laser and was independently stabilized. (b) Transmission spectral lineshapes of the Fabry–Perot interferometer which was commonly used as frequency references for both of the master lasers. The points *A* and *B* represent the frequencies at which the two master lasers were locked.

back to the injection current after being amplified by a proportional amplifier, an integrator, and a differentiator in a PID-controller. The master laser frequency was locked at the steepest point *A* on the slope of the transmission spectral lineshape shown in Fig. 1(c). The bandwidths of the PID-controller and the current source were designed as 1.5 MHz. The gains of the three analog amplifiers in the PID-controller were empirically adjusted in order to get the highest frequency stability by using measured results of the direct frequency modulation characteristics of Fig. 2(a) and FM noise properties.

Fig. 3(a) shows an apparatus used to measure the frequency stability of the master laser, in which one more master laser was prepared to measure the frequency fluctuations of the beat signal between the equally stabilized two master lasers. Frequencies of these master lasers were locked at the points *A* and *B* of a slope of the transmission spectral lineshape of the common Fabry–Perot interferometer used in Fig. 1(a) [see Fig. 3(b)]. The resultant beat frequency was 400 MHz. Magnitudes of residual beat frequency fluctuations $\delta\nu(t)$ were evaluated by using the Allan variance $\sigma_\nu^2(\tau)$, which is an accurate measure popularly used to represent the frequency stabilities of several oscillators [16]. It is defined by

$$\sigma_\nu^2(\tau) \equiv \lim_{N\to\infty} \frac{1}{N-1} \sum_{k=1}^{N-1} \frac{(\overline{\delta\nu}_{k+1} - \overline{\delta\nu}_k)^2}{2} \qquad (1)$$

where N is a number of data, and $\overline{\delta\nu}_k(t)$ is the value of $\delta\nu(t)$ averaged over the integration time τ which is given by

$$\left.\begin{aligned} \overline{\delta\nu}_k &= \frac{1}{\tau}\int_{t_k}^{t_{k+1}} \delta\nu(t)\,dt \\ t_{k+1} &= t_k + \tau \quad (k = 1, 2, 3, \cdots, N-1) \end{aligned}\right\} \qquad (2)$$

Since the feedback loops for the two lasers were independent of each other except for the Fabry–Perot interferometer, it can be assumed that their residual frequency

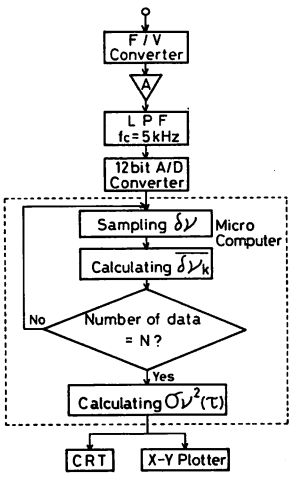

Fig. 4. Block diagram of a computerized Allan variance real-time processing system (ARPS).

fluctuations were mutually uncorrelated, and the fluctuations of the beat frequency were free from the effect of the resonance frequency fluctuations of the Fabry–Perot interferometer. It means that the Allan variance of the frequency fluctuations of the beat signal can be given by a sum of the Allan variances of the frequency fluctuations of the two master lasers. The Allan variance was measured by using a computerized Allan variance real-time processing system (ARPS), whose preliminary setup has been developed by Ohtsu [17]. Fig. 4 shows its block diagram.

The other part of the experimental setup [Fig. 1(b)] is the feedback loop of the frequency offset locking for the slave laser. The beat signal between the master and slave lasers was detected by a Si-APD of 2 GHz bandwidth, and its frequency ν_B was divided by a prescaler after amplified by a wide-band preamplifier. The division rate M of the prescaler was fixed to 500 for $\nu_B < 0.7$ GHz, and to 2000 for $\nu_B \geqq 0.7$ GHz, which was required because of a limited bandwidth of the prescaler used.

Instead of controlling the frequency of the beat signal, its phase, i.e., the time integral of the frequency, was controlled in the present experiments to reduce beat frequency drift and to improve the accuracy of frequency tracking. For this purpose, a phase of the output signal from the prescaler was compared with that of the output signal from a digital frequency synthesizer by a digital phase comparator. This comparator was composed of binary up counters, down counters, full adders, and a D/A converter.

The output signal from the phase comparator was applied to a current source for the slave laser after being amplified by a PID-controller, and the injection current of the slave laser was controlled in order that the divided beat frequency ν_B/M was locked to the synthesizer frequency ν_L. The bandwidths of the PID-controller and current source used here were also 1.5 MHz.

Under a condition of frequency offset locking, the slave laser frequency ν_S is given by

$$\nu_S = \nu_M \pm M \cdot \nu_L \tag{3}$$

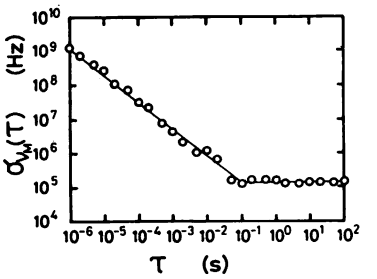

Fig. 5. Square root of the Allan variance $\sigma^2_{\nu M}(\tau)$ of the residual frequency fluctuations of the master laser. τ: Integration time of the measurement.

where ν_M is the frequency of the master laser. This formula represents that the locked frequency of the slave laser possesses an offset ($\pm M \cdot \nu_L$) with respect to the master laser frequency, by which this technique has been called frequency offset locking. The magnitude of residual fluctuations of the beat frequency was evaluated by the computerized ARPS.

As can be deduced from the explanation given above, a part of this technique is equivalent to a phase locked loop for conventional electronic circuits [18]. However, in contrast to such a conventional phase locked loop, the dynamic range of the present phase comparator was designed to be as large as $2\pi \times 2^{11}$ (rad) to detect a large phase fluctuations in lightwaves.

Stable and accurate frequency sweep can be also carried out by slowly sweeping the synthesizer frequency under the condition of frequency offset locking.

III. Experimental Results and Discussions

A. Frequency Stabilization of the Master Laser and Frequency Tracking of the Slave Laser

The spectral linewidth of the beat signal between the two master lasers was measured as 35 MHz by a spectrum analyzer. Since the magnitudes of residual frequency fluctuations of these lasers were approximated as being equal with each other and mutually uncorrelated, the linewidth of field spectrum of each laser was estimated as a half that of the beat signal, i.e., 17.5 MHz. Furthermore, the Allan variance $\sigma^2_{\nu M}(\tau)$ of residual frequency fluctuations of each laser can be also estimated as being a half that of the beat signal. Fig. 5 shows the square root of $\sigma^2_{\nu M}(\tau)$ estimated from that of the beat frequency which can be approximated as

$$\sigma_{\nu M}(\tau) = \begin{cases} 2.3 \times 10^4 \cdot \tau^{-0.8}\ (\text{Hz}) \\ \quad \text{for}\ \ 1\ \mu\text{s} \leqq \tau < 100\ \text{ms} \\ 140\ (\text{kHz}) \\ \quad \text{for}\ \ 100\ \text{ms} \leqq \tau \leqq 100\ \text{s}. \end{cases} \tag{4}$$

That is, the minimum on the curve in this figure was 140 kHz.

This value was 1/100 times that of the free-running laser, from which improvements of the frequency stability was confirmed. Higher frequency stability can be expected by using a more stable frequency reference, e.g.,

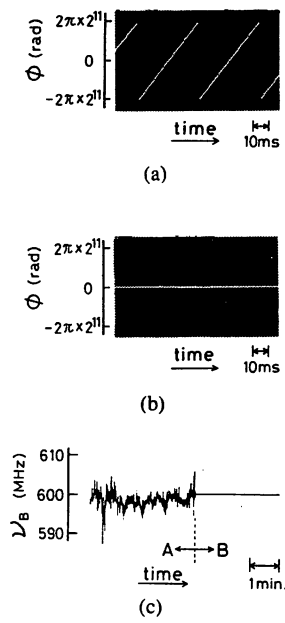

Fig. 6. Output signals from the phase comparator under free-running (a) and frequency offset locked (b) conditions. The ordinates of these figures represent a phase difference between the signal from the frequency synthesizer and the beat signal whose frequency has been divided by M. (c) Fluctuations in the beat frequency ν_B. The parts A and B represent the waveforms under free-running and frequency offset locked conditions, respectively, where M was fixed at 500 and the locked value of ν_B was 0.6 GHz.

absorption spectral lines in stable atoms or molecules [4], [6], [19].

Fig. 6(a) and (b) shows waveforms of output signals from the phase comparator under free-running and frequency offset locked conditions, respectively. Fig. 6(c) shows fluctuations of a beat frequency between the master and slave lasers. It was confirmed from these figures that the present scheme of phase control was effective to lock tightly the beat frequency. As will be shown in subsection B, the lock range of the beat frequency was 1.22 GHz. On the other hand, it was empirically confirmed that the capture range of the beat frequency was also as wide as 1.22 GHz, i.e., the free-running beat frequency ν_B can be captured to be fixed at $M \cdot \nu_L$ if ν_B stayed within this range. Such a large capture range was due to large dynamic range of the phase comparator mentioned in Section II. The capture range was limited mainly by the response speeds of the Si-APD and the prescaler.

Fig. 7(a) shows the square root of the Allan variance $\sigma^2_{\nu B}(\tau)$ of the beat frequency fluctuations. Since directly controlled quantity was not the frequency of the beat signal but its phase, the square root of the Allan variance $\sigma^2_{\phi B}(\tau)$ of the phase fluctuations was also estimated from the result of Fig. 7(a) and is given by Fig. 7(b), where a relation $\sigma^2_{\phi B}(\tau) = (2\pi\tau)^2 \cdot \sigma^2_{\nu B}(\tau)$ was used. Reductions of frequency and phase fluctuations by frequency offset locking are clearly seen in these figures. It is also seen that the effects of locking were remarkable for a longer integration time, which means that the frequency drift was sufficiently reduced by controlling its time integral, i.e., the phase.

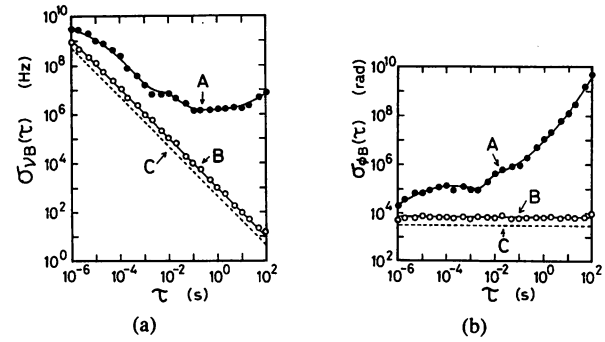

Fig. 7. The square root of the Allan variance $\sigma^2_{\nu B}(\tau)$ of the residual frequency fluctuations (a) and that of $\sigma^2_{\phi B}(\tau)$ of phase fluctuations (b) of the beat signal. A: Results of a free-running condition. B: Results under a condition of frequency offset locking, where $M = 500$ and $\nu_B = 0.6$ GHz. C: Estimated limit given by round-off errors of pulse number counting generated at the D/A converter in the phase comparator.

The value of curve B in Fig. 7(a) is approximated as

$$\sigma_{\nu B}(\tau) = 1.1 \times 10^3 \cdot \tau^{-1}\,(\mathrm{Hz})\ (1\ \mu\mathrm{s} \leqq \tau \leqq 100\ \mathrm{s}), \tag{5}$$

and its minimum is

$$\sigma_{\nu B}(\tau) = 11\ (\mathrm{Hz}) \quad \text{at} \quad \tau = 100\ \mathrm{s}. \tag{6}$$

Analyses of noise magnitudes generated in the feedback loop for frequency offset locking showed that the principal noise source of the residual beat frequency fluctuations was round-off errors of pulse number counting, which was generated at the D/A converter in the phase comparator. The square roots of the Allan variances due to this noise source are expressed as

$$\left.\begin{aligned} \sigma_{\nu B}(\tau) &= M \cdot \tau^{-1}\,(\mathrm{Hz}) \\ \sigma_{\phi B}(\tau) &= 2\pi M\,(\mathrm{rad}) \end{aligned}\right\} \tag{7}$$

which are represented by curve C in Fig. 7(a) and (b). Differences between curves B and C in this figure are due to other noises, e.g., detector noise, noises from the electronic circuits, and so on. Further reductions in the beat frequency fluctuations can be expected by employing a lower division rate M and by using a faster phase comparator and a higher synthesizer frequency.

Since frequencies of the master laser and the beat signal were locked by using different and independent feedback loops, their residual fluctuations can be approximated as being mutually uncorrelated. Therefore, the Allan variance for frequency fluctuations of the slave laser can be expressed as

$$\sigma^2_{\nu S}(\tau) = \sigma^2_{\nu M}(\tau) + \sigma^2_{\nu B}(\tau). \tag{8}$$

Since it can be approximated that $\sigma^2_{\nu B}(\tau) \ll \sigma^2_{\nu M}(\tau)$ for $\tau \geqq 1$ ms by comparing (4) and (5), this equation means that $\sigma^2_{\nu S}(\tau) \cong \sigma^2_{\nu M}(\tau)$, i.e., the residual frequency fluctuations of the slave laser were as low as those of the master laser for $\tau \geqq 1$ ms. Though the value of $\sigma^2_{\nu B}(\tau)$ can not be negligibly smaller than that of $\sigma^2_{\nu M}(\tau)$ for $1\ \mu\mathrm{s} \leqq \tau < 1$ ms, the value of $\sigma_{\nu S}(\tau)$ is still maintained smaller than $\sqrt{2}\,\sigma_{\nu M}(\tau)$, because $\sigma^2_{\nu B}(\tau) \leqq \sigma^2_{\nu M}(\tau)$ in this

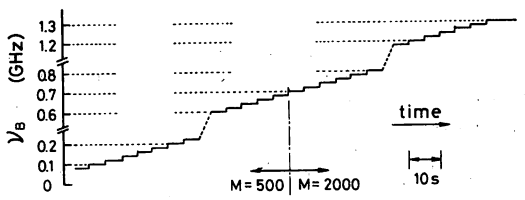

Fig. 8. The beat frequency ν_B which was varied by a stepwise sweep of the synthesizer frequency at 20 MHz interval. The division rate M of the prescaler was fixed at 500 for $\nu_B < 0.7$ GHz, and 2000 for $\nu_B \geqq 0.7$ GHz.

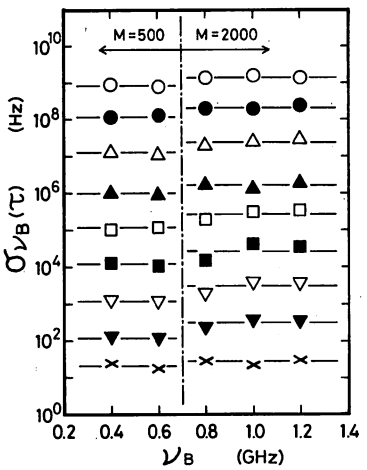

Fig. 9. The relation between the square root of the Allan variance $\sigma^2_{\nu B}(\tau)$ and the beat frequency ν_B within its lock range. The integration times τ of the fluctuation measurements were 1 μs (○), 10 μs (●), 100 μs (△), 1 ms (▲), 10 ms (□), 100 ms (■), 1 s (▽), 10 s (▼), and 100 s (×).

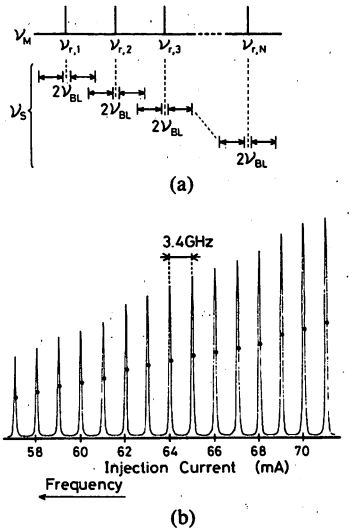

Fig. 10. (a) Schematic explanation of a possible way of extending the range of stable frequency sweep of the slave laser. The master laser frequency ν_M is successively locked to one of the frequency reference grid ($\nu_{r,1} < \nu_{r,2} < \cdots < \nu_{r,N}$). For each locked frequency of the master laser, the frequency offset locking is applied to the slave laser. ν_{BL}: The lock range of the beat frequency. (b) Transmission spectral lineshapes of the Fabry–Perot interferometer which were used as the frequency reference grid for the master laser. The black circles are the points at which the master laser frequency was locked.

range of τ. It can be confirmed from these results that accurate frequency tracking to the master laser was realized, or, in other words, high coherence of the master laser was transferred to the slave laser.

B. Stable and Accurate Frequency Sweep of the Slave Laser

The slave laser frequency can be swept in a stable manner by sweeping the synthesizer frequency with a sweep speed which falls within the bandwidth of the feedback loop (1.5 MHz). Fig. 8 shows the beat frequency ν_B which was varied by a stepwise sweep of the synthesizer frequency at the 20 MHz interval. As shown by this figure, a stable sweep was carried out for 80 MHz $\leqq \nu_B \leqq$ 1.3 GHz, which means that the lock range of the beat frequency was 1.22 GHz and frequency tunable range of the slave laser was 2.44 GHz. This lock range was limited by the following causes. For $\nu_B < 80$ MHz, the level of the input signal to the prescaler was not high enough to be converted into the TTL signal, which is due to a rather broad linewidth of the beat spectrum. For $\nu_B > 1.3$ GHz, on the other hand, the sensitivity of phase comparison was also reduced because of a limited response speeds of the Si-APD and the prescaler.

As shown in Fig. 9, it was confirmed that the magnitudes of residual frequency fluctuations were independent of the beat frequency within the lock range. In this figure, fluctuations for $\nu_B \geqq 0.7$ GHz are slightly larger than those for $\nu_B < 0.7$ GHz because the contributions of round-off errors from the phase comparator are proportional to the division rate M of the prescaler, as was given by (7).

There can be promising ways of further extensions of the range of stable frequency sweep of the slave laser. As shown by Fig. 10(a), one of them is to make a discrete tuning of the master laser frequency by successively locking it to one of the frequency reference grids which are nearly equidistantly distributed along the frequency axis. For each locked frequency of the master laser, the frequency offset locking is applied to the slave laser. By this control scheme, a stable and accurate sweep of the slave laser frequency can be realized. Absorption spectral lines of combination tones or higher harmonics of vibration-rotation transitions in organic molecules can be a candidate for such a frequency reference grid. This is because a great number of lines are distributed with several gigahertz or several tens of gigahertz intervals in the near infrared wavelength region and some of their absolute frequencies have been already calibrated with the accuracies of about $1 \times 10^{-6} \sim 7 \times 10^{-8}$ [6], [19].

In the present experiment, equidistantly distributed resonance frequencies of a Fabry–Perot interferometer of Fig. 1(a) were used as the simpler frequency reference grid. As shown by Fig. 10(b), the master laser frequency was able to be locked to the slopes of its successive fifteen resonance spectral lines. For each locked frequency of the master laser, frequency offset locking was applied to the slave laser to reduce the beat frequency fluctuations as low as those shown by Figs. 7(a) and 9. As a result of

this locking, a range of stable frequency sweep of the slave laser was extended to 36.6 GHz.

The number of lines of frequency reference grid to which the master laser can be locked was limited by mode-hopping phenomena in the laser [20], which also limited the extension of the tunable range of the slave laser frequency. It would be effective to use a laser without mode-hopping to extend this range. A recently developed 1.5 μm GaInAsP/InP DBR laser may be favorably used for this purpose because its wavelength can be continuously varied by varying the ambient temperature within the range of 15 nm without mode-hopping under free-running condition, which corresponds to the frequency range of as wide as 2 THz [21]. A stable and wide-band frequency sweep for more than 1 THz can be expected if this kind of lasers are employed.

IV. Summaries

Frequency offset locking was proposed as a reliable technique for tracking and sweeping of a semiconductor laser frequency. Experiments were carried out by controlling the phase of the beat signal between the master and slave lasers, and their results were quantitatively evaluated. They are summarized as follows.

1) Square root of the Allan variance of residual frequency fluctuations of the master laser was

$$\sigma_{\nu M}(\tau) = \begin{cases} 2.3 \times 10^4 \cdot \tau^{-0.8}\ (\mathrm{Hz}) \\ \quad \text{for}\quad 1\ \mu\mathrm{s} \leqq \tau < 100\ \mathrm{ms} \\ 140\ (\mathrm{kHz}) \\ \quad \text{for}\quad 100\ \mathrm{ms} \leqq \tau \leqq 100\ \mathrm{s}. \end{cases} \tag{9}$$

2) Square root of the Allan variance of residual frequency fluctuations of the beat signal was

$$\sigma_{\nu B}(\tau) = 1.1 \times 10^3 \cdot \tau^{-1}\ (\mathrm{Hz}) \quad \text{for}\quad 1\ \mu\mathrm{s} \leqq \tau \leqq 100\ \mathrm{s}. \tag{10}$$

The minimum was 11 (Hz) at $\tau = 100$ s. Comparisons between this value and that of (9) showed that the residual frequency fluctuations of the slave laser was almost equal to those of the master laser, i.e., the slave laser frequency tracked accurately to that of the master laser. Capture range of the beat frequency was 1.22 GHz.

3) Lock range of the beat frequency was 1.22 GHz, i.e., 0.08 GHz $\leqq \nu_B \leqq$ 1.3 GHz. Frequency tunable range of the slave laser was 36.6 GHz under the condition of frequency offset locking, in which the slave laser frequency fluctuations were maintained as low as the ones given in 2).

References

[1] T. Okoshi, "Recent progress in heterodyne/coherent optical-fiber communications," *J. Lightwave Technol.*, vol. LT-2, pp. 341-346, 1984.

[2] P. Kartaschoff, *Frequency and Time.* London, England: Academic, 1978.

[3] A. Brillet and P. Cerez, "Laser frequency stabilization by saturated absorption," *J. de Physique*, vol. 42, pp. 73-82, 1981.

[4] H. Tsuchida, M. Ohtsu, T. Tako, N. Kuramochi, and N. Oura, "Frequency stabilization of AlGaAs semiconductor laser based on the ^{85}Rb-D_2 line," *Japan. J. Appl. Phys.*, vol. 21, pp. L561-L563, 1982.

[5] M. Ohtsu, H. Fukada, T. Tako, and H. Tsuchida, "Estimation of the ultimate frequency stability of semiconductor lasers," *Japan. J. Appl. Phys.*, vol. 22, pp. 1157-1166, 1983.

[6] M. Ohtsu, H. Kotani, and H. Tagawa, "Spectral measurements of NH_3 and H_2O for pollutant gas monitoring by 1.5 μm InGaAsP/InP lasers," *Japan. J. Appl. Phys.*, vol. 22, pp. 1553-1557, 1983.

[7] M. Ohtsu and S. Kotajima, "Linewidth reduction of a semiconductor laser by electrical feedback," *IEEE J. Quantum Electron.*, vol. QE-21, pp. 1905-1912, Dec. 1985.

[8] S. Kobayashi and T. Kimura, "Injection locking in AlGaAs semiconductor laser," *IEEE J. Quantum Electron.*, vol. QE-17, pp. 681-689, 1981.

[9] F. Favre and D. LeGuen, "Spectral narrowing by optical feedback," in *Proc. Int. Conf. Lasers '83*, 1983, pp. 79-84, STS Press, McLean, VA.

[10] K. Emura, M. Shikada, S. Fujita, I. Mito, H. Honmou, and K. Minemura, "Novel optical FSK heterodyne single filter detection system using a directly modulated DFB-laser diode," *Electron. Lett.*, vol. 20, pp. 1022-1023, 1984.

[11] J. L. Hall and C. J. Borde, "Measurement of methane hyperfine structure using laser saturated absorption," *Phys. Rev. Lett.*, vol. 30, pp. 1101-1104, 1973.

[12] M. Ohtsu, S. Katsuragi, and T. Tako, "Performances of a frequency offset locked He-Xe laser system at 3.51 μm," *IEEE J. Quantum Electron.*, vol. QE-17, pp. 1100-1106, 1981.

[13] H. Tsuchida, T. Tako, and M. Ohtsu, "A novel technique for measuring the frequency deviation of semiconductor lasers under direct modulation," *Japan. J. Appl. Phys.*, vol. 22, pp. L19-L21, 1983.

[14] S. Kobayashi, Y. Yamamoto, M. Ito, and T. Kimura, "Direct frequency modulation in AlGaAs semiconductor lasers," *IEEE J. Quantum Electron.*, vol. QE-18, pp. 582-595, 1982.

[15] G. Jacobsen, H. Olesen, and F. Birkedahl, "Current/frequency-modulation characteristics for directly optical frequency-modulated injection lasers at 830 nm and 1.3 μm," *Electron. Lett.*, vol. 18, pp. 874-876, 1982.

[16] D. W. Allan, "Statistics of atomic frequency standards," *Proc. IEEE*, vol. 54, pp. 221-230, 1966.

[17] I. Siio, M. Ohtsu, and T. Tako, "Development of the Allan variance real-time processor," (in Japanese), *Trans. IECE Japan*, vol. J64-C, pp. 204-208, 1981.

[18] J. Klapper and J. T. Frankle, *Phase-Locked and Frequency-Feedback Systems.* New York: Academic, 1972.

[19] K. Fukuoka, M. Ohtsu, and T. Tako, "Accurate wavelength measurements of the absorption lines in H_2O vapor by a 0.8 μm AlGaAs laser," *Japan. J. Appl. Phys.*, vol. 23, pp. L117-L120, 1984.

[20] M. Ohtsu, Y. Teramachi, Y. Otsuka, and A. Osaki, "Analyses of mode-hopping phenomena in an AlGaAs laser," *IEEE J. Quantum Electron.*, vol. QE-22, pp. 535-543, 1986.

[21] Y. Tohmori, K. Komori, S. Arai, and Y. Suematsu, "Low-threshold-current CW operation of 1.5 μm GaInAsP/InP bundle-integrated-guide distributed-Bragg-reflector (BIG-DBR) lasers," *Electron. Lett.*, vol. 21, pp. 743-745, 1985.

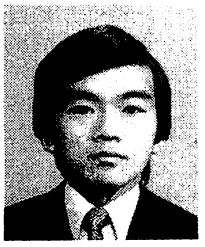

Katsuhiko Kuboki was born in Chiba, Japan, on November 28, 1960. He received the B.S. degree in computer engineering from the Tokyo Institute of Technology, Tokyo, Japan, in 1984.

Currently, he is a doctor-course student at the Graduate School at Nagatsuta, Tokyo Institute of Technology. He is interested in frequency control of semiconductor lasers for coherent optical communications.

Mr. Kuboki is a member of the Institute of Electronics and Communication Engineers of Japan and the Japan Society of Applied Physics.

Motoichi Ohtsu was born in Kanagawa, Japan, on October 5, 1950. He received the B.S., M.S., and Ph.D. degrees in electronics engineering from the Tokyo Institute of Technology, Tokyo, Japan, in 1973, 1975, and 1978, respectively.

At present he is an Associate Professor with the Graduate School at Nagatsuta, Tokyo Institute of Technology. He is interested in frequency control of lasers, analysis of dynamic behavior of lasers, and its applications to coherent optical measurements and optical communications.

Dr. Ohtsu is a member of the Institute of Electronics and Communication Engineers of Japan, the Institute of Electrical Engineers of Japan, the Japan Society of Applied Physics, and the Optical Society of America. In 1982 he was awarded a prize from the Japan Society of Applied Physics. He was also awarded Issac Koga gold medal from the International Union of Radio Science (URSI) in 1984.

談話室

光センサー・計測用の半導体レーザー

東工大国際交流センター　大津　元一
東工大精研　伊賀　健一

1984年秋の本会講演会で「光ファイバーセンサー」と題するシンポジウムが開かれ，多数の出席者を得て活発な討論が行なわれた．筆者らはこの中で，センサー用の半導体光源に関して，デバイス設計，さらに使用者の立場から解説を行なった．従来，この種の解説では，多くの場合，どちらか一方の立場に片寄りがちであったので，筆者らはそれを避けるよう努めた．シンポジウム終了後，多くの方々から，内容に関する問い合わせがあり，何らかの形で小文にまとめてはとのお勧めもいただいた．このような事情をもとに，今回本誌の編集委員の方々のお世話でその機会を得たので，本欄で簡単にまとめてみた．

センサー用光源としての半導体レーザー (LD) の内部構造に起因する特性上の違いは，計測システムの性能を左右する一要因であるが，実用上はむしろLDから出射した光の特性をいかに乱さずに使うかが重要である．このような使い方により，センサーに要求される性能（特に高感度，低ドリフト）をできるだけ向上させる必要がある．この点に注意してLDの性能を概観すると，次のようになろう．

（1） 光出力

実用化されている室温連続発振LDの光出力は 1〜10 mW であり，まだ低レベルである．これによりセンサーの感度が抑えられるので，現状では光伝送系に低損失光学素子を使うことが必要になる．デバイス設計の立場からは 200 mW の高出力化が試みられ[1]，アレイ化により 2.6 W のものが試作されている[2]．

（2） 光束発散角

1 μm×5 μm の楕円形近視野分布をもつLDからの出射光束は，回折により，15°〜30° の非対称発散角をもって広がり，光ファイバーへの集光効率低下，光束平行化困難，光束断面強度，位相分布の乱れを生ずる．後三者では光アイソレーター使用時のアイソレーション低下を招くことが多い．小型の反射防止膜付きコリメートレンズの使用が必要となるが，反射防止膜不十分のときにはレンズ面からの反射光により後述の戻り光誘起雑音が生じてしまう．発散角の小さいデバイスとして，面発光型のLDが試みられている[3]．

（3） 端面反射率

半導体材料の屈折率の値から決まるLDの端面反射率は，約30%である．このように反射率が低いことは外部光，特にLD自身からの戻り光が再入射されやすいことを意味し，それにより誘起される発振不安定（戻り光誘起雑音）[4]がセンサーの感度を低下させる．この発振不安定は，戻り光量が 0.01% 程度でも発生するので，戻り光の十分な抑圧が必要である．

このために用いられる光アイソレーターとしては，ファラデー効果を利用したものが一般的である．その材質は波長 0.7〜0.8 μm 帯では鉛ガラス，1.3〜1.6 μm 帯では YIG が使われる．両者とも約 −30 dB のアイソレーションが可能であるが，後者についてはファラデー回転角の温度依存性が問題である．すなわち，波長 1.15 μm，1.5 μm の光に対して，それはおのおの −0.26 deg/cm·K，+2.0 deg/cm·K の値をもつ．したがって，光アイソレーターの温度制御，または光アイソレーター用の材料開発が必要となる．戻り光の影響を低減するためにビデオディスクでは多モードLDが，非共振型ファイバージャイロでは高輝度発光ダイオードが用いられている．デバイス製作時，端面コーティングによって高反射率を得ることが行なわれており[5,6]，これは今後，より頻繁に使われる技術となろう．

（4） 温度による光出力の変動

素子温度の変化により，しきい値電流，量子効率が変化し，光出力も変動する．その値は約 −50 μW/K である．これは温度変動時のセンサーのドリフトを誘起するので，LD の温度制御，または外付け回路による自動出力制御(APC)が必要である．デバイス設計時に APC 機能のモノリシック化が望ましいが，その第一段階として出力モニター用のフォトダイオードがLDと同一基板上に作製されたものが研究されている．

（5） 温度による波長の変動

LD の波長は，温度により，約 +0.8 nm/K (GaAs 系，InP 系ともにこの程度の値) シフトする[7]．このことは光の可干渉性の低下，すなわちコヒーレントセンサーの感度低下，ドリフト増加につながる．解決法として温度制御，注入電流制御が行なわれる[8]．ただし，注入電流のみにより波長制御すると光出力ドリフトが増加するので，注意が必要である[9]．デバイス設計の際，自動周波数制御(AFC)機能のモノリシック化が望ましいが，波長基準の温度ドリフトの問題を解決しなければならない．この試みの一つとして，変調器をLD共振器内部に作りつけ，波長同調を注入電流調節により行なえるようにしたデバイスも試作されている[10]．

（6） モードホッピング

ファブリー・ペロー共振器型のLDでは，縦モード間でのホッピングが生ずる．ホッピングの頻度は 0.1〜10^7

回/秒の範囲であり，バイアス電流の増加とともに頻度は減少する[11]．さらにまたヒステリシス特性をも有し，これは超低頻度のモードホッピングと考えることができる．これらはすべて，LD の縦モードに混入する自然放出光のゆらぎが原因であることがわかってきた[11,12]．モードホッピングにより光強度雑音が増加し，センサーの感度が低下する．さらに波長の連続同調が困難になる．モードホッピングを抑えるには温度，電流を制御して単一縦モード発振動作を保持することが必要である．動的単一モード LD (DFB 型，DBR 型)[13]はモードホッピングのない LD として有望であり，センサー用の短波長帯 (1 μm 以下) での開発も望まれる．

(7)　波長のばらつき

市販の LD の素子間での波長のばらつきは，GaAs 系の場合，約 ±20 nm である．温度，電流によって波長同調ができるが，上記のモードホッピングも生じるなどのために，特定の波長値への同調が容易でないのが現状である．汚染気体の遠隔測定などの目的で，気体の吸収スペクトル線の一つに波長同調する際には，約0.001 nm の誤差内での確度が要求されるが，それが可能な市販の LD の歩留まりは 1/10～1/4 である．波長可変範囲を拡大する方法として，LD 共振器外部に回折格子を設ける方法があるが[14]，戻り光による発振不安定の可能性があり，まだ信頼性に難点を有する．また，短波長，低出力LDの場合，波長値の経時変化が顕著である．この原因としては，電極ボンディング層の酸化による熱抵抗の経時変化，または共振器端面でのキャリアの非放射再結合による熱効果などが考えられるが[15]，この特性の定量的把握，デバイス設計時の対策も重要である．

(8)　発振スペクトル幅

コヒーレント光源としての LD の性能を左右するパラメーターが発振スペクトル幅であり，10～100 MHz の値が報告されている．これに対しコヒーレントヘテロダイン光通信では 1 MHz 以下，共振型のファイバージャイロ，ドップラー流速計では 0.1 MHz 以下の値が要求されており，その要求を満たすためにスペクトル幅の狭帯域化が必要である．コヒーレントセンサーでは，スペクトル幅が広いと，可干渉低下による感度低下を招くので，この狭帯域化は必須技術である．

その一例として，LD 共振器外部に鏡を設置することにより，共振器Q値を増大させる方法があり，1 kHz の値を得た例がある[16]．同様に LD にファイバーを接続し，ファイバーの他方の端面を外部鏡として用い光を帰還させる方法もあり，30 kHz の値を得た例もある[17]．これらの方法の難点は，戻り光により発振不安定を生じ，スペクトル幅がかえって広くなる可能性を有すること，装置が大型化すること，電流による直接変調効率が著しく減少すること，などである．このような難点をもたない方法として，広帯域の注入電流制御により FM 雑音を抑圧して，狭帯域化を実現することが試みられている[18,19]．これにより，スペクトル幅 330 kHz が実現されている[20]．原理的には，この方法により，1 kHz～100 Hz まで狭くすることが可能である[20]．

(9)　耐電気的サージと寿命

LD は，約 500 V 以下の電気的サージには耐えうるとされている．しかし実際には，波長の経時変化なども含めると，センサー用光源としての LD の実働可能寿命は 10^3～10^4 時間程度であり，実用時の信頼性の問題を含む．低雑音電流源を使用したり，またデバイス設計の面では結晶性，接合部強化が必要である．

以上，主に LD の特性と問題点，その解決法について述べた．入手可能なデバイスを使用者側が工夫して使うという現在の状況では，LD の性能はセンサー用光源として，まだ十分高い信頼性を有しているとはいい難い．光センシングに適した LD のデバイス設計が，他の光通信・光機器などの産業規模で発展中の光エレクトロニクス分野との共通性があるとすれば，高性能デバイス生産も可能となるかもしれない．そうでなければ，LD の根本的設計をするくらいの勇気が，光センシング研究者にも必要であろう．

文　献

1) K. Hamada, M. Wada, S. Shimizu, M. Kume, A. Yoshida, K. Itoh and G. Kano: *Proc. IEEE Semiconductor Laser Conf.* (1984) C-1.
2) D. R. Scifres, C. Lindstrom, R. D. Buhnham, W. Streifer and T. Paoli: Electron. Lett. **19** (1983) 171.
3) H. Soda, Y. Motegi and K. Iga: IEEE J. Quantum Electron. **QE-19** (1983) 1035.
4) R. Lang and K. Kobayashi: IEEE J. Quantum Electron. **QE-16** (1980) 347.
5) M. Ettenberg: Appl. Phys. Lett. **32** (1978) 724.
6) M. Ohtsu, H. Kotani and H. Tagawa: Jpn. J. Appl. Phys. **22** (1983) 815.
7) M. Ohtsu, H. Tagawa and H. Kotani: Jpn. J. Appl. Phys. **22** (1983) 1876.
8) M. Ohtsu, H. Fukada, T. Tako and H. Tsuchida: Jpn. J. Appl. Phys. **22** (1983) 1157.
9) H. Tsuchida and T. Tako: Jpn. J. Appl. Phys. **22** (1983) 1152.
10) Y. Tohmori, Y. Suematsu, H. Tsushima and S. Arai: Electron. Lett. **19** (1983) 656.
11) 大塚祥広，大崎昭雄，大津元一，寺町康昌：電子通信学会技術研究報告 OQE 84-132 (1985).
12) M. Ohtsu, Y. Otsuka and Y. Teramachi: Appl. Phys. Lett. **46** (1985) 108.

13) K. Utaka, K. Kobayashi, K. Kishino and Y. Suematsu: Electron. Lett. **16** (1980) 455.
14) J. A. Rossi, S. R. Chinn and H. Heckscher: Appl. Phys. Lett. **23** (1973) 25.
15) F. Fabre and D. Le Guen: Electron. Lett. **19** (1983) 663.
16) R. Wyatt: *Proc. 8th Conf. Optical Fiber Communication, San Diego, 1985*, TuP 2.
17) F. Fabre, D. Le Guen and J. C. Simon: IEEE J. Quantum Electron. **QE-18** (1982) 1712.
18) S. Saito, O. Nilsson and Y. Yamamoto: Appl. Phys. Lett. **46** (1985) 3.
19) M. Ohtsu and S. Kotajima: Jpn. J. Appl. Phys. **24** (1985) L 256.
20) 古田島真一，大津元一：電子通信学会技術研究報告 OQE 84-130 (1985).

解説B

半導体レーザのコヒーレンスの向上技術

大津　元一

大津元一：正員　東京工業大学大学院総合理工学研究科
Techniques for Improving Coherence in Semiconductor Lasers. By Motoichi OHTSU, Member (The Graduate School at Nagatsuta, Tokyo Institute of Technology, Yokohama-shi).

1. まえがき

レーザのもつ潜在的な特長の一つにその時間的コヒーレンス（Coherence）の高さ，つまり，放出される光波の位相がそろい，正弦波に近いこと，があり，この特長を引き出す試みが 1960 年のレーザ発明以来継続して行われている[1]~[3]．

更にここ数年来，コヒーレント光通信[4],[5]，コヒーレント光計測などへの応用上，半導体レーザのコヒーレンスを向上させる必要が生じ，その努力がなされてきている．しかし半導体レーザは他種レーザと比べ，構造，発振機構などに関し独特の性質を有するためにそのコヒーレンスを向上させる技術について十分整理されているとは言い難い．そこで本稿ではこれらについての解説を試みる．

2. コヒーレンス向上のための基礎概念

以下の議論では半導体レーザは縦，横モードに関し単一モード発振している場合を考える．

半導体レーザの周波数揺らぎの基本的な内部要因は自然放出，キャリヤ密度変動である．AlGaAs レーザの周波数揺らぎのパワースペクトル密度を図 1 に示す[6]．このほか，外来要因として周囲温度揺らぎなどがあるが，それらを含めて図 2 には AlGaAs レーザの公称周波数値で規格化した周波数揺らぎの標準偏差値を示す[7]．こ

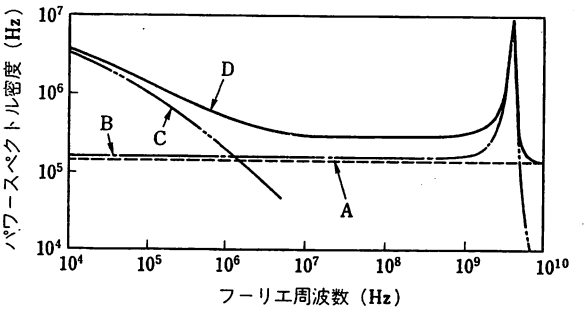

A：自然放出　B：キャリヤ密度揺らぎ　C：電流揺らぎ　D：総和

図 1　AlGaAs レーザの周波数揺らぎのパワースペクトル密度の例[6]

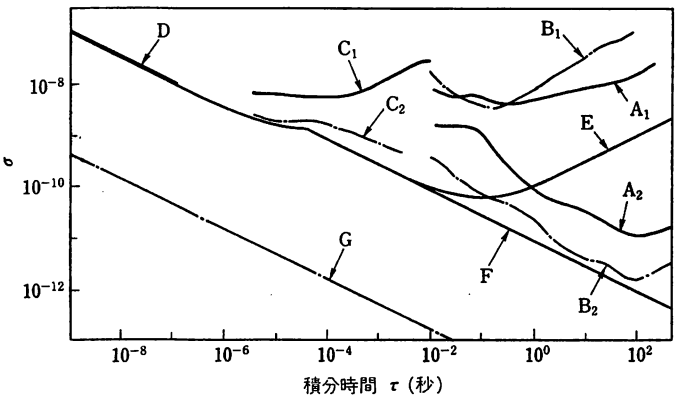

A_1, B_1, C_1, D：フリーランニング時の測定値．A_2, B_2, C_3：周波数制御時の測定値．E：フリーランニング時の理論限界値．F：自然放出，キャリヤ密度変動の寄与の理論値．G：光検出器ショット雑音により制限される理論値．

図 2　AlGaAs レーザの周波数揺らぎの Allan 分散

れは周波数安定度を評価するときにしばしば使われる尺度で，Allan 分散 σ^2[8] の平方根である．横軸の τ は測定に要する時間，すなわち積分時間である．図中の曲線 A_1, B_1, C_1, D に示すようにフリーランニング時の σ の値は 10^{-8} 以上である．これがレーザ発振スペクトルの中心周波数の揺らぎの大きさと考えることができる．

また，発振スペクトル幅の値は自然放出，キャリヤ密度変動によって決まり，通常数 MHz～数 100 MHz である．これは図1の周波数揺らぎのパワースペクトル密度のうちフーリエ周波数約 100 MHz 以下の範囲の積分値，いいかえると図2の σ のうちの積分時間約 10 ns 以上の範囲の値が主な寄与をする．

一方，半導体レーザは共振器寸法が小さいので共振器形状，更に化合物半導体のモル比などのわずかなばらつきにより各素子の発振特性および周波数の再現性が制限される．更には共振器内の大きな注入電流密度，高い光電界強度のために発振スペクトルの経時変化も大きく，例えば AlGaAs レーザのスペクトル中心周波数は数 MHz/h の青方偏移を示すことが確認されている[9]．

以上のようにスペクトル中心周波数の揺らぎとその再現性，およびスペクトル幅がコヒーレンスの高さを議論するときに問題となる量であるが，従来のこれらの値はコヒーレント光通信，コヒーレント光計測などの目的には不十分である．例えば σ の値は約 10^{-9} 以下，スペクトル幅は約 100 kHz 以下が要求されている．これを実現するには新形デバイスを製作すること，光学的，電気的負帰還により特性を改善すること，の3方法が考えられるが，安定性，精度の点で現在のところ電気的負帰還が最も優れている．そこで本章および **3.** では主にこの方法について触れ，光学的負帰還は **3.** で必要に応じて電気的負帰還と比較しながら述べる．新形デバイスについては **4.** で述べる．

電気的負帰還のための外付け電子回路による自動制御系の構成を図3に示す．同図に示すようにレーザ周波数揺らぎに比例した光検出器出力に応じて半導体レーザの動作パラメータを制御して周波数を変化させ，

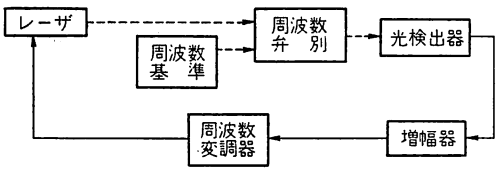

図 3　電気的負帰還のための自動制御

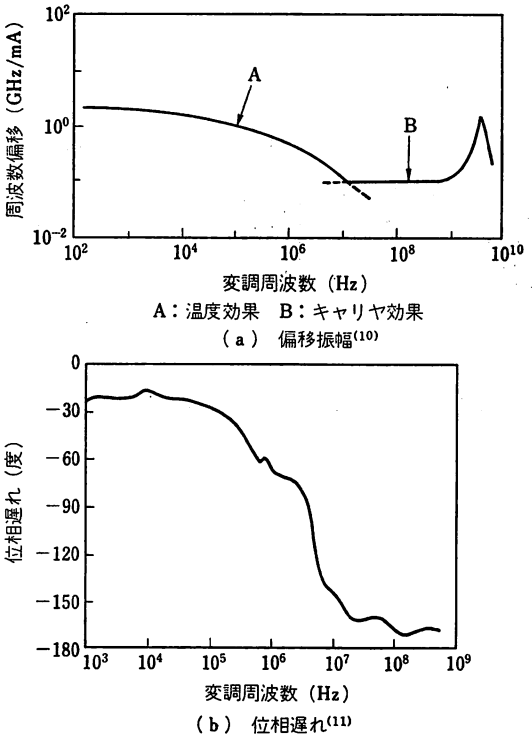

図 4　交流注入電流による AlGaAs レーザの周波数変調特性の例

周波数揺らぎを打ち消す必要がある．このためには温度，または注入電流を調節してレーザ共振器屈折率，長さを変化させ，レーザ共振器の共振周波数を変調すればよい．例えば温度1度当り約 10 GHz，直流注入電流 1 mA 当り約 1 GHz の赤方偏移が得られる．但し温度変化の時定数は長いので注入電流を調節する方が広帯域制御のためには有利である．注入電流を変化させると共振器温度の変化，およびキャリヤ密度変化が生じ共振周波数が変化する．

この場合図4（a）の注入電流による周波数変調特性に見られるように，前者は遮断周波数が数 MHz の高域遮断特性，後者は緩和振動周波数を遮断周波数とする高域遮断特性を示す[10]．図4（b）には応答の位相特性を示すが[11]，温度効果，キャリヤ効果とも位相遅れ特性を有する．周波数制御用の外付け電子回路を設計するには図4の特性をもとにすればよい．

さて，図3のような系で周波数揺らぎを測定でき，更にこれを補償するために周波数を負帰還制御できたとすると，周波数揺らぎは制御系の雑音の大きさによって制限される値まで小さくなる[12]．そこで，制御系

の雑音の基本的要因，すなわち光検出器のショット雑音で制限されるスペクトル中心周波数の残留揺らぎを推定すると図2の曲線Gに示すように $\sigma=1.7\times10^{-14}\tau^{-1/2}$ となり[7]，水素メーザのそれと同程度の小さい値であることがわかる．

同様に光検出器のショット雑音で制限されるスペクトル幅の狭窄(さく)化の限界を推定するとフリーランニング時の約 10^{-6}，すなわち数 Hz になることが確認されている[18]．これらの推定結果により，半導体レーザが極めてコヒーレンスの高い発振器になりうる能力を持っていることが結論される．

3. コヒーレンス向上技術の実際

応用面からの要求，および従来のマイクロ波発振器用技術と比較すると，半導体レーザのコヒーレンスを向上させるためには以下の節で述べる5項目を行う必要があると思われる．

3.1 スペクトル中心周波数安定度の向上

この節では周波数揺らぎのうちフーリエ周波数約1MHz以下の成分を抑圧することによりスペクトル中心周波数の安定度を向上させることを考える．フリーランニング時，このような低フーリエ周波数範囲のレーザ周波数ドリフトの主要因はレーザの温度変動である．これを抑圧するには低周波数領域で高利得の増幅器，すなわち積分増幅器を使うことが有効である．一般には更に補助的に比例，微分増幅器も付加しPID制御を施す．

使用できる周波数基準のうち簡単なものは安定な外部共振器，例えばファブリーペロー干渉計である．しかし干渉計の周囲温度が変化すると基準周波数としての干渉計共振周波数自身がドリフトする．但し，フーリエ周波数が約 100 Hz 以上（積分時間約 10 ms 以下）ではこのドリフトの効果は小さいので，石英ブロックを用いた簡単な干渉計が十分使用可能である．図2の曲線 C_2 はこのような干渉計により得られた結果である．より高度の安定度を得るには，より安定な周波数基準を使う必要がある．それには安定な原子，分子の共鳴スペクトルが使える．

例えば波長 0.7～1.6 μm の半導体レーザに対しては H_2O, NH_3 などの有機分子の振動回転準位間の遷移の結合調または高調波の吸収スペクトル[14],[15]，更にこれらよりも周波数弁別感度が高いものとして波長 0.8 μm 帯にある Cs, Rb などのアルカリ金属蒸気の電子遷移の共鳴線が使える[16],[17]．図2の曲線 A_2, B_2 はそれぞれ H_2O, Rb を周波数基準に用いた結果である．このうち特に曲線 B_2 は積分時間 100 秒において $\sigma=1.4\times10^{-12}$ に達しており，温度変動によるドリフトが十分抑圧されたことがわかる．波長 1.5 μm InGaAsP レーザに対しては H_2O, NH_3 が周波数基準として使われており図2の曲線 A_2 と同程度の安定度が得られている[14],[18]．

3.2 スペクトル中心周波数の再現性の向上

温度変動による周波数ドリフトを抑圧するには特に積分増幅器の利得を大きくする必要があるが，実際に得られる利得には上限があるので制御可能なフーリエ周波数の範囲は通常約 1 mHz 以上に限られる．すなわち現状では積分時間1,000秒以上の長期変動は抑圧不十分で，これが周波数再現性を制限する原因の一つになる．今後超低フーリエ周波数領域での制御利得の大きい電子回路の開発が必要である．

一方，長期変動として 2. で述べたような青方偏移が観測されているがこれは電極ボンディング層の酸化による熱抵抗の経時的減少などによる熱効果であることが指摘されている[19]．従って再現性を向上させるには熱抵抗の小さいデバイスの製作およびその経時的な安定化が必要である．これに加え，デバイス加工精度の向上による発振特性の素子間ばらつきの減少，スクリーニングなどが重要である．

3.3 スペクトル幅の狭窄化

レーザの発振スペクトル幅を狭くするには $f \leqq \Delta\nu_{FR}$ なるフーリエ周波数 f の範囲の周波数揺らぎを抑圧する必要がある．ここで $\Delta\nu_{FR}$ はフリーランニング時のスペクトル幅である．しかし当初は各種の要因により周波数揺らぎが大きく，スペクトル幅が約 100 MHz まで広がっていたので，これに合せ約 100 MHz の広帯域周波数制御が必要であった．これは技術的に困難を伴うので従来は電気的な負帰還制御ではなく，光学的方法を用いていた．

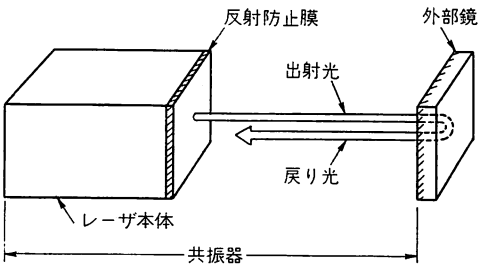

図5　スペクトル幅狭窄化のための外部鏡設置の構成図

これはスペクトル幅を決定する要因のうち，自然放出により発生した光子がランダムにレーザモードに混入してくる頻度を少なくすること，すなわちレーザ共振器内の光子寿命を長くすることにより行われる．そのためには図5のようにレーザの外部に鏡を置いてこれをレーザ共振器の一方の高反射率端面として使い，これからの反射光をレーザに再入射させ光子寿命を長くする．これによりスペクトル幅を 10 kHz まで狭くした例が報告されている[20]．同様にレーザ端面にファイバを接続し，ファイバの自由端面を反射鏡として用い，長い共振器を作って 30 kHz を得た例がある[21]．以上の光学的方法では光子寿命を長くしているのみであるので，位相のドリフトを補償するように負帰還を施しているわけではない．

従って動作パラメータの変化に応じた不安定性を含む．例えば反射鏡の振動などにより戻り光の位相が変化すると光子寿命が変化し，従ってスペクトル幅は変動する．更にレーザ共振器の大型化，直接周波数変調効率の低下，などの問題を含む．しかし，これは簡便な方法なので従来頻繁に使われている．

一方，ここ数年のレーザ素子製造技術の進歩により十分に単一モード性が向上し，品質の優れたレーザが現れてきた．このためにフリーランニング時のスペクトル幅も数 10 MHz 以内となり，電気的な負帰還制御に必要な制御帯域に対する要求が緩和されてきた．これに伴い最近になって光学的方法のもつ問題を含まない方法として電気的負帰還が試みられるようになった[22]．原理的には **4.1** の中心周波数安定化と同じであるが，制御帯域はその場合より広く，数 10 MHz である．このため制御ループを短くしたり，更には図4(b) の位相遅れを補償する制御系を使用する．周波数基準と弁別にはファブリーペロー干渉計[22]~[24] や他のより高いコヒーレンスを有するレーザとのヘテロダイン[25]などが使われている．既存の実験装置で 10 kHz まで狭くなることが検証されている[18]．

3.4 コヒーレンスのより高いレーザへの周波数追随

3.3 までの方法によりコヒーレンスの高いレーザができれば，これをマスターレーザとして用い，この高コヒーレンスを他のレーザ，すなわちスレーブレーザに移乗させること，いいかえればスレーブレーザの周波数をマスターレーザのそれに追随させること，ができる．これはコヒーレント光通信におけるヘテロダイン，ホモダイン検波，光直接増幅，更にコヒーレント光計測において有用な技術である．これはマイクロ波に対しては確立された技術である．

これを実現するための一つとして注入同期の方法がある[26]．すなわち，マスターレーザの光をスレーブレーザに注入するとスレーブレーザの周波数はマスターレーザのそれに引き込まれる．これが注入同期であり，この状態ではスレーブレーザの周波数はマスターレーザのそれに忠実に追随する．

注入同期が成立するためにはフリーランニング時のスレーブレーザ周波数はマスターレーザ周波数のまわりの一定の範囲内になければならないが，その範囲は両レーザのパワー比に依存する．従ってレーザパワーに対する条件が要求され系が複雑になる．

これより安定で簡潔な方法として周波数オフセットロック法とよばれる電気的方法が試みられている[27]．これはマスターレーザとスレーブレーザとのヘテロダインによるビート信号の位相または周波数を，別に用意した局部発振器のマイクロ波のそれと一致するようにスレーブレーザの注入電流を負帰還制御する方法である．これによるとビート周波数の揺らぎをマスターレーザのそれ以下に抑圧することができ，周波数の追随精度が高い．これは FSK ヘテロダイン検波のためにも試みられている[28],[29]．

3.5 周波数の広帯域可変

周波数を広帯域にわたって可変にするために従来採用されている簡便な方法は図5中の外部鏡のかわりに回折格子を置き，その面を回転させることにより発振縦モードを選択するものである．周波数の微調整をするためにレーザと回折格子の間にファブリーペローエタロンを設置することもある．この方法により波長 1.5 μm InGaAsP レーザを波長範囲 0.5 nm (周波数範囲 67 GHz) にわたって連続可変にした例がある[30]．これは気体，色素レーザなどにも用いられている一般的で簡便な光学的方法であるが，**3.3** に述べたように図5の方法に付随する問題がこの場合にもあてはまる．

このような問題点を解決しうる方法として **3.4** の電気的方法すなわち周波数オフセットロック法を流用することが考えられる．すなわち，スレーブレーザをマスターレーザに周波数オフセットロックしたまま局部発振器のマイクロ波周波数を掃引するとスレーブレーザの周波数もそれに追随して安定に連続掃引される．現在までに可変範囲 12 GHz が得られている[31]．この範囲は使用したレーザのモードホッピング特性に

より制限されているが，最近ではフリーランニング時，約 1 THz の範囲にわたって周波数連続可変の波長 1.5 μm InGaAsP レーザも開発されており[82]，これらを使えば，周波数オフセットロック法による周波数連続可変範囲が更に拡大するであろう．

4. コヒーレンス向上のための新形レーザ設計

高コヒーレンスを得るにはデバイス作製の段階で低雑音，単一モード発振するレーザを実現することが望ましいが，これに関しては DFB, DBR 形[83]，量子井戸構造を採り入れる方法[84]，などが試みられている．

しかしながらデバイス構造の工夫のみでは必ずしも十分ではないので，将来的にも外付け素子を用いて光学的，または電気的な負帰還を併用することが必要であろう．これは電子回路においてトランジスタに外付け回路素子を使って安定な動作を引き出すのと同様，半導体能動素子には不可欠の手法といえる．そうであるならば負帰還を施すのに適した構造のレーザを開発するのが望ましい．例えば図5の方式にならい，スペクトル幅狭窄化のためにレーザと同一基板上に外部導波路を作製した例がある[85],[86]．これは光学的方法によるコヒーレンス向上を推進するためのデバイス面からのアプローチといえよう．

一方，電気的負帰還を施すのに適したデバイス構造としては図3の中のブロックの一部をレーザと共に集積化するものである．このような例として，レーザ共振器内に位相変調器を作りつけた二分割電極形 DBR レーザ[87]，DFB, DBR 両者の構造を組み合せた二分割電極形レーザ[88]が開発されている．更に，二分割電極形 DFB レーザでは変調器に流す電流を制御することにより，図4に見られる温度効果による不均一な周波数変調特性を補正している[89]．このように共振器内に位相変調器が組み込まれると図4のような周波数変調特性を電気的負帰還に適したように変形できるので都合がよい．

位相変調器が共振器内に設置されていると実際には共振器損失の変化に伴う発振パワーの変化を誘起するので制御系設計上不都合が生ずることがある．

これを避けるには変調器はレーザ共振器外に集積化されるべきであり，実際に気体，色素レーザのようにスペクトル幅 1 Hz 以内[40]の高コヒーレンスを実現しているレーザではすでに外部変調器使用への方式移行が完了している．

以上のほかに図3中の光検出器および増幅器をレーザと集積化することも可能で[41]，将来は図3のかなりの部分が集積化された機能レーザの実現が期待される．

5. 高コヒーレンス半導体レーザの応用

半導体レーザは小形，低消費電力，長寿命であるため工業的応用には極めて適しているが，これに加えそのコヒーレンスが十分高い場合には以下に列挙するような分野への応用が可能になるであろう：コヒーレント光通信（光ファイバ伝送[4],[5]，および衛星間通信[42]）．ドップラー流速計による血流速度測定や振動面の振動速度測定[43]．ホログラフィー．1 m～1 km の範囲の距離測定用の測距儀．半導体材料を加工する際の露光用マスクの位置決め．慣性航法用ファイバジャイロ[44]．地震予知，地球の極運動測定，惑星探査用高感度ファイバジャイロ[45]．大気中の汚染気体測定およびレーザレーダ[46]．マイクロ波領域の高精度セシウム，ルビジウム原子発振器の光励起[9]．計測用波長標準．長さ標準．

6. おわりに

半導体レーザのコヒーレンスを向上させる技術には以上のように他種レーザ，マイクロ波発振器に対して確立した電気的負帰還の手法が採用されているが，それは現在のところこの方法が他に比べ最も信頼性が高いからである．この手法の利点を更に生かすにはそれに適した構造のデバイスの開発が重要であろう．

また，レーザの発振機構に含まれる非線形光学効果を利用した光学的方法は物理的には興味深いが信頼性と精度に問題がある．しかし今後，発振機構のより詳しい研究，および新機能デバイスの開発によりレーザ特有の光学的手法が出現することの期待も捨て切れない．

更に高コヒーレンスを十分に生かすには光アイソレータを始めとする周辺光素子が不可欠で，これらの性能向上と低価格化が望まれる．

文　献

（1）大津元一：“レーザと原子時計―マイクロ波と光を結ぶ新技術―”，オーム社（昭 61）．

（2）M. Ohtsu, S. Katsuragi and T. Tako: “Performances of a frequensy offset locked He-Xe laser system at 3.51 μm”, IEEE J. Quantum Electron., **QE-17**, 6, pp. 1100-1106 (June 1981).

(3) A. Brillet and P. Cerez : "Laser frequency stabilization by saturated absorption", J. de Physique, **42**, 12, pp. 73-82 (Dec. 1981).
(4) Y. Yamamoto : "Receiver performance evaluation of various digital optical modulation-demodulation systems in the 0.5-10 μm wavelength region", IEEE J. Quantum Electron., **QE-16**, 11, pp. 1251-1259 (Nov. 1980).
(5) T. Okishi and K. Kikuchi : "Heterodyne-type optical fiber communication", J. Opt. Commun., **2**, 3, pp. 82-88 (Sept. 1981).
(6) Y. Yamamoto, S. Saito and T. Mukai : "AM and FM quantum noise in semiconductor lasers-Part II : Comparison of theoretical and experimental results for AlGaAs lasers", IEEE J. Quantum Electron., **QE-19**, 1, pp. 47-58 (Jan. 1983).
(7) M. Ohtsu, H. Fukuda, T. Tako and H. Tsuchida : "Estimation of the ultimate frequency stability of semiconductor lasers", Jpn. J. Appl. Phys., **22**, 7, pp. 1157-1166 (July 1983).
(8) D. Allan : "Statistics of atomic frequency standards", Proc. IEEE, **54**, 2, pp. 221-230 (Feb. 1966).
(9) M. Ohtsu, M. Hashimoto and H. Ozawa : "A Highly Stabilized Semiconductor Laser and Its Application to Optically Pumped Rb Atomic Clock", Proc. 39 th Annual Symposium on Frequency Control, IEEE Catalog No. 85 CH 2186-5, Philadelphia, pp. 43-53 (May 1985).
(10) S. Kobayashi, Y. Yamamoto, M. Ito and T. Kimura : "Direct frequency modulation in AlGaAs semiconductor lasers", IEEE J. Quantum Electron., **QE-18**, 4, pp. 582-595 (April 1982).
(11) G. Jacobsen, H. Olesen and F. Birkedahl : "Currents/frequency-moduration characteristics for directly optical frequency-modulated injection lasers at 830 nm and 1.3 μm", Electron. Lett., **18**, 20, pp. 874-876 (Sept. 1982).
(12) Y. Yamamoto, O. Nilsson and S. Saito : "Theory of a negative frequency feedback semiconductor laser", IEEE J. Quantum Electron., **QE-21**, 12, pp. 1919-1928 (Dec. 1985).
(13) 田淵 昇, 尾内敏彦, 大津元一 : "半導体レーザの超高コヒーレンス化 (I)—線幅の狭帯域化", 第33回応用物理関係連合講演会予稿, 3 pK 11, (昭 61-04).
(14) M. Ohtsu, H. Kotani and H. Tagawa : "Spectral measurements of NH_3 and H_2O for pollutant gas monitoring by 1.5 μm InGaAsP/InP lasers", Jpn. J. Appl. Phys., **22**, 10, pp. 1553-1557 (Oct. 1983).
(15) K. Fukuoka, M. Ohtsu and T. Tako : "Accurate wavelength measurements of the absorption lines in H 20 vapor by a 0.8 μm AlGaAs laser", Jpn. J. Appl. Phys., **23**, 2, pp. L 117-L 120 (Feb. 1984).
(16) T. Yabuzaki, A. Ibaragi, H. Hori, M. Kitano and T. Ogawa : "Frequency-locking of a GaAlAs laser to a Doppler-free spectrum of the Cs-D_2 line", Jpn. J. Appl. Phys., **20**, 6, pp. L 451-L 454 (June 1981).
(17) H. Tsuchida, M. Ohtsu, T. Tako, N. Kuramochi and N. Oura : "Frequency stabilization of AlGaAs semiconductor laser based on the ^{85}Rb-D_2 line", Jpn. J. Appl. Phys., **21**, 9, pp. L 561-L 563 (Sept. 1982).
(18) T. Yanagawa, S. Saito and Y. Yamamoto : "Frequency stabilization of 1.5 μm InGaAsP distributed feedback laser to NH_3 absorption lines", Appl. Phys. Lett., **45**, 8, pp. 826-828 (Oct. 1984).
(19) F. Favre and D. Le Guen : "Emission frequency stability in single-mode-fibre optical feedback controlled semiconductor lasers", Electron. Lett., **19**, 17, pp. 663-665 (Aug. 1983).
(20) R. Wyatt and W.J. Devlin : "10 kHz linewidth 1.5 μm InGaAsP external cavity laser with 55 nm tuning range", Electron., Lett., **19**, 3, pp. 110-112 (Feb. 1983).
(21) F. Favre, D. Le. Guen and J.C. Simon : "Optical feedback effects upon laser diode oscillation field spectrum", IEEE J. Quantum Electron., **QE-18**, 10, pp. 1712-1717 (Oct. 1982).
(22) 古田島真一, 大津元一 : "1.5 μm InGaAsP レーザのスペクトル幅測定とその狭帯域化", 第 45 回応用物理学会学術講演会予稿, 13 aR 9, (昭 59-09).
(23) M. Ohtsu and S. Kotajima : "Linewidth reduction of a 1.5 μm InGaAsP laser by electrical feedack", Jpn. J. Appl. Phys., **24**, 4, pp. L 256-L 258 (April 1985).
(24) M. Ohtsu and S. Kotajima : "Linewidth reduction of a semiconductor laser by electrical feedback", IEEE J. Quantum Electron., **QE-21**, 12, pp. 1905-1912 (Dec. 1985).
(25) S. Saito, O. Nilsson, and Y. Yamamoto : "Frequency modulation noise and linewidth reduction in a semiconductor laser by means of negative frequency feedback technique", Appl. Phys. Lett., **46**, 1, pp. 3-5 (Jan. 1985).
(26) S. Kobayashi and T. Kimura : "Injection locking in AlGaAs semiconductor laser", IEEE J. Quantum Electron., **QE-17**, 5, pp.681-689 (May 1981).
(27) 久保木勝彦, 大津元一 : "半導体レーザの周波数オフセット・ロックに関する研究", 信学技報, **MW 85-29** (1985-06).
(28) K. Emura, M. Shikada, S. Fujita, I. Mito, H. Hanmou and K. Minemura : "Novel optical FSK heterodyne single filter detection system using a directly modulated DFB-laser diode", Electron. Lett., **20**, 24, pp. 1022-1023 (Nov. 1984).
(29) F. Favre and D. Le Guen : "Spectral narrowing by optical feedback", Proc. Int. Conf. on Lasers '83, pp. 79-84, ed. R.C. Powell, STS Press, McLean (Dec. 1983).
(30) K.H. Cameron, M.R. Matthews, T.G. Hodgkinson and W.J. Devlin : "Frequency-stable packaged 20-kHz linewidth 1.5-μm InGaAsP external cavity laser used in an experimental heterodyne optical fiber system", Technical Digest of Conference on Lasers and Electro-Optics, TUC 5, Baltimore, USA (May 1985).

(31) 久保木勝彦，瀬上雅博，大津元一："半導体レーザの超高コヒーレンス化（II）—周波数追随と広帯域可変—"，第 33 回応用物理学関係連合講演会予稿，3 pK 12（昭 61-04）.
(32) B. Broberg, F. Koyama, Y. Tohmori and Y. Suematsu : "1.53 μm DFB lasers by mass transport", Electron. Lett., **20**, 17, pp. 692-694 (Aug. 1984).
(33) 末松安晴編著："半導体レーザと光集積回路"，オーム社（昭 59）.
(34) Y. Arakawa and A. Yariv : "Enhanced modulation performance and reduced quantum noise in quantum well lasers", Technical Digest of Conference on Lasers and Electro-Optics, WH 5, Baltimore, USA (May 1985).
(35) T. Fujita, J. Ohya, K. Matsuda, M. Ishino, H. Sato and H. Serizawa : "Narrow spectral linewidth characteristics of monolithic integrated-passive-cavity InGaAsP/InP semiconductor lasers", Electron. Lett., **21**, 9, pp. 374-376 (April 1985).
(36) 村田　茂，水戸郁夫："外部共振器をモノリシック集積化した DFB レーザ"，第 46 回応用物理学会学術講演会予稿，1 pM 6（昭 60-10）.
(37) T. Tohmori, Y. Suematsu, H. Tsushima and S. Arai : "Wavelength tuning of GaInAsP/InP integrated laser with butt-jointed built-in distributed Bragg reflector", Electron. Lett., **19**, 17, pp. 656-657 (Aug. 1983).
(38) L.D. Westbrook, A.W. Nelson, P.J. Fiddyment and J.V. Collins : "Monolithic 1.5 μm hybrid DFB/DBR lasers with 5 nm tuning range", Electron. Lett., **20**, 23, pp. 957-959 (Nov. 1984).
(39) Y. Yamazaki, K. Emura, M. Shikada, M. Yamaguchi and I. Mito : "Realisation of flat FM response by directly modulating a phase tunable DFB laser diode", Electron. Lett., **21**, 7, pp. 283-285 (March 1985).
(40) J.L. Hall, D. Hils, C. Salomon and M. Rayman: "Stable lasers : progress and applications", Technical Digest of Conference on Lasers and Electro-Optics, FM 3, Baltimore, USA (May 1985).
(41) K. Iga and B.I. Miller : "GaInAsP/InP laser with monolithically integrated monitoring detector", Electron. Lett., **16**, 9, pp. 342-343 (April 1980).
(42) V.W.S. Chan, L.L. Jeromin and J.E. Kaufmann: "Heterodyne lasercom systems using GaAs lasers for ISL application", IEEE Int. Conference of Communications, E 1-5, Boston, USA (1983).
(43) F. Durnst, A. Melling and J.H. Whitelaw : "Principle and Practice of Laser-Doppler Anemometry", Academic Press, New York (1976).
(44) T.G. Giallorenzi, J.A. Bucaro, A. Dandridge, G.H. Sigel Jr., J.H. Cole, S.C. Rashleigh and R.C. Priest : "Optical fiber sensor technology", IEEE J. Quantum Electron., **QE-18**, 4, pp. 626-665 (April 1982).
(45) 荒木聡彦，大津元一："地震検出・予知用リング Fabry-Perot 共振器形ファイバジャイロスコープ"，信学技報，**OQE 85**-170 (1986-03).
(46) N. Takeuchi, H. Baba, K. Sakurai and T. Ueno: "Diode-laser random-modulation cw lidar", Appl. Opt., **25**, 1, pp. 63-67 (Jan. 1986).

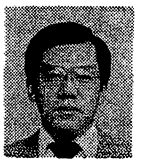

大津　元一（正員）
昭 48 東工大・工・電子卒．昭 53 同大学院博士課程了．同年東工大助手．昭 57 同大助教授．レーザ制御，レーザ計測に従事．工博．57 年度応用物理学会賞（B），59 年電波科学国際連合（URSI）より I. Koga Gold Medal 受賞．著書「レーザと原子時計」など

Conference on Lasers and Electro-Optics (CLEO'86), June 1986, San Francisco, CA, WB4, p.154

WB4 Demonstration and application of frequency stabilization and linewidth reduction in semiconductor lasers

MOTOICHI OHTSU, Tokyo Institute of Technology, Graduate School at Nagatsuta, 4259 Nagatsuta, Midori-ku, Yokohama, Kanagawa 227, Japan.

We report on the progress in improving the coherence of semiconductor lasers and demonstrate applications of these highly coherent lasers.

The following must be simultaneously improved to achieve high coherence in semiconductor lasers: (1) linewidth narrowing of field spectrum; (2) center frequency stabilization of field spectrum; (3) frequency tracking to another coherent laser; (4) wideband frequency tunability; (5) frequency reproducibility. We proposed that electrical feedback is effective for these improvements,[1,2] whose electronic components may be integrated with lasers in the future.

Stable linewidth narrowing was carried out for a 1.5-μm DFB laser by electrical feedback without changing the laser cavity configuration. The minimum linewidth obtained so far was 200 kHz, which was 25 times narrower than in a free-running laser. This linewidth was confirmed to be narrower than the one limited by quantum noise, which is consistent with theory.[3] A 10-kHz linewidth is expected by improving the postdetector amplifier of our present experimental setup; our estimate showed that the theoretical limit is 100 Hz.

Stability of the center frequency of the field spectrum was improved to 1×10^{-12} by employing absorption spectra in alkali vapor or organic molecules as a frequency reference,[4,5] which was as high as a quantum noise level. A theoretical estimate showed that a 1×10^{-15} stability can be expected, which is limited by the detector shot noise in the feedback loop.[4]

Frequency tracking of a slave laser to a highly coherent master laser was achieved by reducing PM noise in the beat signal between the two lasers. High stability of the beat frequency (1×10^{-13}) indicates that high coherence in the master laser was precisely transferred to the slave laser. The frequency of the slave laser was varied in the 2.4-GHz range by sweeping the microwave frequency of the local oscillator used for PM noise reduction of the beat signal. This range was limited by the APD bandwidth for beat signal detection. A wider tunability of $\sim$1 THz is expected with this technique if a frequency reference grid, e.g., resonance frequencies of a Fabry-Perot etalon, is also employed for frequency locking of the master laser.

Frequency reproducibility of 1×10^{-8} has been obtained so far by using absorption spectra in organic molecules as frequency references.[6,7] To improve the reproducibility, it is important to investigate the long-term frequency drift of the longitudinal mode. For this purpose, the frequency drifts of 0.78-μm AlGaAs lasers were traced for 1 yr in stable operating conditions. A frequency drift of +8.6 MHz/h was observed, which was attributed to a decrease in thermal resistance of the laser.

Two applications of these coherent lasers are now under investigation: (1) a ring Fabry-Perot resonator-type fiber gyro was constructed and tested to measure fluctuations in the rotational speed of the earth. The purpose of this measurement is earthquake prediction by detecting the anomalous Chandler motion. (2) A microwave Rb atomic clock was optically pumped by this coherent laser. A microwave frequency shift induced by the laser frequency shift was accurately measured, which was 0.2 Hz/MHz. Furthermore, two-quanta transitions in ^{87}Rb were observed by this coherent laser. Improvement of the frequency stability of this atomic clock was also obtained.

(Invited paper, 25 min)

1. M. Ohtsu and S. Kotajima, Jpn. J. Appl. Phys. **24**, L256 (1985).
2. M. Ohtsu and S. Kotajima, IEEE J. Quantum Electron. **QE-21** (Dec. 1985).
3. Y. Yamamoto, O. Nilsson, and S. Saito, IEEE J. Quantum Electron. **QE-21** (Dec. 1985).
4. M. Ohtsu, H. Fukada, T. Tako, and H. Tsuchida, Jpn. J. Appl. Phys. **22**, 1157 (1983).
5. M. Ohtsu, H. Kotani, and H. Tagawa, Jpn. J. Appl. Phys. **22**, 1553 (1983).
6. K. Fukuoka, M. Ohtsu, and T. Tako, Jpn. J. Appl. Phys. **23**, L117 (1984).
7. M. Ohtsu, M. Hashimoto, and H. Ozawa, in *Proceedings, Thirty-ninth Annual Symposium on Frequency Control*, Philadelphia (May 1985), pp. 43–53.

Electrical feedback for attaining ultrahigh coherence in semiconductor lasers

K.Kuboki, M.Ohtsu, N.Tabuchi, and T.Ouchi

Graduate School at Nagatsuta, Tokyo Institute of Technology
4259 Nagatsuta, Midori-ku, Yokohama, Kanagawa 227, Japan

Abstract

Electrical negative feedback was proposed to carry out simultaneously the four subjects in order to attain ultrahigh coherence in semiconductor lasers. Their experimental results were presented. They were: (1) Linewidth of field spectrum was reduced to 200 kHz, which was narrower than the value given by the Schawlow-Townes' formula, i. e., the one limited by spontaneous emission. (2) Fluctuations of center frequency of field spectrum were reduced to 500 Hz at the integration time of 100 s. (3) Frequency tracking of the slave laser to the master laser was carried out with the frequency stability as high as that of the master laser given (2). (4) Wideband frequency tuning of the slave laser was carried out under the condition of (3). The resultant lock range was 47.3 GHz, in which the stability of the slave laser was maintained as high as that of (3).

Introduction

Attempts at improving temporal coherence in semiconductor lasers have been made in recent years for coherent optical measurements, coherent optical communications [1], and so on.

It can be deduced from well developed techniques for coherent microwave oscillators [2] (H masers, Cs or Rb atomic clocks) and gas lasers [3] that at least four subjects should be simultaneously carried out for this improvement, which are (1) linewidth reduction, (2) stabilization of center frequency of field spectrum, (3) frequency tracking to the other highly coherent laser, (4) wideband frequency tuning.

One of the authors (M. O.) has proposed that electrical negative feedback can be used as a promising technique to carry out these four subjects simultaneously.

Electrical negative feedback was employed to attain ultrahigh coherence in semiconductor lasers. Theoretical analysis, based on quantum mechanical Langevin's equation, has shown that electrical feedback can reduce the FM noise to the level lower than the value limited by quantum noise [4]. Following four subjects are presented.

Linewidth reduction

Since a field spectrum is given by Fourier transform of an autocorrelation function of an amplitude of the laser electric field, its spectral lineshape depends on the magnitude of phase fluctuations of a slowly varying amplitude. Therefore, the spectral linewidth depends on magnitude of phase fluctuations or that of frequency fluctuations.

Linewidth can be measured by observing a beat spectrum between the two independent lasers, by a technique of delayed self-heterodyning [5], or by using a high-resolution scanning Fabry-Perot interferometer [6]. For accurate measurements, an integration time of measurements should be taken long enough to maintain a high resolution, which is a consequence of the uncertainty principle between frequency and time. At the same time, this integration time should be taken short enough to avoid an effect of frequency drift, which is because the frequency of the free-running laser exhibits a random walk due to the fluctuations of ambient temperature or injection current. Because of such the inevitable requirement of optimal adjustment of the integration time, spectral linewidth is not necessarily an accurate measure for representing properties of coherence. The power spectral density or the Allan variance [7] of frequency fluctuations should be used as a primary measure. However, since spectral linewidth has attracted attentions for several applications, discussions will be focused on spectral linewidth in this section. For this discussion, it is assumed that the above mentioned optimal adjustment of integration time has been made.

To reduce such a large linewidth by electrical negative feedback, frequency fluctuations at $f \leq \Delta\nu_{FR}$ should be reduced, where f is the Fourier frequency [8]. If the bandwidth of the feedback loop is larger than $\Delta\nu_{FR}$, the linewidth can be reduced to a value limited by noises contained in the feedback signal.

Experiments have shown that the linewidth of a 1.5 μm InGaAsP laser was reduced to 330 kHz by electrical negative feedback, where it has been about 5 MHz under a free-running condition [8]. Furthermore, recent experiments have proved that it was reduced to 200 kHz, which is 1/25 times that of a free-running laser. Figure 1(a) shows the gain of the electrical negative feedback loop. The curve A of Fig. 1(b) shows the phase delay of the feedback loop. Contributions from the phase delay of the laser frequency modulation, bias T, servo-amplifier and filter, and delay time due to the finite loop length are represented by curve B, C, D, and E, respectively.

Figure 2 shows an example of simulated results of a power spectral density of frequency fluctuations under electrical negative feedback. For this simulation, transfer functions of all the components in the feedback loop were estimated by measuring their response characteristics as well as above mentioned phase delay [9]. It shows an oscillation at the phase delay of 180 degree, by which FM sidebands can be induced and optical carrier components are decreased, which gives an upper limit of the feedback gain to be increased. The Fourier frequency for this oscillation depends on the phase delay of the laser and length of the feedback loop. When the loop length is shorter than about 10 cm, the peak of this oscillation becomes lower. At the same time, since this frequency becomes higher than 100 MHz, which is away from the required bandwidth for feedback, the oscillation can be suppressed by appropriate design of the servo-amplifier and a low-pass filter. Therefore, it is important to reduce the size of this system to improve the linewidth reduction, which is compatible to realize an integrated, miniature ultrahigh-coherent light source.

Further increases in a total gain of the feedback loop can be expected if the sensitivity of frequency discrimination is increased. It can be realized if a higher resolution Fabry-Perot interferometer is employed. Figure 3 shows a relation between the width of a resonance curve of the Fabry-Perot interferometer $\Delta\nu_{FP}$ and the detector-noise-limited linewidth $\Delta\nu_{FB}$ of the laser under feedback [9]. For this estimation, it was assumed that required phase compensations discussed above has been made by an optimal design of the servo-amplifier. Since $\Delta\nu_{FP}$ is inversely proportional to the sensitivity of frequency discrimination, the noise-limited linewidth is decreased with decreasing $\Delta\nu_{FP}$, which is represented by the curve A. Such an increase in the sensitivity is equivalent to the technique of employing a ultranarrow spectral line of two-photon optical Ramsey spectroscopy [10]. However, in the present case, decreases in $\Delta\nu_{FP}$ would also reduce the bandwidth of the feedback loop and induce a re-broadening of the laser linewidth because $\Delta\nu_{FP}$ gives the response bandwidth of the interferometer. This effect is represented by the meshed area between the curves B and C in this figure. This figure shows that the linewidth of about $10^{-8} \sim 10^{-7}$ times that of a free-running laser, i. e., a subhertz linewidth, can be expected when $\Delta\nu_{FP}$ is about 1 MHz ~ 10 MHz. In such a case of subhertz linewidth, the effect of increases in power fluctuations of a conventional laser was also neglected because its estimated value was less than 5 % of that of a free-running laser [9].

Stabilization of center frequency of field spectrum

By using ^{87}Rb vapor as a frequency reference, fluctuations of center frequency of a 0.8 μm AlGaAs laser were reduced to 500 Hz at $\tau = 100$ s, where τ represents the integration time of measurements [11]. This was as low as quantum noise level [4].

Frequency tracking to the other highly coherent laser

A technique of frequency tracking of the slave laser to the other highly coherent master laser would be useful for applications to coherent/heterodyne optical communications, heterodyne optical measurements, and so on. The authors have proposed a frequency offset locking as a stable and accurate technique for such a tracking [12, 13].

Experimental setup for a 0.8 μm AlGaAs laser is shown in Fig. 4, where injection current of the slave laser is controlled in order to lock the divided beat frequency between the master and slave lasers to the frequency from a digital frequency synthesizer. By this electrical negative feedback, the frequency of the slave laser ν_S is given by

$$\nu_S = \nu_M \pm \nu_B = \nu_M \pm M \cdot \nu_L \quad , \qquad (1)$$

where ν_M, ν_B, and ν_L are frequencies of the master laser, beat signal, and the synthesizer, respectively. An integer M represents a division rate of the beat frequency provided by a prescaler. This formula represents that the locked frequency of the slave laser possesses an offset ($\pm M \cdot \nu_L$) with respect to the master laser frequency, by which this technique has been called frequency offset locking [14, 15].

Instead of controlling the frequency of the beat signal, its phase, i. e., the time integral of frequency, was controlled in the present experiments to reduce frequency drift

and to improve accuracy of frequency tracking. For this purpose, a phase of the beat signal was compared with that of the signal from the frequency synthesizer by using a digital phase comparator, which was composed of binary up counters, down counters, full adders, and a D/A converter. Figures 5(a) and (b) show waveforms of output signals from the phase comparator under free-running and frequency offset locked conditions, respectively. Figure 5(c) shows fluctuations of a beat frequency between the master and slave lasers. It was confirmed from these figures that the present scheme of phase control was effective to lock tightly the beat frequency.

Figure 6(a) shows the square root of the Allan variance $\sigma\nu_B^2(\tau)$ of the beat frequency fluctuations. Since directly controlled quantity was not the frequency of the beat signal but its phase, the square root of the Allan variance $\sigma\phi_B^2(\tau)$ of the phase fluctuations was also estimated from the result of Fig. 6(a) and is given by Fig. 6(b), where a relation $\sigma\phi_B^2(\tau) = (2\pi\tau)^2 \cdot \sigma\nu_B^2(\tau)$ was used. Reductions of frequency and phase fluctuations by frequency offset locking are clearly seen in these figures. It is also seen that the effects of locking were remarkable for a longer integration time, which means that the frequency drift was sufficiently reduced by controlling its time integral, i. e., the phase.

The value of curve B in Fig. 6(a) is approximated as

$$\sigma\nu_B(\tau) = 1.1 \times 10^3 \cdot \tau^{-1} \ (\mathrm{Hz}) \quad (1\,\mu\mathrm{s} \leq \tau \leq 100\ \mathrm{s}) \ , \tag{2}$$

and its minimum is

$$\sigma\nu_B(\tau) = 11 \ (\mathrm{Hz}) \quad \text{at} \quad \tau = 100\ \mathrm{s} \ . \tag{3}$$

Analysis of noise magnitudes generated in the feedback loop for frequency offset locking showed that the principal noise source of the residual beat frequency fluctuations was round-off errors of pulse number counting, which was generated at the D/A converter in the phase comparator. The square roots of the Allan variance due to this noise source are expressed as

$$\left.\begin{aligned} \sigma\nu_B(\tau) &= M \cdot \tau^{-1} \ (\mathrm{Hz}) \\ \sigma\phi_B(\tau) &= 2\pi \cdot M \ \ (\mathrm{rad}) \end{aligned}\right\} \ , \tag{4}$$

which are represented by the curves C in Figs. 6(a) and (b).

Since frequencies of the master laser and the beat signal were locked by using different and independent feedback loops, their residual fluctuations are mutually uncorrelated. Therefore, the Allan variance for frequency fluctuations of the slave laser can be expressed as

$$\sigma\nu_S^2(\tau) = \sigma\nu_M^2(\tau) + \sigma\nu_B^2(\tau) \ . \tag{5}$$

Since it was confirmed that $\sigma\nu_B^2(\tau) \ll \sigma\nu_M^2(\tau)$ for $1\,\mu\mathrm{s} \leq \tau \leq 100$ s, this equation means that $\sigma\nu_S^2(\tau) \cong \sigma\nu_M^2(\tau)$, i. e., the residual frequency fluctuations of the slave laser were as low as those of the master laser. It can be confirmed from these results that accurate frequency tracking to the master laser was realized, or, in other words, high coherence of the master laser was transferred to the slave laser.

Wideband frequency tuning

A highly stable, reproducible, and accurate technique for wideband frequency tuning would be required for several improved applications. Frequency offset locking can be also used as a candidate for such a reliable technique. In this technique, the slave laser frequency can be swept in a stable manner by sweeping the synthesizer frequency with a sweep speed which falls within the bandwidth of the feedback loop (1.5 MHz). Figure 7 shows the beat frequency ν_B which was varied by a stepwise sweep of the synthesizer frequency at 20 MHz interval. Here, the division rate M of the prescaler was fixed to 500 for $\nu_B < 0.7$ GHz, and to 2000 for $\nu_B \geq 0.7$ GHz, respectively, which was required because of a limited bandwidth of the prescaler used. As shown by this figure, a stable sweep was carried out for 0.08 GHz $\leq \nu_B \leq$ 1.6 GHz, which means that the lock range of the beat frequency was 1.52 GHz and frequency tunable range of the slave laser was 3.04 GHz. Furthermore, recent experiments have proved that it was carried out for 0.024 GHz $\leq \nu_B \leq$ 1.6 GHz, which means that the lock range of the beat frequency was 1.58 GHz and frequency tunable range of the slave laser was 3.15 GHz. This lock range was limited by the following causes : For $\nu_B <$ 0.024 GHz, the level of the input signal to the prescaler was not high enough to be converted into the TTL signal, which is due to a rather broad linewidth of the beat spectrum. For $\nu_B >$ 1.6 GHz, on the other hand, the sensitivity of phase comparison was also reduced because of a limited response speeds of the Si-APD and the prescaler.

There can be promising ways of further extensions of the range of stable frequency tuning of the slave laser. One of them is to make a discrete tuning of the master laser frequency by successively locking to one of the frequency reference grid which are nearly equidistantly distributed along the frequency axis. For each locked frequency of the master laser, the frequency offset locking is applied to the slave laser. By this control scheme, a stable and accurate tuning of the slave laser frequency can be realized. Absorption spectral lines of combination tones or higher harmonics of vibration-rotation transitions in organic molecules can be a candidate for such a frequency reference grid. This is because a great number of lines are distributed with several GHz or several tens of GHz interval in the near infrared wavelength region and some of their absolute frequencies have been already calibrated with the accuracies of about $1 \times 10^{-6} \sim 7 \times 10^{-8}$ [16, 17].

In the present experiment, equidistantly distributed resonance frequencies of a Fabry-Perot interferometer were used as the simpler frequency reference grid. The master laser frequency was able to be locked to the slopes of its successive fifteen resonance spectral lines. For each locked frequency of the master laser, frequency offset locking was applied to the slave laser to reduce the beat frequency fluctuations as low as those shown by Fig. 6. As a result of this locking, a range of stable frequency sweep of the slave laser was extended to 47.3 GHz.

The number of lines of frequency reference grid to which the master laser can be locked was limited by mode-hopping phenomena in the laser, which also limited the extension of the tunable range of the slave laser frequency. It would be effective to use a laser without mode-hopping to extend this range. A recently developed 1.5 μm InGaAsP DFB laser may be favorably used for this purpose because its wavelength can be continuously varied by varying the ambient temperature within the range of 15 nm without mode-hopping under free-running condition, which corresponds to the frequency range of as wide as 2 THz [18]. A stable and wideband frequency tuning for more than 1 THz can be expected if this kind of lasers are employed.

Summaries

Electrical negative feedback was proposed as a promising synthesized technique to carry out simultaneously the four subjects which were required to attain ultrahigh coherence in semiconductor lasers. Experimental results are summarized as follows :

(1) Linewidth of field spectrum : 200 kHz, which is 1/25 times that of the free-running laser (for a 1.5 μm InGaAsP laser). It was estimated as being narrower than the value given by the Schwlow-Townes' formula, i. e., limited by spontaneous emission.

(2) Stability of center frequency of field spectrum : $\sigma\nu(\tau) = 500$ Hz at $\tau = 100$ s (for a 0.8 μm AlGaAs laser).

(3) Frequency tracking : Stability of the beat frequency was
$\sigma\nu_B(\tau) = 11$ Hz at $\tau = 100$ s (for a 0.8 μm AlGaAs laser) .

(4) Stable and wideband frequency tuning : Lock range of the beat frequency was 1.58 GHz, and the total range of frequency tuning of the slave laser was 47.3 GHz, in which a stability of the beat frequency was maintained as high as that of (3) (for a 0.8 μm AlGaAs laser) .

An improved experimental setup is now under preparation to realize higher coherence. Further improvement in the performances of this system can be expected by using a novel integrated laser devices with lower drift and improved FM response characteristics in the future.

References

1. Okoshi, T., "Recent Progress in Heterodyne/Coherent Optical-Fiber Communications", J. Lightwave Technol., Vol. LT-2, pp. 341-346, 1984
2. Kartaschoff, P., Frequency and Time, London: Academic Press, 1978
3. Brillet, A. and Cerez, P., "Laser Frequency Stabilization by Saturated Absorption", J. de Physique, Vol. 42, pp. 73-82, 1981
4. Ohtsu, M., Fukada, H., Tako, T., and Tsuchida, H., "Estimation of the Ultimate Frequency Stability of Semiconductor Lasers", Jpn. J. Appl. Phys., Vol. 22, pp. 1157-1166, 1983
5. Okoshi, T., Kikuchi, K., and Nakayama, A., "Novel method for high resolution measurement of laser output spectrum", Electron. Lett., Vol. 16, pp. 630-631, 1980
6. Takakura, T., Iga, K., and Tako, T., "Linewidth Measurements of a Single Longitudinal Mode AlGaAs Laser with a Fabry-Perot Interferometer", Jpn. J. Appl. Phys., Vol.

19, pp. L725-727, 1980
7. Allan, D. W., "Statistics of atomic frequency standards", Proc. IEEE, Vol. 54, pp. 221-230, 1966
8. Ohtsu, M. and Kotajima, S., "Linewidth Reduction of a Semiconductor Laser by Electrical Feedback", IEEE J. Quantum Electron., Vol. QE-21, pp. 1905-1912, 1985
9. Tabuchi, N., Ouchi, T., and Ohtsu, M., "Linewidth Reduction of a Semiconductor Laser by Electrical Feedback" (in Japanese), Pap. Tech. Group IECE Japan, no. OQE86-29, June 27, 1986
10. Beausoleil, R. G. and Hansch, T. W., "Two-photon optical Ramsey spectroscopy of freely falling atoms", Opt. Lett., Vol. 10, pp. 547-549, 1985
11. Tsuchida, H., Ohtsu, M., Tako, T., Kuramochi, N., and Oura, N., "Frequency Stabilization of AlGaAs Semiconductor Laser Based on the ^{85}Rb-D_2 Line", Jpn. J. Appl. Phys., Vol. 21, pp. L561-L563, 1982
12. Kuboki, K. and Ohtsu, M., "Frequency Offset Locking of Semiconductor Lasers" (in Japanese), Pap. Tech. Group IECE Japan, no. MW85-29, June 17, 1985
13. Kuboki, K., Segami, M., and Ohtsu, M., "Frequency Offset Locking of Semiconductor Lasers II" (in Japanese), Pap. Tech. Group IECE Japan, no. OQE86-2, April 21, 1986
14. Hall, J., L., and Borde, C., J., "Measurement of Methane Hyperfine Structure Using Laser Saturated Absorption", Phys. Rev. Lett., Vol. 30, pp. 1101-1104, 1973
15. Ohtsu, M., Katuragi, S., and Tako, T., "Performances of a Frequency Offset Locked He-Xe Laser System at 3.51 μm", IEEE J. Quantum Electron., Vol. QE-17, pp. 1100-1106, 1981
16. Fukuoka, K., Ohtsu, M., and Tako, T., "Accurate Wavelength Measurements of the Absorption Lines in H_2O Vapor by a 0.8 μm AlGaAs Laser", Jpn. J. Appl. Phys., Vol. 23, pp. L117-120, 1984
17. Ohtsu, M., Kotani, H., and Tagawa, H., "Spectral Measurements of NH_3 and H_2O for Pollutant Gas Monitoring by 1.5 μm InGaAsP/InP Lasers", Jpn. J. Appl. Phys., Vol. 22, pp. 1553-1557, 1983
18. Tohmori, Y., Komori, K., Arai, S., and Suematsu, Y., "Low-Threshold-Current CW Operation of 1.5 μm GaInAsP/InP Bundle-Integrated-Guide Distributed-Bragg-Reflector (BIG-DBR) Lasers", Electron. Lett., Vol. 21, pp. 743-745, 1985

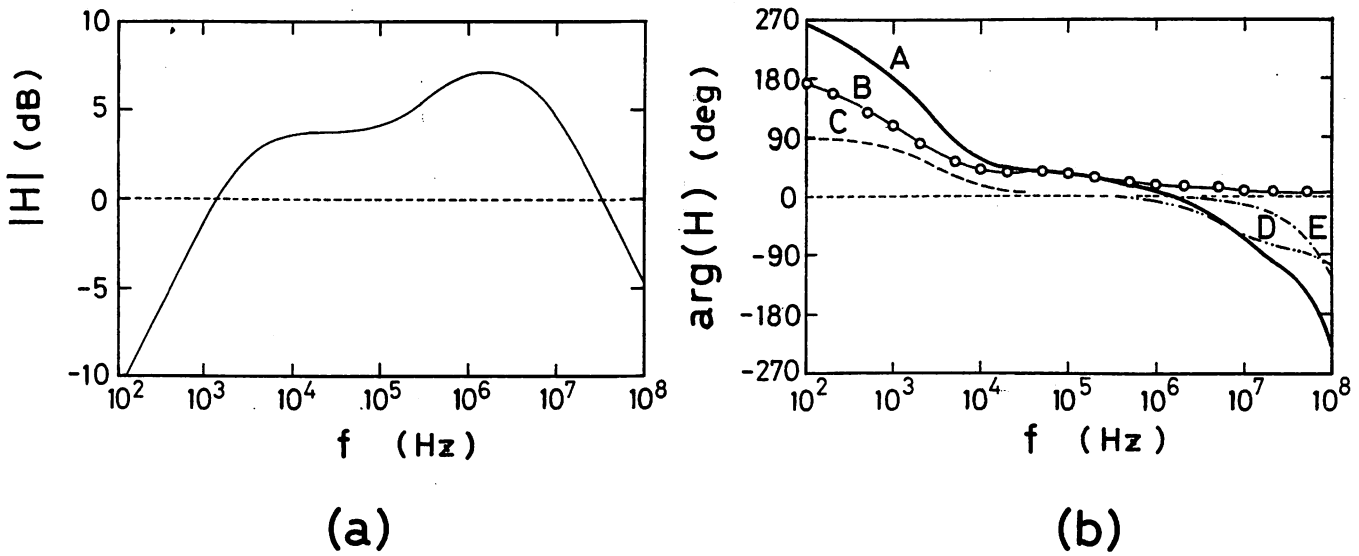

Fig. 1 (a) The gain of the electrical negative feedback loop. (b) The phase delay of the electrical negative feedback loop (curve A). Contributions from the phase delay of the laser frequency modulation, bias T, servo-amplifier and filter, and delay time due to a finite loop length are represented by curves B, C, D, and E, respectively.

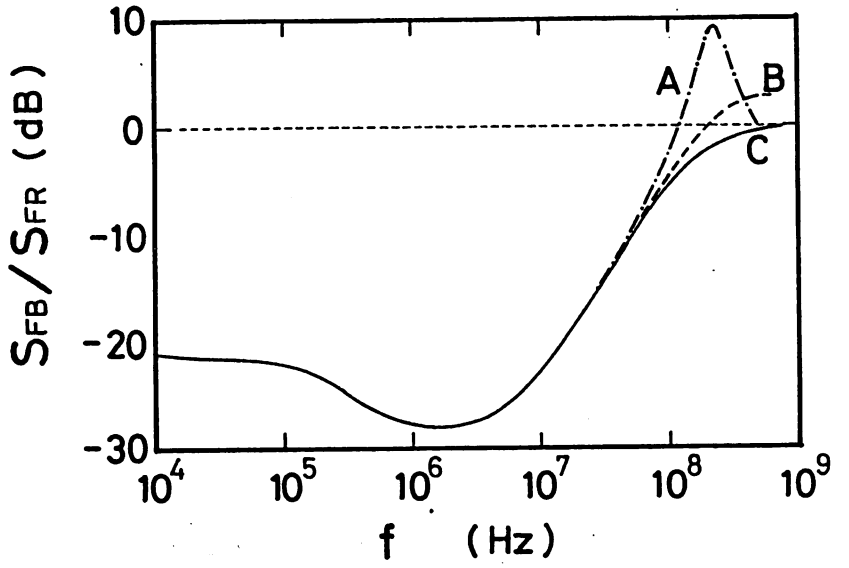

Fig. 2 An example of simulated results of the power spectral densities $S_{FB}(f)$ of frequency fluctuations under electrical negative feedback. This value is normalized to that of the free-running laser $S_{FR}(f)$. The curves A, B, and C represent the results when the loop length is 30 cm, 10cm, and 0, respectively.

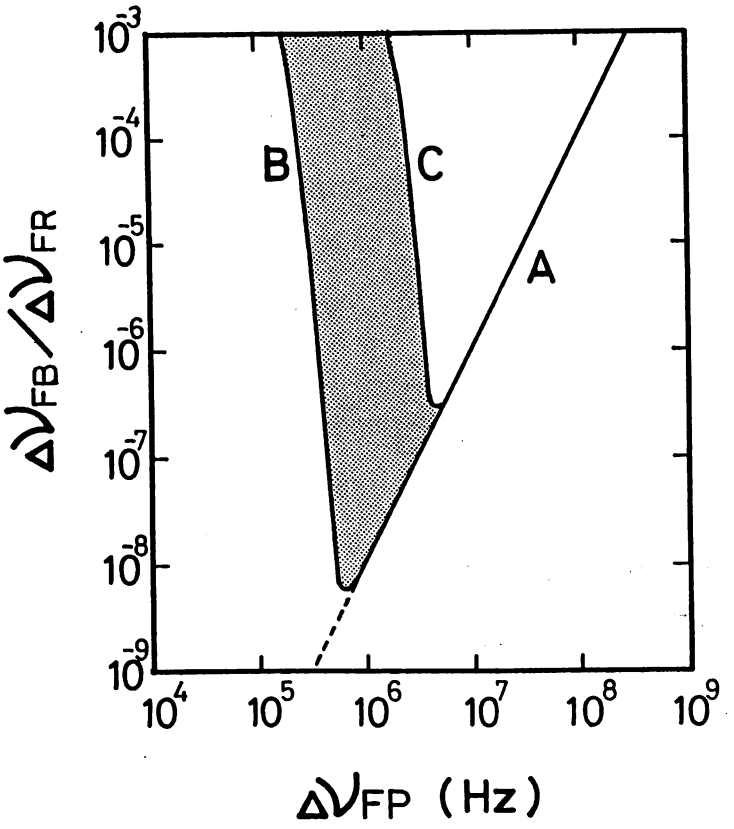

Fig. 3 Relation between the detector-noise-limited linewidth $\Delta\nu_{FB}$ of a 1.5 μm InGaAsP laser under feedback and the width of a resonance curve of a Fabry-Perot interferometer $\Delta\nu_{FP}$ used as a frequency discriminator. The linewidth $\Delta\nu_{FB}$ is normalized to that of the free-running laser $\Delta\nu_{FR}$. The linewidth $\Delta\nu_{FB}$ is decreased with decreasing $\Delta\nu_{FP}$, i.e., increasing the feedback gain, which is represented by the curve A. Further decreases in $\Delta\nu_{FP}$ would induce a re-broadening of $\Delta\nu_{FB}$, which is represented by the meshed area between the curves B and C. Since the accuracy of estimating a required bandwidth of the feedback loop was not high enough, the re-broadening was represented by such a meshed area.

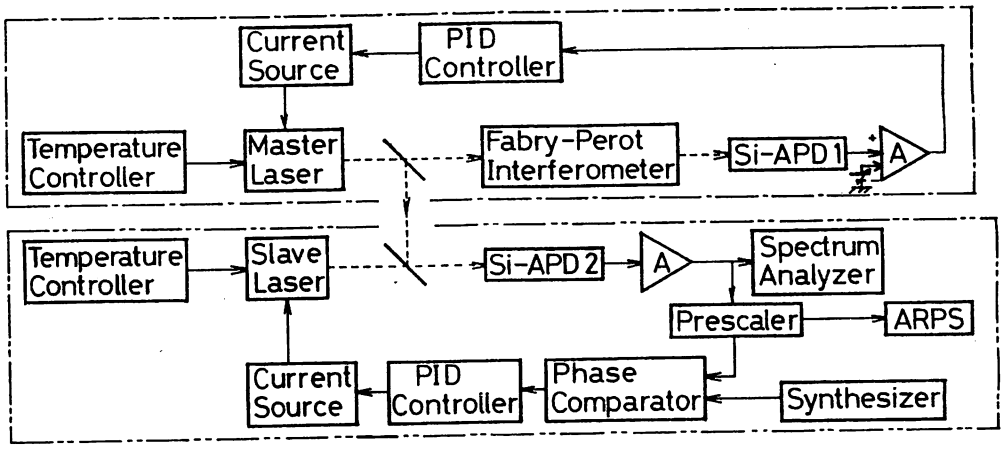

Fig. 4 Experimental setup for frequency offset locking. ARPS : Computerized Allan variance real-time processing system.

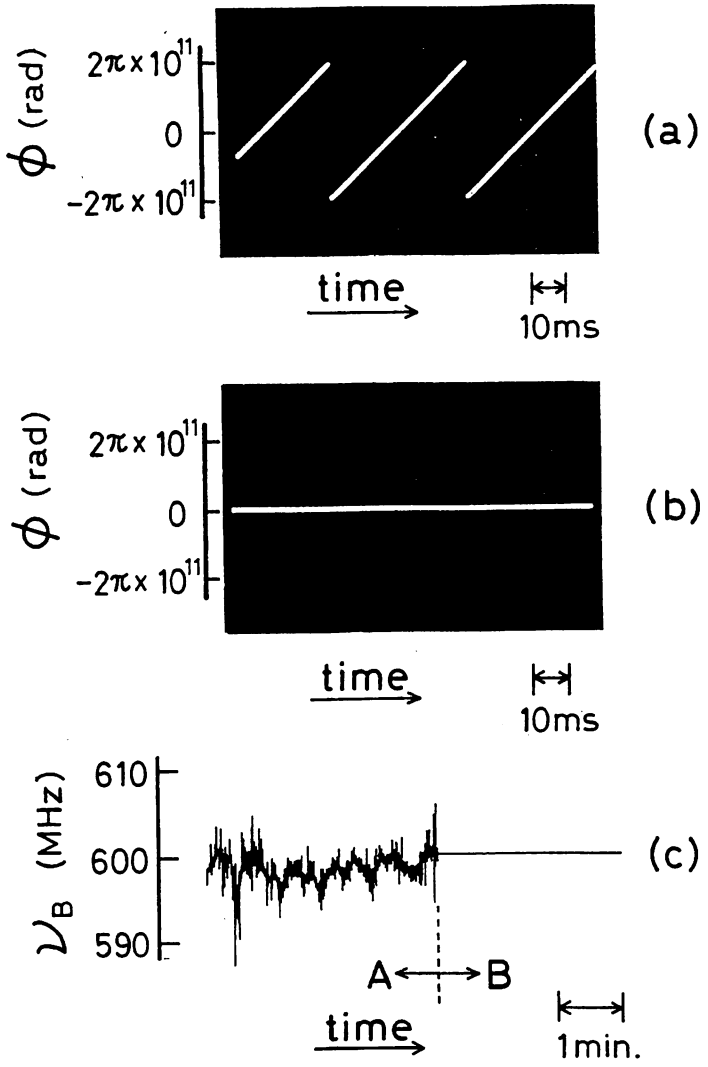

Fig. 5 Output signals from the phase comparator under free-running (a) and frequency offset locked (b) conditions. The ordinates of these figures represent a phase difference between the signal from the frequency synthesizer and the beat signal whose frequency has been divided by M. (c) : Fluctuations in the beat frequency ν_B. The parts A and B represent the waveforms under free-running and frequency offset locked conditions, respectively, where M was fixed at 500 and the locked value of ν_B was 0.6 GHz.

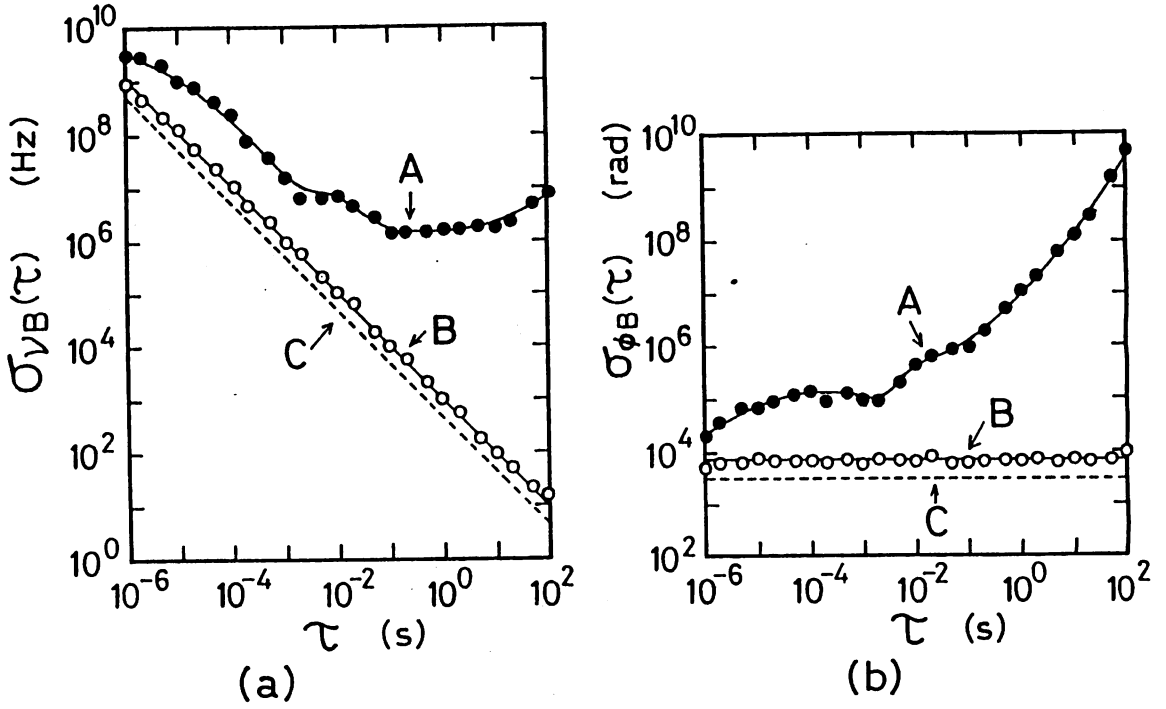

Fig. 6 The square root of the Allan variance $\sigma\nu_B^2(\tau)$ of the residual frequency fluctuations (a) and that of $\sigma\phi_B^2(\tau)$ of phase fluctuations (b) of the beat signal. A : Results of a free-running condition. B : Results under a condition of frequency offset locking, where M = 500 and ν_B = 0.6 GHz. C : Estimated limit given by round-off errors of pulse number counting generated at the D/A converter in the phase comparator.

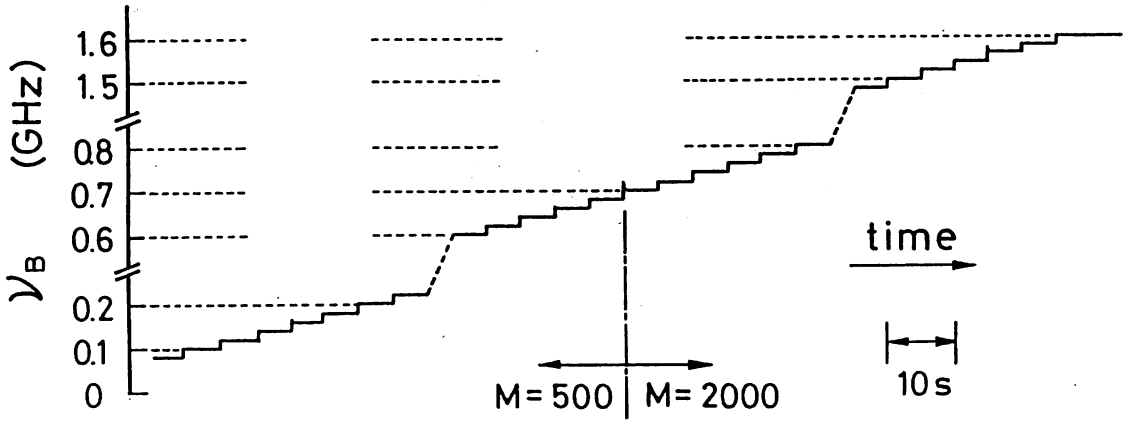

Fig. 7 The beat frequency ν_B which was varied by a stepwise sweep of the synthesizer frequency at 20 MHz interval. The division rate M of the prescaler was fixed at 500 for ν_B < 0.7 GHz, and 2000 for $\nu_B \geq 0.7$ GHz.

Sixth International Conference on Integrated Optics and Optical Fiber Communication (OFC/IOOC'87), January 1987, Reno, Nevada, TUC5

TUC5 Ultrahigh coherence in semiconductor lasers

M. OHTSU, K. KUBOKI, N. TABUCHI, Tokyo Institute of Technology, Graduate School at Nagatsuta, 4259 Nagatsuta, Midori-ku, Yokohama, Kanagawa 227, Japan.

Electrical feedback was employed to attain ultrahigh coherence in semiconductor lasers. A theoretical analysis, based on the quantum mechanical Langevin equation, has proved that electrical feedback can reduce the FM noise to a value lower than the quantum FM noise of the laser. The following four techniques were studied:

(1) Linewidth reduction: A compact external Fabry-Perot interferometer was used as a frequency discriminator for feedback. The linewidth was reduced to 200 kHz, which was narrower than the value limited by the quantum FM noise of the laser. Network analyses were carried out to make an optimum design of the wideband low-phase-delay servo amplifier, from which it was found that the linewidth can be reduced to as narrow as 10 kHz. Furthermore, it was found that integration of the feedback loop with the laser devices is not necessarily required, simplifying the experimental setup. It was estimated that the linewidth can be ultimately reduced to 1 Hz by employing an optimum fiber ring Fabry-Perot interferometer of $\sim$1 m as the frequency discriminator.

(2) Stabilization of the center frequency of field spectrum: Fluctuations of the center frequency were reduced to 500 Hz at 100-s integration time by using ^{85}Rb vapor as the frequency reference, which was as low as that limited by the quantum FM noise of the laser. This value was estimated by measuring the fluctuations of the beat frequency between the two independently stabilized lasers. The theoretical limit of this fluctuation was estimated at 0.5 Hz.

(3) Frequency tracking to the other highly coherent laser: A highly coherent laser [i.e., a master laser prepared by (1) and (2)] and a slave laser were heterodyned, and the IF signal was phase-locked to a microwave local oscillator by applying electrical feedback to the slave laser. The feedback bandwidth was 1.5 MHz, and the capture range of this optical PLL was 1.9 GHz. Fluctuations of IF frequency were reduced to 30 Hz at 100-s integration time, which was less than that of the master laser. This means that high coherence of the master laser was accurately transferred to the slave laser. Its theoretical limit was estimated as subhertz.

(4) Wideband frequency tuning: By sweeping the microwave frequency in the PLL condition of (3), the slave laser frequency was varied while maintaining high coherence. The frequency variable range, i.e., lock range of the PLL, was 58 GHz. It was estimated that this range can be extended to as wide as 1 THz if a dynamic single-mode laser is employed, which means that a highly coherent tunable laser can be developed.

Based on the results above, a synthesized system was proposed employing an electrical feedback to use the above four techniques simultaneously to achieve an ultrahigh coherence in semiconductor lasers.

(Invited paper, 25 min)

US-Japan Seminar, Quantum Mechanical Aspects of Quantum Electronics, July 1987, Monterey, CA, Session III, Paper number 4

Ultrahigh Coherent Semiconductor Lasers And Their Applications To Rb Atomic Clock

M. Ohtsu*, K. Kuboki, and M. Hashimoto

Tokyo Institute of Technology
4259 Nagatsuta, Midori-ku, Yokohama, Kanagawa 227, Japan

*Presently, AT&T Bell Laboratories
Crawford Hill Laboratory, Holmdel, NJ 07733, USA

ABSTRACT

We demonstrate that the FM noise in semiconductor lasers can be reduced to a value lower than the quantum noise limit by using negative electrical feedback. A synthesized method of electrical feedback (Fig. 1) is proposed to realize such ultrahigh temporal coherence in semiconductor lasers. The center frequency fluctuations of the field spectrum are reduced as low as 2×10^{-12} by this feedback. The linewidth of the field spectrum is reduced to 100 kHz, which is narrower than the value given by the qu..tum noise limit of the free-running laser (Fig. 2). Optical phase-locked loop realizes a frequency tracking accuracy of 3×10^{-14}, capture range of 1.2 GHz, and locking range of 53 GHz.

As an alternative scheme to realize ultrahigh coherence in semiconductor lasers, we present a novel experimental method for accurate frequency tracking using the correlated spontaneous emission between the two longitudinal modes [1,2]. We employ a method of resonant coupling between the two optical transitions via optical sidebands produced by parametric modulation of the laser gain. By this modulation, the linewidth of the heterodyned signal was reduced to 25 kHz (Fig. 3: The minimum of the linewidth obtained is limited by resolution of our linewidth measurement system). This value corresponds to suppression of the relative phase noise between the two modes to less than one-twentieth of the quantum noise limit of the free-running laser.

As an application of these ultrahigh coherent lasers, we have used them as optical pumping sources for Rb atomic clock of 6.8 GHz frequency. A novel optical-microwave double resonance spectral shape with the linewidth as narrow as 20 Hz is demonstrated by utilizing FM sidebands of the laser induced by nonlinear susceptibility of the three-level Rb atoms (Fig. 4). Theoretical analysis shows that by optimizing the modulation parameters one can realize ultra-sensitive microwave frequency discrimination, which is about 7500 times more sensitive than a conventional Rb atomic clocks.

REFERENCES

(1) M. O. Scully, Phys. Rev. Lett., 55, 2802 (1980)

(2) P. E. Toschek and J. L. Hall, Technical Digest of 15th International Quantum Electronics Conference, April 1987, Baltimore, WDD2.

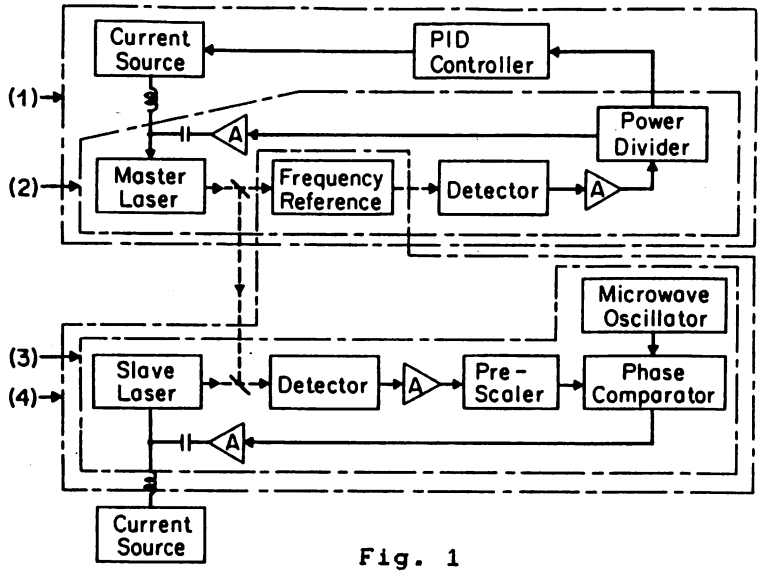

Fig. 1

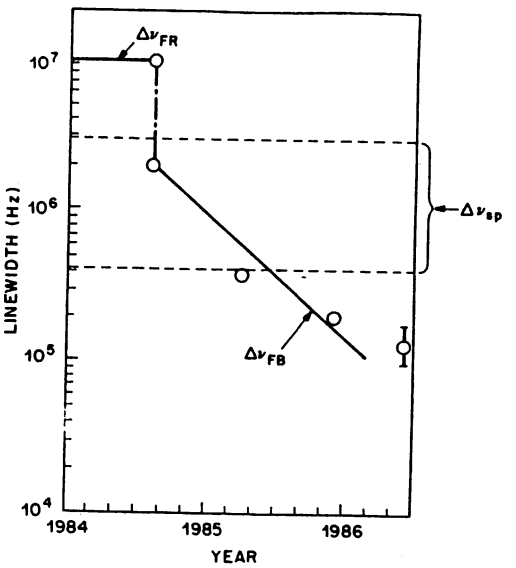

Fig. 2

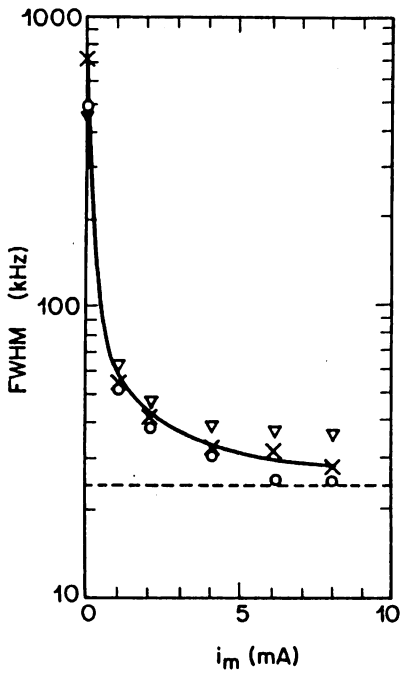

Fig. 3

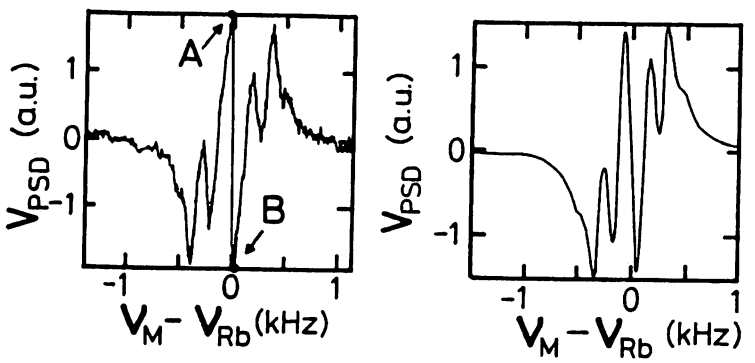

Fig. 4

Analyses of Mode-Hopping Phenomena in an AlGaAs Laser

MOTOICHI OHTSU, YASUAKI TERAMACHI, YOSHIHIRO OTSUKA, AND AKIO OSAKI

Abstract—**Intensity fluctuations of the longitudinal modes of a 0.8 μm AlGaAs laser were precisely measured during the occurrence of hopping between two modes. It was found from this result that mode hopping follows the stochastics of a Poisson process. The frequency of mode hopping was measured as $f_c = [\exp[-95(I/I_{th} - 1)]] \times 10^7$ (Hz), where I/I_{th} is the injection current normalized to its threshold value. Results of analog computer simulations showed that spontaneous emission worked as a triggering force for mode hopping. Results of the analysis based on the Fokker–Planck equation were compared to the experimental results, from which the root-mean-square value of the fluctuating electric field of spontaneous emission was estimated as 2.3×10^2 (V/m) $\leqq \langle \tilde{E}_N \rangle \leqq 3.2 \times 10^2$ (V/m). It is concluded that an effective reduction of mode hopping is achieved if the laser is operated at a higher bias or if the coupling constant between the two modes is increased.**

I. Introduction

THE performance of semiconductor lasers has recently been improved to the extent that they can be used for a variety of applications. They can, for example, be used as light sources for video and audio disk systems [1]. For these applications, their intensity fluctuations should be reduced to a sufficiently low level. However, it has been empirically found that high level fluctuations are induced in the low Fourier frequency range when the laser is operated with multilongitudinal modes [1]. This has been attributed to hopping between longitudinal modes. Ito *et al.* [2] have carried out several experiments and have discussed several correlation characteristics between the intensity fluctuations of each mode when multimode oscillation occurred. A theoretical analysis of the intensity fluctuations was first given by McCumber [3]. However, systematic studies on quantitative measurements and precise theoretical analysis of mode-hopping phenomenon have not been performed.

In order to reduce the intensity fluctuations induced by mode hopping, we have carried out precise measurements of these fluctuations as well as an analog computer simulation for a 1.5 μm InGaAsP laser [4]. As a result of this, it was found that mode hopping follows the stochastics of a Poisson process and spontaneous emission acts as a trigger to this hopping.

Manuscript received July 30, 1985.

M. Ohtsu, Y. Teramachi, and Y. Otsuka are with the Graduate School at Nagatsuta, Tokyo Institute of Technology, Midori-ku, Yokohama 227, Japan.

A. Osaki is with the Precision Engineering Research Laboratory, Hitachi, Ltd., Totsuka-ku, Yokohama 244, Japan.

IEEE Log Number 8407193.

In this paper, the results of a systematic study (precise measurements, analog computer simulations, theoretical analysis based on the Fokker–Planck equation) on mode-hopping phenomena of a 0.8 μm AlGaAs laser are presented, which are based on the results of the previous paper [4].

II. Precise Measurements of Intensity Fluctuations by Mode Hopping

A. Experimental Apparatus

An AlGaAs laser (channeled-substrate-planar type [5]) of 0.8 μm wavelength was employed for the experiments. Fig. 1 shows the experimental apparatus. The laser was installed in a small vacuum chamber, and temperature of the heat sink for the laser made of a copper block was controlled by using a Peltier element for which a thermistor bridge was used as a sensor. As a result of this control, the temperature fluctuations of the heat sink were reduced to ranges as low as 1×10^{-5}–3×10^{-4} K. The laser was driven by a low-noise dc current source with a current noise (root-mean-square value) of 0.6 nA/$\sqrt{\text{Hz}}$ at the Fourier frequency of 1 kHz. By realizing such extremely stable conditions of temperature and injection current, reproducible experimental results were obtained, i.e., the effects of temperature and injection current fluctuations on the laser intensity could be neglected in the present experiments.

Hatched areas in Fig. 2(a) give the regions of the heat sink temperature T and the injection current I where the laser showed a single longitudinal mode oscillation which was measured by a conventional grating monochromator. Here, the single longitudinal mode oscillation was defined to be the situation in which the intensities of satellite longitudinal modes were less than 5 percent of that of the main mode. For example, modes $M1$ and $M2$ in this figure are adjacent to each other, while two nonoscillating longitudinal modes exist between modes $M7$ and $M10$. In the present study, the intensity fluctuations under the two-mode oscillation [see Fig. 2(b)], which is the simplest case of multimode oscillation, were investigated for simplicity. Here, the two-mode oscillation was defined to be the situation in which the intensity difference between the two longitudinal modes was less than 10 percent. This two-mode oscillation was obtained by setting the temperature and injection current at several points between the two hatched areas in Fig. 2(a). Laser beams of two modes

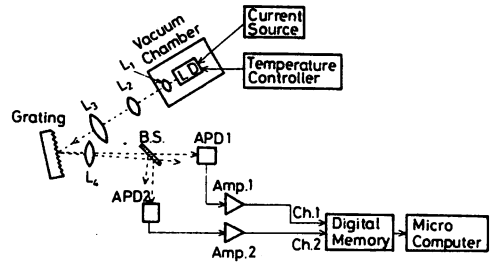

Fig. 1. Experimental apparatus. LD: laser diode. APD: silicon avalanche photodiode.

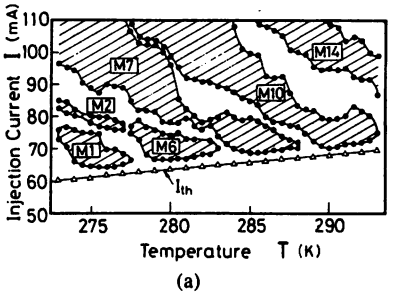

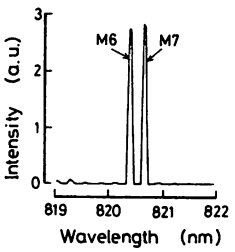

Fig. 2. (a) Regions of the temperature T of the heat sink of the laser and the injection current I where single longitudinal mode oscillation was observed (hatched areas). $M1$-$M14$ represent a series of longitudinal modes whose typical wavelengths are: $M1$: 820.0 nm, $M2$: 820.3 nm, $M6$: 821.6 nm, $M7$: 822.0 nm, $M10$: 822.9 nm, $M14$: 824.2 nm. I_{th} represents the threshold current. (b) Intensities of modes $M6$ and $M7$ measured by a grating monochromator.

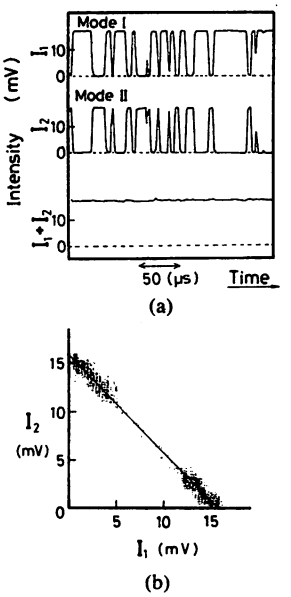

Fig. 3. (a) Temporal intensity fluctuations of the two modes and their sum. These values are represented by the output voltage of the preamplifier from the Si-APD. Modes I and II in this figure correspond to $M6$ and $M7$ in Fig. 2, respectively. The value of I/I_{th} was 1.07. (b) A phase space of the intensities of the two modes. The dots in this figure represent the distributions of the intensities of Fig. 3(a) sampled at a time interval of 50 ns. The solid line was drawn by a least square fitting to these data.

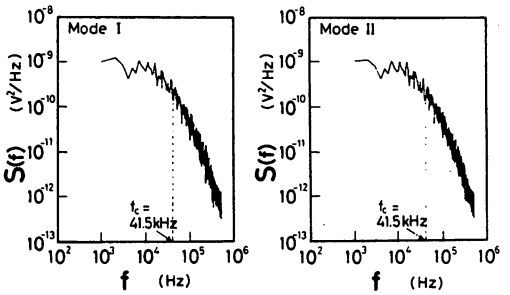

Fig. 4. Power spectral densities $S(f)$ of intensity fluctuations of both modes of Fig. 3(a). The cutoff frequency f_c was defined as $S(f_c) \equiv S(0)/2$.

were spatially separated by a grating as shown in Fig. 1 and were simultaneously detected by two silicon avalanche photodiodes (Si-APD). The output signals of Si-APD's were recorded by a two-channel digital memory. The bandwidth of the detection system was 50 MHz.

B. Results

Fig. 3(a) gives the fluctuations of the intensities of both modes and that of their sum. It can be clearly seen that the two modes do not oscillate simultaneously, but show switching phenomena, which can be interpreted as mode hopping. Fig. 3(b) gives a phase space, which represents the distributions of the intensities of both modes of Fig. 3(a) sampled at time intervals of 50 ns. The value of cross-correlation coefficient R between the intensities of both modes were calculated as being -0.998, where the following definition of R [6] and all the values of the sampled data in Fig 3(b) were used for calculation:

$$R = \sigma_{12}/\sqrt{\sigma_1 \cdot \sigma_2}. \quad (1)$$

In this case, σ_i is the self variance of the intensity variation of the ith mode and σ_{12} is the cross variance between the two modes. Switching phenomena can be also concluded from Fig. 3(b) and from a large negative value of R. Fig. 4 gives the power spectral densities of the intensity fluctuations of both modes calculated from the signal recorded by the two-channel digital memory. These curves show typical Lorentzians with a cutoff frequency f_c of 41.5 kHz, which means that mode hopping follows the stochastics of a Poisson process [7], i.e., mode hopping occurs completely at random in time. This also has been found for a 1.5 μm InGaAsP laser [4]. Furthermore, these curves imply that the average duration time corresponds to $1/\pi f_c$ [7], i.e., f_c represents the average frequency of mode hopping. Fig. 5 shows the relation between the injection current I normalized to its threshold value I_{th} and f_c. The solid curve was calculated by least square fitting to the experimental results, which is

$$f_c = [\exp[-95(I/I_{th} - 1)]] \times 10^7 \text{ (Hz)}. \quad (2)$$

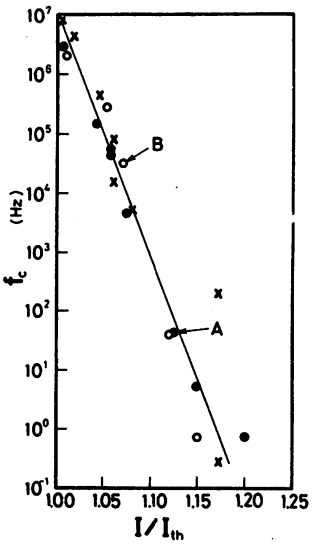

Fig. 5. Relation between the injection current normalized to its threshold value I/I_{th} and the cutoff frequency f_c. •: Hopping between modes $M1$ and $M2$ of Fig. 2(a). ○: Hopping between modes $M6$ and $M7$ of Fig. 2(a). ×: Hopping between modes $M7$ and $M10$ of Fig. 2(a). The solid line was drawn by least square fitting to the experimental values. The condition of the point A was used to obtain Figs. 10–12 and 16. Point B corresponds to the result of Figs. 3 and 4.

It is seen from Fig. 5 and (2) that the value of f_c, i.e., the frequency of mode hopping, decreases with increasing I/I_{th}, which was almost independent of the fact of whether or not the two modes were adjacent to each other. From this result, it can be concluded that an effective way of reducing mode hopping is to operate the laser at a higher value of I/I_{th}, i.e., at a higher bias.

III. Analog Computer Simulations

An analog computer simulation was carried out to investigate the origin of mode-hopping phenomenon. One of the most precise models of semiconductor laser oscillations, as it was proposed by Yamada and Suematsu [8], was employed. According to this model, the electric field of the laser under two-mode oscillation is given by

$$E(r, t) = \tilde{E}_1(t) \cdot F_1(r) \cdot e^{i\omega_1 t} + \tilde{E}_2(t) \cdot F_2(r) \cdot e^{i\omega_2 t} + \text{c.c} \tag{3}$$

where $\tilde{E}_i(t)$ is the slowly varying amplitude, $F_i(r)$ is the spatial distribution function, ω_i is the angular frequency, and c.c represents the complex conjugate of the first two terms. The fluctuations of $\tilde{E}_i(t)$ are described by van der Pol equations which are given by

$$\frac{d\tilde{E}_i^2}{dt} = \frac{1}{n_I\sqrt{\epsilon_0\mu_0}} [\tilde{\alpha}_i^{(1)} - \alpha_{th} - \tilde{\alpha}_i^{(3)}\tilde{E}_i^2 - \tilde{\alpha}_{i(j)}^{(3)}\tilde{E}_j^2]\,\tilde{E}_i^2 \qquad (i, j = 1, 2;\ i \neq j) \tag{4}$$

where n_I is the refractive index of the laser medium, ϵ_0 is the permittivity constant of vacuum, μ_0 is the permeability constant of vacuum, and α_{th} is the loss of the laser cavity. The quantities $\tilde{\alpha}_i^{(1)}$, $\tilde{\alpha}_i^{(3)}$, and $\tilde{\alpha}_{i(j)}^{(3)}$ represent a linear gain, self-saturation coefficient, and cross-saturation coefficient, respectively. These quantities are derived from the density matrix formulation, and are given by [8]

$$\tilde{\alpha}_i^{(1)} = \xi^{(1)} g^{(1)} [\bar{n}^{(0)} - n_G^{(1)} - h'(\lambda_i - \lambda_0)^2], \tag{5}$$

$$\tilde{\alpha}_i^{(3)} = \frac{9}{2} (\xi^{(1)})^2 \left(\frac{\tau_{in}}{\hbar}\right)^2 \langle M^2 \rangle\, g^{(1)} (\bar{n}^{(0)} - n_G^{(3)}), \tag{6}$$

$$\tilde{\alpha}_{i(j)}^{(3)} = \frac{6(\xi^{(1)})^2 \left(\frac{\tau_{in}}{\hbar}\right)^2 \langle M^2 \rangle\, g^{(1)} (\bar{n}^{(0)} - n_G^{(3)})}{1 + \tau_{in}^2 (\omega_i - \omega_j)^2}, \tag{7}$$

and

$$\alpha_{th} = \xi^{(1)} g^{(1)} (\bar{n}_{th}^{(0)} - n_G^{(1)}). \tag{8}$$

The quantities of (5)–(8) are defined in [8] and are summarized as follows.

- $\bar{n}^{(0)}$: Carrier density injected into the active region.
- $\xi^{(1)}$: Laser power confinement ratio in the active region.
- $g^{(1)}$: Inclination of the linear gain to the injected carrier density $\bar{n}^{(0)}$.
- $n_G^{(1)}$: Carrier density required to get positive value of the linear gain.
- h': Broadening of the linear gain on photon energy.
- λ_i: Wavelength of the ith longitudinal mode.
- λ_0: Wavelength of the center of the gain spectrum.
- τ_{in}: Relaxation time of the dipole which consists of an electron and hole.
- $\langle M^2 \rangle$: Square of the dipole moment.
- $n_G^{(3)}$: Carrier density required to get positive value of the saturation coefficients.
- $\bar{n}_{th}^{(0)}$: Threshold value of $\bar{n}^{(0)}$.

Since all the quantities in (5)–(8) can be measured through appropriate experiments as given in [8], the model employed here is concrete and it can be compared to experimental results.

The following approximation is valid because it was confirmed by several preliminary calculations that the fluctuations of $\tilde{\alpha}_i^{(3)}$ and $\tilde{\alpha}_{i(j)}^{(3)}$ with a change of $\bar{n}^{(0)}$ are much less than that of $\tilde{\alpha}_i^{(1)} - \tilde{\alpha}_{th}$:

$$\left.\begin{aligned} \tilde{\alpha}_i^{(3)}(\bar{n}^{(0)}) &\cong \tilde{\alpha}_i^{(3)}(\bar{n}_{th}^{(0)}) \\ \tilde{\alpha}_{i(j)}^{(3)}(\bar{n}^{(0)}) &\cong \tilde{\alpha}_{i(j)}^{(3)}(\bar{n}_{th}^{(0)}) \end{aligned}\right\}. \tag{9}$$

On the other hand, the time dependency of the carrier density $\bar{n}^{(0)}$ is given by

$$\frac{d\bar{n}^{(0)}}{dt} = -n_I\sqrt{\frac{\epsilon_0}{\mu_0}} \left(\frac{2}{\hbar\omega_1} \tilde{\alpha}_1^{(1)} \tilde{E}_1^2 + \frac{2}{\hbar\omega_2} \tilde{\alpha}_2^{(1)} \tilde{E}_2^2\right) - \frac{\bar{n}^{(0)}}{\tau_s} + \frac{I}{V_I e} \tag{10}$$

where greek τ_s is the mean lifetime related to spontaneous emission, I is the injection current, V_I is the volume of

the active region, and e is the electron charge. Further explanations of the quantities appearing in (5)–(10) can be found in [8]. Numerical values used for calculations in the present paper were derived by referring to the discussions in [8] and are summarized in the following:

$$\left.\begin{aligned}
&\langle M^2\rangle = 2.0 \times 10^{-57}\ (\mathrm{C}^2 \cdot \mathrm{m}^2),\\
&g^{(1)} = 2.4 \times 10^{-20},\\
&h' = 3 \times 10^{39}\ (\mathrm{m}^{-5}),\quad n_G^{(1)} = 1.6 \times 10^{24}\ (\mathrm{m}^{-3}),\\
&|\lambda_i - \lambda_0| = 5\ (\mathrm{nm}),\\
&\omega_1 \cong \omega_2 \cong 2.36 \times 10^{15}\ (\mathrm{rad/s}),\\
&\xi^{(1)} = 0.2,\quad \tau_{in} = 3 \times 10^{-13}\ (\mathrm{s}),\\
&n_G^{(3)} = 1.7 \times 10^{24}\ (\mathrm{m}^{-3})\quad V_l = 2.4 \times 10^{-16}\ (\mathrm{m}^3),\\
&n_l = 3.6,\quad \alpha_{\mathrm{th}} = 5 \times 10^{3}\ (\mathrm{m}^{-3}),\\
&\tau_s = 3 \times 10^{-9}\ (\mathrm{s}),\ \bar{n}_{\mathrm{th}}^{(0)} = 2.6 \times 10^{24}\ (\mathrm{m}^{-3})
\end{aligned}\right\} \tag{11}$$

Because we expected that spontaneous emission acts as a triggering force for mode hopping, several analog computer simulations were carried out by adding the square of the amplitude $\tilde{E}_{Ni}$ $(i = 1, 2)$ of the fluctuating electric field of spontaneous emission to the right side of (4). This treatment has already led to a successful result with reference to mode hopping in a 1.5 μm InGaAsP laser [4].

Two uncorrelated Gaussian white noises, generated from two noise generators, were applied to the analog computer as the additional spontaneous emission terms $\tilde{E}_{Ni}^2$ of (4). The amplitudes of the output signals from the noise generators were adjusted so that the root-mean-square values of $\tilde{E}_{Ni}$ could be fixed around a value which will be estimated in Section IV [see (25)]. Furthermore, as long as the wavelength separation between the two modes was less than about 1 nm, it was found that the following approximation was valid using (5)–(7) and the numerical values of (11);

$$\left.\begin{aligned}
&\bar{n}^{(0)} - n_G^{(1)} \gg h'(\lambda_i - \lambda_0)^2\\
&1 \gg \tau_{in}^2(\omega_i - \omega_j)^2
\end{aligned}\right\}. \tag{12}$$

This also leads to the following approximation:

$$\left.\begin{aligned}
&\tilde{\alpha}_1^{(1)} \cong \tilde{\alpha}_2^{(1)}\\
&\tilde{\alpha}_1^{(3)} \cong \tilde{\alpha}_2^{(3)}\\
&\tilde{\alpha}_{1(2)}^{(3)} \cong \tilde{\alpha}_{2(1)}^{(3)}
\end{aligned}\right\}. \tag{13}$$

which means that this model can be used to describe the situation in which the intensities of two modes are almost equal, as was experimentally investigated [Fig. 2(b)]. Fig. 6 shows the output waveforms of $\tilde{E}_1^2$, $\tilde{E}_2^2$, $\tilde{E}_1^2 + \tilde{E}_2^2$, and $\bar{n}^{(0)}$ from the analog computer. Switching of the intensities between the two modes is clearly seen in this figure, which means that mode hopping occurred by spontaneous emission. Fig. 7 gives the power spectral densities of the

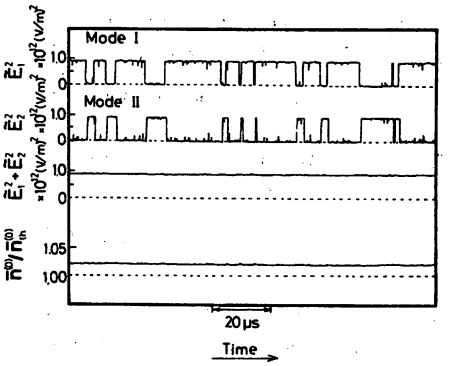

Fig. 6. Output waveforms of $\tilde{E}_1^2$, $\tilde{E}_2^2$, $\tilde{E}_1^2 + \tilde{E}_2^2$, and $\bar{n}^{(0)}$ as calculated by analog computer. $\langle \tilde{E}_{Ni} \rangle = 3.0 \times 10^2$ (V/m) $(i = 1, 2)$.

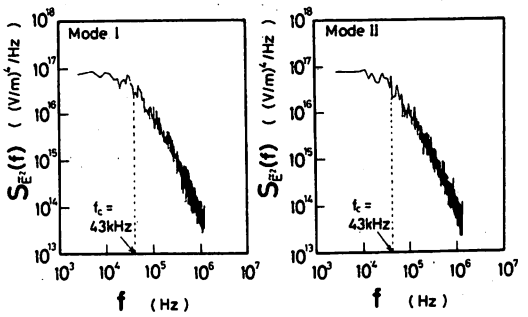

Fig. 7. Power spectral densities of $\tilde{E}_1^2$ and $\tilde{E}_2^2$ shown in Fig. 6.

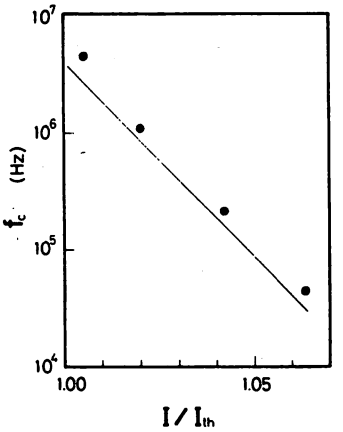

Fig. 8. Relation between I/I_{th} and f_c as calculated by analog computer. •: The results obtained by fixing $\langle \tilde{E}_N \rangle = 3.0 \times 10^2$ (V/m). The solid line corresponds to that of Fig. 5.

fluctuations of $\tilde{E}_i^2$ $(i = 1, 2)$. These curves also show typical Lorentzians, from which it can be confirmed again that mode hopping is induced by spontaneous emission and follows the stochastics of a Poisson process. Fig. 8 gives the relation between I/I_{th} and the cutoff frequency f_c. The cutoff frequency f_c also exponentially decreases with increasing I/I_{th}, which is consistent with the experimental results of Fig. 5. It is seen from Fig. 6 that the value of $\bar{n}^{(0)}$ is almost constant in time, which is due to the fact that the stimulated emission rate is kept constant even though mode hopping occurs. This is concluded from the fact that the value of $\tilde{E}_1^2 + \tilde{E}_2^2$ of Fig. 6 is kept constant, even under mode-hopping conditions. Therefore,

when the two modes oscillate with almost equal intensities as shown in Fig. 2(b), it can be confirmed that the values of $\tilde{\alpha}_i^{(1)}$, $\tilde{\alpha}_i^{(3)}$, and $\tilde{\alpha}_{i(j)}^{(3)}$ do not vary in time.

IV. Analysis Based on the Fokker–Planck Equation

A. Cutoff Frequency and Electric Field of Spontaneous Emission

Dynamics of hopping between two modes of a ring gas laser and a ring dye laser have been investigated through an analysis based on the Fokker–Planck equation [9]–[11]. In this section, this approach is applied to investigate the results obtained in Sections II and III.

The values of $\tilde{\alpha}_i^{(1)}$, $\tilde{\alpha}_i^{(3)}$, and $\tilde{\alpha}_{i(j)}^{(3)}$ of (5)–(7) can be considered as constants because the value of $\bar{n}^{(0)}$ does not vary in time as long as intensities of the two modes are nearly equal, which has been pointed out in the last part of Section III. Therefore, the equation we have to solve in order to describe mode hopping is (4) only, and (10) does not have to be taken into account. This means that the formulations used for a gas laser and a dye laser can also be applied for a semiconductor laser as long as the intensities of the two modes are equal. The analysis based on this formulation is given in the following.

The normalized set of equations of motion, i.e., the Langevin equation for the electric fields of the laser, is

$$\frac{dE_i}{d\tau} = (a_i - |E_i|^2 - \xi|E_j|^2)\,E_i + q_i(\tau) \qquad (i, j = 1, 2;\ i \neq j) \tag{14}$$

where E_i ($i = 1, 2$,) is the normalized amplitude of the electric field of the ith mode, τ is the normalized time, and a_i and τ are the pump parameter and coupling constant defined in [10], respectively. All the quantities in these equations are dimensionless. The quantities $q_i(\tau)$ ($i = 1, 2$) are Langevin noise terms which are supposed to be delta-correlated Gaussian random processes with a zero mean and

$$\langle q_i^*(\tau) \cdot q_j(\tau')\rangle = 4 \cdot \delta_{ij} \cdot \delta(\tau - \tau') \qquad (i, j = 1, 2) \tag{15}$$

where * means the complex conjugate, δ_{ij} is the Kronecker's delta, and $\delta(\tau - \tau')$ is the delta function. The quantities $q_i(\tau)$ represent the fluctuations of spontaneous emission and are proportional to $\tilde{E}_{Ni}$ appearing in Section III. The Langevin equations corresponding to (14) also can be derived from (4) and are

$$\frac{d\tilde{E}_i}{dt} = \frac{1}{2n_l\sqrt{\epsilon_0\mu_0}}[\tilde{\alpha}_i^{(1)} - \alpha_{th} - \tilde{\alpha}_i^{(3)}|\tilde{E}_i|^2 - \tilde{\alpha}_{i(j)}^{(3)}|\tilde{E}_j|^2]\,\tilde{E}_i + \frac{1}{2n_l\sqrt{\epsilon_0\mu_0}}\alpha_{th}\,\tilde{E}_{Ni} \qquad (i, j = 1, 2;\ i \neq j). \tag{16}$$

Comparison between (14) and (16) gives the following relationship:

$$\left.\begin{aligned} \zeta_{Ei} &= \left[\frac{1}{4}\left(\frac{\alpha_{th}}{\tilde{\alpha}_i^{(3)}}\right)^2 r_{N1}r_{N2}\,\frac{\tilde{\alpha}_i^{(1)} - \alpha_{th}}{\tilde{\alpha}_i^{(3)}}\right]^{1/6} \\ \zeta_t &= \frac{2n_l\sqrt{\epsilon_0\mu_0}}{\tilde{\alpha}_i^{(3)}\zeta_{Ei}^2} \\ a_i &= (\tilde{\alpha}_i^{(1)} - \alpha_{th})/\tilde{\alpha}_i^{(3)}\zeta_{Ei}^2 \\ \xi &= \tilde{\alpha}_{i(j)}^{(3)}/\tilde{\alpha}_i^{(3)}. \end{aligned}\right\} \tag{17}$$

where normalized constants ζ_{Ei} and ζ_t are defined as

$$\left.\begin{aligned} \zeta_{Ei} &= \tilde{E}_i/E_i = \tilde{E}_{Ni}/q_i \qquad (i = 1, 2) \\ \zeta_t &= t/\tau \end{aligned}\right\} \tag{18}$$

The value of the coupling constant ξ was easily found to be $\frac{4}{3}$ from (6), (7), and (18). The quantity r_{Ni} of (17) represents the ratio between the root-mean-square value of the fluctuation of the spontaneous emission $\langle\tilde{E}_{Ni}\rangle$ and the stationary value of the electric field of the ith mode, which is expressed as

$$r_{Ni} = \langle\tilde{E}_{Ni}\rangle/[(\tilde{\alpha}_i^{(1)} - \alpha_{th})/\tilde{\alpha}_i^{(3)}]^{1/2} \qquad (i = 1, 2). \tag{19}$$

If we express the normalized complex field amplitude E_i in terms of real and imaginary parts

$$E_i = x_i + i \cdot y_i \qquad (i = 1, 2), \tag{20}$$

the vector $\vec{x}$ [$= (x_1, x_2, y_1, y_2)$] represents the state of the laser, and its components obey a set of coupled Langevin equations of motion given by (14). The Fokker–Planck equation for the probability density $p(\vec{x}, \tau)$ associated with these Langevin equations is given by [10]

$$\frac{\partial}{\partial\tau}p(\vec{x}, \tau) = \sum_{i=1}^{2}\left[-\frac{\partial}{\partial x_i}A_i^{(x)}p - \frac{\partial}{\partial y_i}A_i^{(y)}p + \left(\frac{\partial^2}{\partial x_i^2} + \frac{\partial^2}{\partial y_i^2}\right)p\right] \tag{21}$$

where

$$A_i^{(\eta)} = [a_i - (x_i^2 + y_i^2) - \xi(x_j^2 + y_j^2)]\eta_i \qquad (i, j = 1, 2;\ i \neq j,\ \eta = x, y). \tag{22}$$

The eigenvalue γ of the time-dependent solution for $p(\vec{x}, \tau)$ of (21) has been obtained [10, eq. (8.4)]. The cutoff frequency f_c of Fig. 4 can be derived from γ, and it is

$$f_c = \gamma/\pi\zeta_t = \frac{1}{\pi\zeta_t}\,a^2\,\frac{\sqrt{1 + \xi} - 1}{\sqrt{\pi(1 + \xi)}} \cdot \exp\left[-\frac{a^2(\sqrt{1 + \xi} - 1)^2}{1 + \xi}\right]. \tag{23}$$

In this equation, the approximation $a_1 = a_2$ ($\equiv a$) is used, which is allowed according to (13). Fig. 9 gives the relation between a and f_c derived from (17) and (23). For this derivation, the carrier density is fixed to be

$$\bar{n}^{(0)} = 1.02\,\bar{n}_{th}^{(0)}, \tag{24}$$

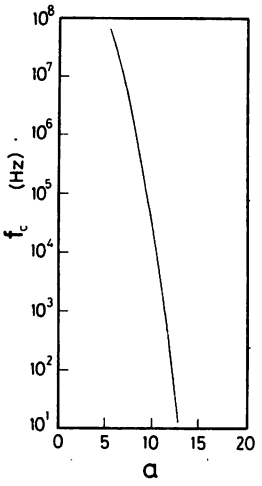

Fig. 9. Relation between a ($\equiv a_1 = a_2$) and f_c given by (23).

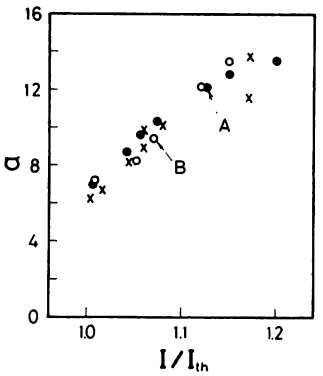

Fig. 10. Relation between I/I_{th} and a estimated using the experimental results of Fig. 5 and the calculated results of Fig. 9. All the points (•, ○, ×) and the meanings of A and B in this figure correspond to those of Fig. 5.

as has been given in Fig. 6. The value of $\bar{r}^{(0)}$ is slightly larger than $\bar{n}_{th}^{(0)}$ as given by this equation, and this difference between $\bar{n}^{(0)}$ and $\bar{n}_{th}^{(0)}$ depended on the intensity of spontaneous emission. However, since this slight difference did not give any notable effects on the values of $\tilde{\alpha}_i^{(1)}$, $\tilde{\alpha}_i^{(3)}$, and $\tilde{\alpha}_{i(j)}^{(3)}$, the value of $\bar{n}^{(0)}$, as given by (24), was used in the following calculations.

The value of f_c in this figure exponentially decreases with increasing a, which is consistent with the experimental results shown in Fig. 5 because a is proportional to $\tilde{\alpha}_i^{(1)} - \alpha_{th}$, i.e., $I/I_{th} - 1$, as given by (17). Experimentally realized values of a can be estimated by comparing Figs. 5 and 9; they are given in Fig. 10 as a function of I/I_{th}.

The root-mean-square value of $\langle \tilde{E}_N \rangle$ ($\equiv \langle \tilde{E}_{N1} \rangle = \langle \tilde{E}_{N2} \rangle$) of the electric field of the spontaneous emission can be estimated from (17)–(19) and Fig. 10 under the approximation $a_1 = a_2$. Estimated values of $\langle \tilde{E}_N \rangle$ are given in Fig. 11. This figure shows that the value of $\langle \tilde{E}_N \rangle$, which contributes as a triggering force to mode hopping, is almost independent of I/I_{th}, and is estimated as being

$$2.3 \times 10^2 \text{ (V/m)} \leqq \langle \tilde{E}_N \rangle \leqq 3.2 \times 10^2 \text{ (V/m)}. \quad (25)$$

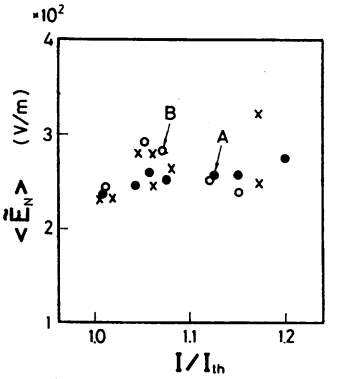

Fig. 11. The root-mean-square values $\langle \tilde{E}_N \rangle$ of the fluctuating electric field of the spontaneous emission as estimated from (17)–(19) and Fig. 10. All the points (•, ○, ×) and the meanings of A and B in this figure correspond to those of Figs. 5 and 10.

The value of $\langle \tilde{E}_N \rangle$ given by (25) is almost equal to the one which has been experimentally obtained for the laser operating near the threshold condition [12], which confirms the present estimation reasonably.

For derivation of Figs. 6–8 in Section III, the values of $\langle \tilde{E}_N \rangle$ were fixed around the value given by (25).

B. Estimation of the Potential

The stationary-state solution of (21) gives the following steady-state probability density $p_s(\vec{x})$:

$$p_s(\vec{x}) = B^{-1} \exp [-U(\vec{x})] \quad (26)$$

where B is the normalization constant and the potential $U(\vec{x})$ is given in [10]

$$U(\vec{x}) = -\tfrac{1}{2} a_1(x_1^2 + y_1^2) - \tfrac{1}{2} a_2(x_2^2 + y_2^2) + \tfrac{1}{4}[(x_1^2 + y_1^2)^2 + (x_2^2 + y_2^2)^2 + 2\xi(x_1^2 + y_1^2)(x_2^2 + y_2^2)]. \quad (27)$$

In this equation, $x_i^2 + y_i^2 (= |E_i|^2)$ is proportional to the intensity of the ith mode. Therefore, it can be transformed into the following expression by representing $x_i^2 + y_i^2$ as I_i:

$$U(I_1, I_2) = -\frac{1}{2}\left\{a(I_1 + I_2) + \frac{\Delta a}{2}(I_1 - I_2)\right\} + \frac{1}{4}(I_1^2 + I_2^2 + 2\xi I_1 I_2) \quad (28)$$

where

$$\left.\begin{aligned} a &= (a_1 + a_2)/2 \\ \Delta a &= a_1 - a_2 \end{aligned}\right\}. \quad (29)$$

The potential $U(I_1, I_2)$ can be estimated if a and Δa are derived from the experimental results. Since the approximation $a_1 = a_2$ is valid for the experiments as shown in Fig. 2(b), Δa may be fixed to zero and the value of a

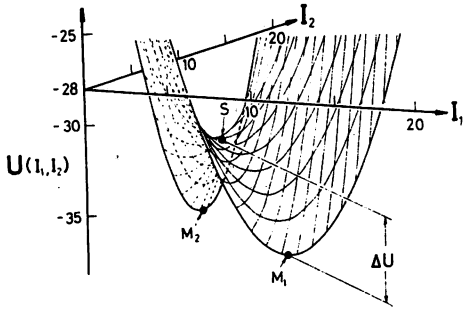

Fig. 12. The form of the potential $U(I_1, I_2)$ where $a = 12.09$ and $\Delta a = 0.05$ (see Appendix). M_1 and M_2 represent the minima, and S is the saddle point of the potential. ΔU represents the depth of the minima measured from the saddle point.

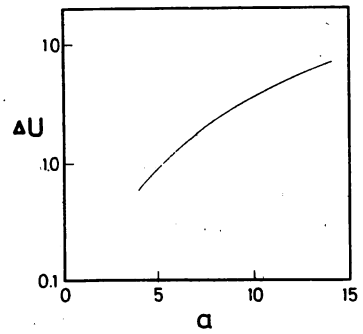

Fig. 13. Relation between a and ΔU calculated from (30) where the approximation $\Delta a = 0$ was used. The value of ξ was fixed to $\frac{4}{3}$.

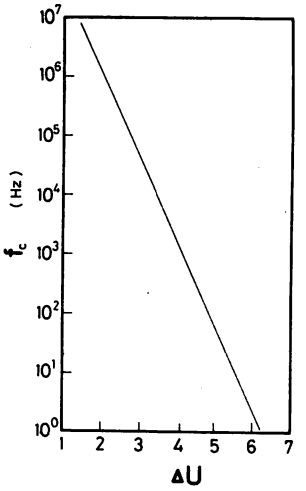

Fig. 14. Relation between ΔU and f_c derived from (23) and (30) where the approximation $\Delta a = 0$ was used. The value of ξ was fixed to $\frac{4}{3}$.

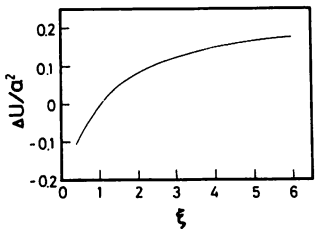

Fig. 15. Relation between the coupling constant ξ and ΔU derived from (30) where the approximation $\Delta a = 0$ was used.

given by Fig. 10 may be employed here. However, it is also possible to evaluate the value of Δa more accurately by following the derivation given by Lett *et al.* [11]. This evaluation is given in the Appendix.

Then the potential $U(I_1, I_2)$ can be obtained using (28) and the value of Δa given in the Appendix. It is given in Fig. 12 and has two minima (M_1, M_2) separated by a saddle point (S). Both of these minima correspond to highly probable states for which one mode intensity is zero, while the other is nonzero. Fluctuations by spontaneous emission drive the representation point in phase space [it also corresponds to Fig. 3(b)] from one minimum to the other at random times. The intensity of each mode therefore tends to jump randomly between zero and nonzero values, which corresponds to the mode-hopping phenomena shown in Fig. 3. The difference between the minimum and the saddle point can be derived from (28) as

$$\Delta U = -(a_1^2 - 2\xi a_1 a_2 + a_2^2)/4(1 - \xi^2) + \frac{a_i^2}{4}. \quad (30)$$

($i = 1$ for the points S and M_1, $i = 2$ for the points S and M_2 in Fig. 12).

Fig. 13 gives the value of ΔU where $\Delta a = 0$ is used. It is seen from this figure that ΔU increases with increasing a. Fig. 14 gives the relation between ΔU and f_c derived from (23) and (30) where $\Delta a = 0$ is also used. It can be clearly seen that f_c decreases with increasing ΔU. From these results, it can be concluded again that an effective way of reducing mode hopping is to increase a, i.e., to increase I/I_{th}, which has been pointed out in Section II. The alternative way for this reduction is to increase the coupling constant ξ between both modes. Fig. 15 gives the relation between $\Delta U/a^2$ and ξ. The negative value of ΔU for $\xi < 1$ means that the potential has a single minimum. This means that both modes oscillate simultaneously, which corresponds to the situation of weak coupling mentioned by Lamb [13]. In the present case, however, the coupling between the modes is strong because $\xi = \frac{4}{3}(> 1)$. Fig. 15 shows that mode hopping can be reduced by increasing ξ. Referring to the detailed derivations of $\tilde{\alpha}_i^{(3)}$ and $\tilde{\alpha}_{i(j)}^{(3)}$ given in [8], it is found that the value of ξ can be increased with increasing overlap of the spatial distributions of the electric fields of both modes in the laser cavity, i.e., with increasing the spatial integral of the term $|F_1(r)\ F_2(r)|$ [cf. (3)]. This should be possible through an appropriate design of the laser cavity.

V. Discussions and Summary

It has sometimes been mentioned that mode hopping is induced by fluctuations of temperature or injection current [14], injected light from the external mirrors into the laser cavity [15], and other deterministic mechanisms [16]. However, it is not probable that the mode hopping we observed was caused by the fluctuations of temperature or injection current because the magnitudes of these fluctuations were so low that jumping between the two hatched areas in Fig. 2(a) was not likely to occur. Furthermore,

mode hopping was actually observed in the present experiment even though the injection of reflected lights into the laser cavity was carefully avoided. These facts suggest that mode hopping is induced by other origins.

Since the typical Lorentzian power spectral density of intensity fluctuations was clearly observed under stable conditions of the present experiments, it is seen that the occurrence of mode hopping is completely random in time, i.e., mode hopping follows the statistics of a Poisson process. Furthermore, the relation between I/I_{th} and the cutoff frequency f_c of this Lorentzian agreed well with the results of the analyses by means of the Fokker–Planck equation [10]. From these facts, it is quite reasonable to believe that mode hopping in a semiconductor laser is induced by the fluctuations of spontaneous emission.

For more detailed discussions, quantum mechanical treatment is required, following the basic theory given by Haken [17], Louisell [18], Sargent *et al.* [19], Yamamoto [20], and Marcuse [21]. However, considered as a first-order approximation, the present treatment can be accurate enough to describe the results of the present experiments.

The experimental and theoretical analyses presented in this paper are for the special case where $a_1 \cong a_2$. If the more general case where $a_1 \neq a_2$ should be treated, the approximation of the constant carrier density $\bar{n}^{(0)}$, as derived from Fig. 6, cannot be valid because the total intensity of the laser may vary in time as a consequence of mode hopping. Therefore, several modifications of the analysis based on the Fokker–Planck equation are required.

Experiments and calculations are now in progress to generalize and improve the accuracy of the analysis.

The results obtained in this study are summarized as follows.

Intensity fluctuations of the longitudinal modes of a 0.8 μm AlGaAs laser were precisely measured under stable experimental conditions during the occurrence of hopping between two modes. Power spectral densities of the fluctuations were typical Lorentzians, from which it was found that mode hopping follows the statistics of a Poisson process. The cutoff frequency of the Lorentzian, i.e., the frequency of mode hopping, was

$$f_c = [\exp[-95(I/I_{th} - 1)]] \times 10^7 \text{ (Hz)}.$$

Results of analog computer simulations showed that spontaneous emission worked as a triggering force for mode hopping. Furthermore, analysis based on the Fokker–Planck equation was carried out. Comparison between this result and experimental results gave the estimated value of the root mean square of the fluctuating electric field of spontaneous emission as

$$2.3 \times 10^2 \text{ (V/m)} \leqq \langle \tilde{E}_N \rangle \leqq 3.2 \times 10^2 \text{ (V/m)}.$$

The form of the potential was also estimated through this analysis. From the discussions given above, it was concluded that an effective reduction of mode hopping is achieved if the laser is operated at a higher bias or if the coupling constant between the two modes is increased.

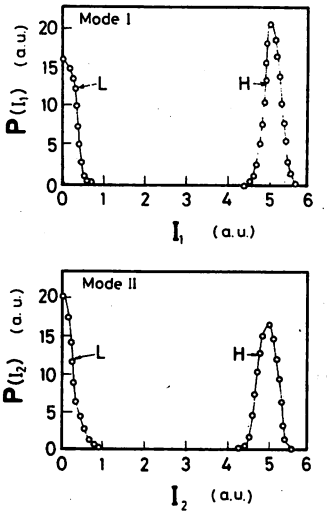

Fig. 16. Histograms, i.e., the probability distributions $P(I_i)$ $(i = 1, 2)$ estimated using the sampled values of the waveforms of the intensity variations of the ith mode. The sampling time was 50 ns. This figure was obtained from the condition corresponding to point A in Fig. 5.

Appendix
Evaluation of Δa

The value of Δa can be estimated more accurately by the following procedure.

The probability distribution $P(I_i)$ of the ith mode has to be calculated for this purpose, which is given by

$$P(I_i) = \int_0^\infty p_s(\vec{x})\, dI_j \qquad (i, j = 1, 2 : i \neq j). \tag{A.1}$$

The value of $P(I_i)$ also can be derived from the experimental results as the histogram of the sampled values of the waveforms of the intensity fluctuations of the ith mode. For a sampling time of 50 ns, this histogram, i.e., the form of the probability distribution $P(I_i)$, is given in Fig. 16. It has two peaks, corresponding to one peak at $I_i = 0$, the low-intensity peak L, and a high-intensity peak H at $I_i \neq 0$. The areas under these two peaks yield the probabilities P_L and P_H that the intensity I_i is low or high, respectively. Their ratio has been theoretically derived from (A.1) as [11]

$$P_H/P_L = \exp(a \cdot \Delta a/2 - 3 \cdot \Delta a/a). \tag{A.2}$$

Therefore, substitution of the value of P_H/P_L obtained from Fig. 16 and the value of a given by Fig. 10 (=12.09) into (A.2) gives for Δa, a value of 0.05. This result was used to obtain the form of the potential of Fig. 12.

Acknowledgment

The authors would like to express their thanks to Prof. Musha and Dr. Asada of the Tokyo Institute of Technology for their valuable discussions. They also wish to thank Prof. Suematsu of the Tokyo Institute of Technology for his encouragement during this work.

REFERENCES

[1] A. Arimoto and M. Ojima, "Diode laser noise at control frequencies in optical disc players," in *Proc. 13th Congr. Int. Commission for Opt.*, Sapporo, Japan, Aug. 1984, p. B4-3.

[2] T. Ito, S. Machida, K. Nawata, and T. Ikegami, "Intensity fluctuations in each longitudinal mode of multimode AlGaAs laser," *IEEE J. Quantum Electron.*, vol. QE-13, pp. 574-579, 1977.

[3] D. E. McCumber, "Intensity fluctuations in the output of CW laser oscillations I," *Phys. Rev.*, vol. 141, pp. 306-322, 1966.

[4] M. Ohtsu, Y. Otsuka, and Y. Teramachi, "Precise measurements and computer simulations of mode-hopping phenomena in semiconductor lasers," *Appl. Phys. Lett.*, vol. 46, pp. 108-110, 1985.

[5] K. Aiki, M. Nakamura, T. Kuroda, J. Umeda, R. Ito, N. Chinone, and M. Maeda, "Transverse mode stabilized $Al_xGa_{1-x}As$ injection lasers with channelled-substrate-planar structure," *IEEE J. Quantum Electron.*, vol. QE-14, pp. 89-94, 1978.

[6] J. S. Bendat and A. G. Piersol, *Random Data: Analysis and Measurement Procedures.* New York: Wiley, 1971.

[7] A. Papoulis, *Probability, Random Variables, and Stochastic Process.* New York: McGraw-Hill, 1984.

[8] M. Yamada and Y. Suematsu, "Analysis of gain suppression in undoped injection lasers," *J. Appl. Phys.*, vol. 52, pp. 2653-2664, 1981.

[9] M. M. Tehrani and L. Mandel, "Intensity fluctuations in a two-mode ring laser," *Phys. Rev. A*, vol. 17, pp. 694-700, 1978.

[10] F. T. Hioe and S. Singh, "Correlations, transients, bistability, and phase-transition analogy in two-mode lasers," *Phys. Rev. A*, vol. 24, pp. 2050-2074, 1981.

[11] P. Lett, W. Christian, S. Singh, and L. Mandel, "Macroscopic quantum fluctuations and first-order phase transition in a laser," *Phys. Rev. Lett.*, vol. 47, pp. 1892-1894, 1981.

[12] Y. Suematsu, S. Akiba, and T. Hong, "Measurement of spontaneous-emission factor of AlGaAs double-heterostructure semiconductor lasers," *IEEE J. Quantum Electron.*, vol. QE-13, pp. 214-218, 1977.

[13] W. E. Lamb, Jr., "Theory of an optical maser," *Phys. Rev.*, vol. 134, pp. A1429-A1450, 1964.

[14] A. Arimoto, M. Ojima, and K. Tatsuno, "Characteristics of laser diodes in optical disc systems" (in Japanese), *Kogaku*, vol. 11, pp. 629-633, 1982.

[15] J. W. M. Biesterbos, A. J. Den Boef, W. Linders, and G. A. Acket, "Low-frequency mode-hopping optical noise in AlGaAs channeled substrate lasers induced by optical feedback," *IEEE J. Quantum Electron.*, vol. QE-19, pp. 986-990, 1983.

[16] G. L. Lippi, J. R. Tredice, N. B. Abraham, and F. T. Arecchi, "Deterministic mode alternation, giant pulses, and chaos in a bidirectional CO_2 ring laser," *Opt. Commun.*, vol. 53, pp. 129-132, 1985.

[17] H. Haken, *Encyclopedia of Physics*, vol. XXV/2c, S. Flugge Ed. Berlin: Springer-Verlag, 1970.

[18] W. H. Louisell, *Quantum Statistical Properties of Radiation.* New York: Wiley, 1973.

[19] M. Sargent III, M. O. Scully, and W. E. Lamb, Jr. *Laser Physics.* Reading, MA: Addison-Wesley, 1974.

[20] Y. Yamamoto, "AM and FM quantum noise in semiconductor laser—Part I: Theoretical analysis," *IEEE J. Quantum Electron.*, vol. QE-19, pp. 34-46, 1983.

[21] D. Marcuse, "Computer simulation of laser photon fluctuations: Theory of single-cavity laser," *IEEE J. Quantum Electron.*, vol. QE-20, pp. 1139-1155, 1985.

Motoichi Ohtsu was born in Kanagawa, Japan, on October 5, 1950. He received the B.S., M.S., and Ph.D.. degrees in electronics engineering from the Tokyo Institute of Technology, Tokyo, Japan, in 1973, 1975, and 1978, respectively.

At present he is an Associate Professor of Graduate School at Nagatsuta, Tokyo Institute of Technology. He is interested in frequency control of lasers, analysis of dynamic behavior of lasers, and its applications to coherent optical measurements and optical communications.

Dr. Ohtsu is a member of the Institute of Electronics and Communication Engineers of Japan, the Institute of Electrical Engineers of Japan, the Japan Society of Applied Physics, and the Optical Society of America. In 1982 he was awarded a prize from the Japan Society of Applied Physics. He was also awarded Issac Koga gold medal from the International Union of Radio Science (URSI) in 1984.

Yasuaki Teramachi was born in Japan in 1947. He received the Doctor's degree in electrical engineering from the Tokyo Institute of Technology, Tokyo, Japan, in 1975.

Since 1976 he has been a Research Associate in the Department of Applied Electronics, Tokyo Institute of Technology. He has been involved in the research program on the body surface potential mapping system and on nonlinear instability of lasers.

Dr. Teramachi is a member of the Physical Society of Japan and the Japan Society of Medical Electronics and Biological Engineering.

Yoshihiro Otsuka was born in Gifu, Japan, on February 2, 1961. He received the B.E. degree in electronics engineering from Kanazawa University in 1983, and the M.E. degree in electronics engineering from the Tokyo Institute of Technology, Tokyo, Japan, in 1985.

He is currently with the NTT Corporation, Japan.

Mr. Otsuka is a member of the Institute of Electronics and Communication Engineers of Japan and the Japanese Society of Applied Physics.

Akio Osaki was born in Niigata, Japan, on October 23, 1962. He joined Hitachi, Ltd., Japan, in 1981. From April 1984 to March 1985, he joined the Tokyo Institute of Technology, Tokyo, Japan, as a Research Student.

ANALYSES OF SUPPRESSION OF MODE HOPPING IN AN AlGaAs LASER BY SATURABLE ABSORBER

Motoichi OHTSU, Yasuaki TERAMACHI [1] and Tetsuya MIYAZAKI
Graduate School at Nagatsuta, Tokyo Institute of Technology, 4259 Nagatsuta, Midori-ku, Yokohama, Kanagawa 227, Japan

Received 19 August 1986

A novel stochastic model based on a formulation by the Fokker–Planck equation was proposed to describe a drastic suppression of mode hopping in an AlGaAs laser, which has been observed when tellurium was doped in its n-type cladding layer. It was found that this suppression was caused by a decrease in the self-saturation coefficient of the laser oscillation due to saturable optical absorption by DX centers. Furthermore, the dependence of this suppression on the laser power confinement ratio in the active layer was evaluated. Calculated results obtained with this model agreed well with the experimental results.

1. Introduction

It has been pointed out that single-longitudinal mode oscillation of an AlGaAs laser can be stabilized by saturable optical absorption from DX centers, i.e., deep-level states or traps, which are created by tellurium (Te) doped in its n-type cladding layer [1,2]. By increasing the amount of Te in a MCSP (modified channeled substrate planar) laser over a threshold value, drastic suppression of mode hopping has been observed [3].

Though some of the effects of this saturable absorber have been theoretically investigated, it should be pointed out that conventional theoretical models present the following problems:

(1) The suppression of mode hopping has been attributed to the spatial variation in the optical loss created by the saturable absorber due to the standing-wave pattern of the single predominant mode [2,3]. Even though the values of the width of the hysteresis loop of mode hopping can be evaluated by this model [2], it is rather difficult to discuss any stochastics of mode hopping which governs the properties of laser power fluctuations. Furthermore, at the edge of the hysteresis loop, the predominant mode cannot be distinguished from the sub-mode because both modes have an equal linear gain at this point. It should be noticed for these discussions that mode hopping is a stochastic process induced by fluctuations of the spontaneous emission, which would require a stochastic model. A relation between Te density N_T and the average frequency f_c of mode hopping, i.e. average number of occurrences of the mode hopping event per unit time, should be derived by using such a model because it has been pointed out that f_c can be used as a measure of describing the stochastic properties of the mode hopping [4].

(2) No theoretical models have been proposed for evaluating quantitatively experimental results of dependences of f_c on N_T, laser power confinement ratio in the active layer, and so on.

A novel theoretical model is proposed in this communication in order to overcome these difficulties and to evaluate quantitatively the effect of a saturable absorber on the mode hopping.

2. Theoretical model

Hopping between two longitudinal modes in a 0.8 μm AlGaAs laser is treated in this paper. The absorption coefficient of a DX center has been given in ref. [5], by which a steady-state value the absorption coefficient for the ith mode can be expressed as

[1] Present address: Institute of Vocational Training, 1960 Aihara, Sagamihara, Kanagawa 229, Japan.

0 030-401/87/$03.50

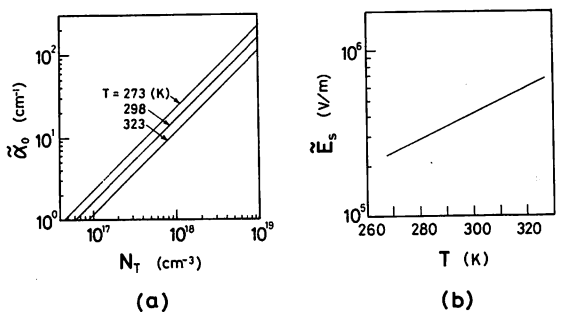

Fig. 1. (a) Relation between N_T and $\tilde{\alpha}_0$ at several temperatures T. (b) Relation between temperature T and saturation parameter $\tilde{E}_s$.

$$\tilde{\alpha}_{ai} = \frac{\tilde{\alpha}_0}{1+(\tilde{E}_i^2+\kappa_{ij}\tilde{E}_j^2)/\tilde{E}_s^2}$$

$$\approx \tilde{\alpha}_0[1-(\tilde{E}_i^2+\kappa_{ij}\tilde{E}_j^2)/\tilde{E}_s^2] ,$$

$$(i,j=1,2;\, i\neq j) , \qquad (1)$$

where $\tilde{\alpha}_0$ is the unsaturated absorption coefficient, $\tilde{E}_i$ is the electric field of the ith mode, and $\tilde{E}_s$ is a saturation parameter. Figs. 1(a) and (b) show the dependences of $\tilde{\alpha}_0$ on N_T and that of E_s on temperature T, respectively, which were calculated by using the numerical values given in ref. [5]. The quantity κ_{ij} in this equation is an overlapping factor which represents the degree of spatial overlap between the profiles of the two modes in the cavity. Straightforward calculations showed that κ_{ij} can be approximated as unity as long as the wavelength difference between the two modes is less than several nanometers, which is a typical case for the mode hopping in an AlGaAs laser. An approximation made at the right hand side of this equation by using a power-series expansion is justified by the experimental results of $\tilde{E}_i^2/\tilde{E}_s^2 < 1/5$ [3]. By this approximation, the effect of saturable absorption can be introduced into the rate equations for $\tilde{E}_i^2$ [4], which are

$$d\tilde{E}_i^2/dt = (1/n_I\sqrt{\epsilon_0\mu_0})$$

$$\times[\tilde{\alpha}_i^{(1)'} - \alpha'_{th} - \tilde{\alpha}_i^{(3)'}\tilde{E}_i^2 - \tilde{\alpha}_{i(j)}^{(3)'}\tilde{E}_j^2]\tilde{E}_i^2 ,$$

$$(i,j=1,2;\, i\neq j) . \qquad (2)$$

Quantities $\tilde{\alpha}_i^{(1)'}$, α'_{th}, $\tilde{\alpha}_i^{(3)'}$, $\tilde{\alpha}_{i(j)}^{(3)'}$ in this equation are the linear gain, cavity loss, self-saturation coefficient, and cross saturation coefficient, respectively, in which contributions from the saturable optical absorption of eq. (1) has been included. They are expressed as

$$\tilde{\alpha}_i^{(1)'} = \tilde{\alpha}_i^{(1)} , \qquad (3)$$

$$\alpha'_{th} = \alpha_{th}(1+\epsilon_{th}\tilde{\alpha}_0) , \qquad (4)$$

$$\tilde{\alpha}_i^{(3)'} = \tilde{\alpha}_i^{(3)'}(1-\epsilon_{3i}\tilde{\alpha}_0/\tilde{E}_s^2) , \qquad (5)$$

$$\tilde{\alpha}_{i(j)}^{(3)'} = \tilde{\alpha}_{i(j)}^{(3)}[1-(1/\xi)\kappa_{ij}\epsilon_{3i}\tilde{\alpha}_0/\tilde{E}_s^2] ,$$

$$(i,j=1,2;\, i\neq j) , \qquad (6)$$

where $\tilde{\alpha}_i^{(1)}$, α_{th}, $\tilde{\alpha}_i^{(3)}$, and $\tilde{\alpha}_{i(j)}^{(3)}$ are the values at $N_T=0$. These quantities have been derived by density matrix formulation [6,7]. The details have been summarized in ref. [4], in which it has been also pointed out that $\tilde{\alpha}_1^{(1)'} \approx \tilde{\alpha}_2^{(1)'}$, $\tilde{\alpha}_1^{(3)'} \approx \tilde{\alpha}_2^{(3)'}$, and $\tilde{\alpha}_{1(2)}^{(3)'} \approx \tilde{\alpha}_{2(1)}^{(3)'}$ as long as the wavelength difference between the two modes is less than several nanometers. The quantities of eqs. (3), (5), and (6) depend on the carrier density $\bar{n}^{(0)}$ in the active layer. The quantity ϵ_{th} and ϵ_{3i} of eqs. (4)–(6) are constants derived by using the material constants of an AlGaAs laser, which are 8.5×10^{-5} (m) and 7.0×10^{9} (V^2/m), respectively. The quantity ξ in eq. (6) is a coupling constant between the two modes at $N_T=0$, which is 4/3. Since $\tilde{\alpha}_0$ is proportional to N_T, eqs. (4)–(6) mean that the cavity loss α'_{th} is increased, and saturation coefficients $\tilde{\alpha}_i^{(3)'}$ and $\tilde{\alpha}_{i(j)}^{(3)'}$ are decreased with increasing N_T, respectively.

The equation of motion for carrier density $\bar{n}^{(0)}$ in the active layer is given by

$$d\bar{n}^{(0)}/dt = -n_I\sqrt{\epsilon_0/\mu_0}[(2/\hbar\omega_1)\tilde{\alpha}_1^{(1)'}\tilde{E}_1^2$$

$$+(2/\hbar\omega_2)\tilde{\alpha}_2^{(1)'}\tilde{E}_2^2] - \bar{n}^{(0)}/\tau_s + I/V_I e , \qquad (7)$$

where detailed descriptions of the quantities in this equation have been given in ref. [4].

In this equation of motion, contributions of a fraction of the carrier density, which is trapped by or released from the DX center in the cladding layer, were neglected. This is based on the plausible assumption that the amount of such carrier density, which may diffuse between the cladding layer and the active layer, can be considerably lower than that of $\bar{n}^{(0)}$ [8].

It is assumed in the following discussions that the steady-state values of the two mode powers are equal with each other. This assumption is satisfied at the edge of the hysteresis loop, at which the mode hopping can most likely occur. In this case, the value of the stimulated emission rate (the quantity given in the parenthesis of the right hand side of eq. (7)) is kept unchanged with time because $\tilde{\alpha}_1^{\{1\}'} \approx \tilde{\alpha}_2^{\{1\}'}$ and the value of $\tilde{E}_1^2 + \tilde{E}_2^2$ is kept constant even under the mode hopping conditions. This means that the carrier density $\bar{n}^{(0)}$ of eq. (8), the value of $\tilde{\alpha}_i^{\{1\}'}$, $\tilde{\alpha}_i^{\{3\}'}$, and $\tilde{\alpha}_{i(j)}^{\{3\}'}$ in eq. (2) are also kept constant, as have been confirmed also by an analog computer simulation [4]. The constant value of the carrier density can be expressed as

$$\bar{n}^{(0)}/n_{\mathrm{th}} = 1 + \epsilon_{\mathrm{n}} , \qquad (8)$$

where n_{th} is the value of the carrier density at the threshold of laser oscillation, and ϵ_{n} is a constant which depends on the magnitude of the fluctuations of spontaneous emission and takes a value between 1×10^{-4} and 2×10^{-2} [4].

As the carrier density is fixed at the constant value of eq. (8), eq. (7) does not have to be taken account in the following discussions. The equation we have to solve is eq. (2) only. Since all the coefficients of eq. (2) are assumed as constant, it makes it easy to treat the mode hopping phenomenon by a formulation of the Fokker–Planck equation. As the first step of this formulation, the normalized set of equation of motion, i.e., the Langevin equation for the electric fields of the laser, is derived from eq. (2) by adding to it the Langevin terms, which is

$$\mathrm{d}E_i/\mathrm{d}\tau = (a_i' - E_i^2 - \xi' E_j^2)E_i + q_i(\tau) ,$$

$$(i, j = 1, 2;\ i \neq j) , \qquad (9)$$

where E_i $(i=1, 2)$ is the normalized amplitude of the electric field of the ith mode, and τ is the normalized time. The quantities a_i' and ξ' are a pump parameter of the ith mode and coupling constant between the two modes, respectively. The quantities $q_i(\tau)$ $(i=1, 2)$ are Langevin noise terms representing fluctuations of spontaneous emission which are supposed to be delta-correlated gaussian random processes with a zero mean. The pump parameter a_i' corresponds to the bias level for the laser oscillation, which is given by the ratio between the steady-state mode power and the mean square value of the fluctuations of spontaneous emission $\langle \tilde{E}_{\mathrm{N}i}^2 \rangle$ which works as a triggering force for the oscillation of the ith longitudinal mode. This is expressed as

$$a_i' = (\tilde{\alpha}_i^{\{1\}'} - \alpha_{\mathrm{th}}')/\tilde{\alpha}_i^{\{3\}'} \langle \tilde{E}_{\mathrm{N}i}^2 \rangle , \quad (i=1, 2). \qquad (10)$$

In the present case, $a_1' = a_2'$ ($\equiv a'$) because the steady-state values of the two mode powers are equal. The coupling constant ξ' is given by

$$\xi' = \alpha_{i(j)}^{\{3\}'}/\tilde{\alpha}_i^{\{3\}'} , \qquad (i, j=1, 2:\ i \neq j). \qquad (11)$$

The values of a_i' and ξ' depend on N_{T}, which means that the mode hopping properties also depend on N_{T}.

As the second step, the Fokker–Planck equation for the probability density $p(E_1^2, E_2^2, \tau)$ associated with these Langevin equations is derived. A time-dependent solution of the Fokker–Planck equation takes the form of $\exp(-\gamma\tau)$ [4,10], from which the average frequency of mode hopping is expressed as

$$f_{\mathrm{c}} = \frac{\gamma}{\pi\zeta_{\mathrm{t}}} = \frac{1}{\pi\sqrt{\pi}\zeta_{\mathrm{t}}} \left(1 - \frac{1}{\sqrt{1+\xi'}}\right)$$

$$\times (a')^2 \exp\left\{-\left[a'\left(1 - \frac{1}{\sqrt{1+\xi'}}\right)\right]^2\right\} , \qquad (12)$$

where ζ_{t} is a normalization constant used to derive the dimensionless time τ of eq. (9) from the real time t of eq. (2) [4].

3. Calculated results and discussions

Since the value of f_{c} of eq. (12) depends on the quantities of eqs. (3)–(6), it can be connected with the material constants of the laser. Fig. 2 shows the dependence of f_{c} on N_{T} derived from eq. (12). A drastic decrease in the value of f_{c} can be seen at $N_{\mathrm{T}} \geqslant 5\times10^4 \sim 5\times10^{16}$ (cm^{-3}) ($\equiv N_{\mathrm{Tth}}$) for 273 K $\leqslant T \leqslant$ 323 K, where N_{Tth} is the threshold Te density which was conveniently defined by $f_{\mathrm{c}}(N_{\mathrm{T}}=N_{\mathrm{Tth}}) = (1/10)\, f_{\mathrm{c}}(N_{\mathrm{T}}=0)$. The value of N_{Tth} can therefore be used as a measure of the Te density required to suppress the mode hopping. The phenomenon of such a drastic decrease in f_{c} is consistent with the experimental results [3]. That is, a drastic suppression of mode hopping has been experimentally observed at

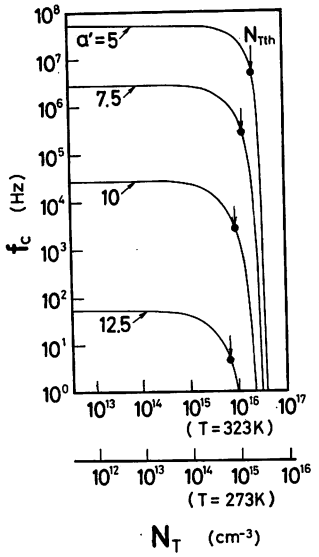

Fig. 2. Relation between N_T and f_c for several values of pump parameters a'. $\xi^{(1)}=0.2$.

$$N_T \geqslant N_{Tth}=4\times10^{17}/[(1-\xi^{(1)})/2] \ (\mathrm{cm}^{-3}), \quad (13)$$

at 273 K$\leqslant T\leqslant$323 K, where $\xi^{(1)}$ is the laser power confinement ratio in the active layer on which the quantities of eqs. (3)–(6) depend. However, the value of N_{Tth} of fig. 2 is lower than the one given by this equation, which can be due to the inaccuracies of estimating the values of T, $\tilde{\alpha}_0$, $\tilde{E}_s$, and so on. More accurate estimations of these parameters will improve the accuracy of estimation of N_{Tth}. Fig. 2 also shows that the mode hopping can be suppressed by a lower N_{Tth} if the laser is operated with a higher bias, i.e., with a larger a'.

Figs. 3(a) and (b) show dependences of f_c and N_{Tth} on the laser power confinement ratio $\xi^{(1)}$, respectively. It can be seen from these figures that the value of N_{Tth} increases with increasing $\xi^{(1)}$, which is because the contribution of the saturable absorber in the cladding layer decreases if a larger fraction of the light power is confined in the active layer. This dependence is consistent with the experimental results given by the empirical formula of eq. (4).

To investigate the origins of these drastic decreases in f_c, the dependence of the pump parameter a' on N_T was derived and is shown by fig. 4(a), in which a drastic increase in a' can be seen with increasing N_T. In spite of the fact that the cavity loss α'_{th} of eq. (4)

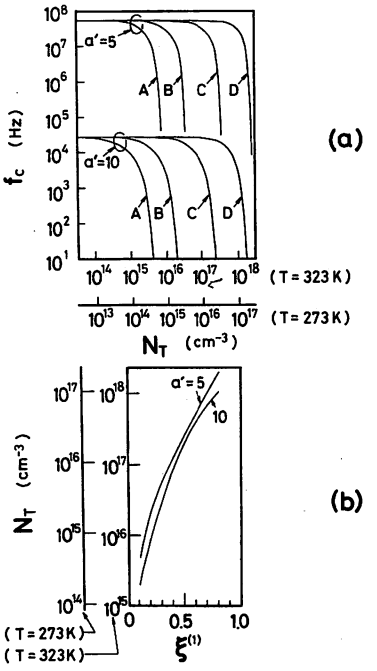

Fig. 3. (a) Relation between N_T and f_c for several values a' and $\xi^{(1)}$. $\xi^{(1)}=0.1$ (A), 0.2 (B), 0.5 (C), 0.8 (D). (b) Relation between $\xi^{(1)}$ and N_{Tth}, where N_{Tth} was defined as $f_c(N_T=N_{Tth})=(1/10)\,f_c(N_T=0)$.

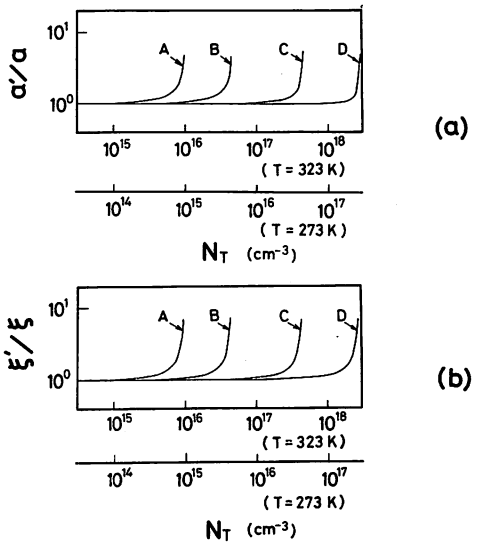

Fig.4. (a) Relation between N_T and a' for several values of $\xi^{(1)}$, where a is the value of a' at $N_T=0$. $\xi^{(1)}=0.1$ (A), 0.2 (B), 0.5 (C), 0.8 (D). (b) Relation between N_T and ξ' for several values of $\xi^{(1)}$, where ξ ($=4/3$) is the value of ξ' at $N_T=0$. $\xi^{(1)}=0.1$ (A), 0.2 (B), 0.5 (C), 0.8 (D).

is increased with increasing N_T, a simultaneous decrease of self-saturation coefficient $\tilde{\alpha}_i^{(3)'}$ of eq. (5) induced such a drastic increase in a', which can be confirmed by referring to eq. (10). By this drastic increase in a', a drastic decrease in f_c is induced, as can be seen from eq. (13).

Furthermore, fig. 4(b) shows the dependence of the coupling constant ξ' on N_T, where $\xi' = 4/3$ ($\equiv \xi$) at $N_T = 0$ [4,6,7]. A drastic increase in ξ' can be also seen in this figure with increasing N_T. This can be understood by noticing that a decrease in the self-saturation coefficient $\tilde{\alpha}_i^{(3)'}$ induced by increasing N_T is ξ times larger than that in the cross-saturation coefficient $\tilde{\alpha}_{ij}^{(3)'}$, as can be confirmed by comparing eqs. (5) and (6). The difference of the decreases in these two saturation coefficients could induce an increase in ξ' of eq. (11). And by this increase in ξ', the value of f_c drastically decreased, as can be seen from eq. (13).

It can therefore be concluded that the origins of the drastic decrease in f_c are twofold, i.e., increases in a' and ξ'. Both of them are induced mainly by decreases in the self-saturation coefficient, which is caused by saturable optical absorption.

4. Summary

A phenomenon of drastic suppression of mode hopping observed above a certain value of doped Te density was successfully explained by employing a stochastic model. It was found that this suppression was caused by decreases in the self-saturation coefficient of the laser oscillation due to saturable optical absorption, and by the resultant increases in bias level and coupling constant between the two modes. Furthermore, a dependence on the laser power confinement ratio was quantitatively evaluated, for which only an emperical formula has been given so far. It was confirmed that the average frequency of mode hopping can be used as an appropriate measure to analyze the stochastic properties of the mode hopping.

Acknowledgements

The authors would like to express their thanks to Dr. Chinone of Hitachi Ltd. for the demonstrations of his experimental results. They also wish to thank Dr. Asada of the Tokyo Institute of Technology for his valuable comments on the theoretical model.

References

[1] J.L. Merz, J. van der Ziel and R.A. Logan, Phys. Rev. B. 20 (1979) 654.
[2] J.A. Copeland, IEEE J. Quantum Electron. QE-16 (1980) 721.
[3] N. Chinone, T. Kuroda, T. Otoshi, T. Takahashi and T. Kajimura, IEEE J. Quantum Electron. QE-21 (1985) 1264.
[4] M. Ohtsu, Y. Teramachi, Y. Otsuka and A. Osaki, IEEE J. Quantum Electron. QE-22 (1986) 535.
[5] T. Ikoma and S. Kumashiro, Seisan Kenkyu (in Japanese) 35 (1983) 53.
[6] M. Yamada and Y. Suematsu, J. Appl. Phys. 52 (1981) 2653.
[7] M. Asada and Y. Suematsu, IEEE J. Quantum Electron. QE-21 (1985) 434.
[8] N. Chinone, private communication, 1986.
[9] J.A. Copeland, Electron. Lett. 14 (1978) 809.
[10] F.H. Hioe and S. Singh, Phys. Rev. A 24 (1981) 2050.

Instabilities in Laser Diodes by Optical Feedback, Modulation and Mode-Hopping

Yasuaki Teramachi*, Tetsuya Miyazaki and Moto-ichi Ohtsu

Graduate School at Nagatsuta, Tokyo Institute of Technology
Nagatsuta,Midoriku,Yokohama,Kanagawa,JAPAN

Abstract

In the deeply modulated laser diode, chaotic behaviors are observed. There are two types of routes to chasos depending on the modulation frequency. When the modulation frequency is at least 1.7 times higher than the relaxation frequncy, period-two instabilties are easily induced the period-two and the period-four instabilties are observed on the way to chaos.

Introduction

Laser diodes are used as light sources for high speed optical communication systems because direct injection current modulation is available. High frequency modulations of laser diodes are sometimes used to suppress optical feedback noise(1). Direct modulation of laser diodes is an important technique for applications of laser diodes. If modulation index is increased, it shows period doubling phenomena in output light intensity. Further increasing modulation index, results chaotic instability. This phenomenon was theoretically predicted by Lee et. al.(2). Kawaguchi(3) calculated this phenomenon in the laser diode with saturable absorber. Chen et.al.(4) experimentally observed subharmonic bifurcations and irregular pulsations in semiconductor lasers. Winful et. al.(5) showed that there is a different route to chaos through quasiperiodic oscillations in the laser diode with selfsustained pulsations. Thus there are a variety of chaotic fluctuations in laser diodes. On the otherhand, Wiesenfelt et. al.(6) showed the possibility of small signal amplification by period-doubling system if the system is near the onset of period-doubling. Derighetti et.al.(7) experimentally showed this small signal amplification phenomenon in the NMR laser. Then we tried experiments on modulation induced fluctuations in the D.F.B.(Distributed Feed-Back) laser diode and analogue computer simulations. In the D.F.B. laser diode, longitudinal mode is kept single even if it is modulated deeply. This makes it easy to compare experimental results and theoretical analyses.

Experiment

The sample laser diode is the D.F.B. type and its wavelength is 1.5 micron-meter. In this type of laser diode, single longitudinal mode operation is available under deeply modulated conditions. The block diagram of the experimental apparatus is shown in Fig.1.

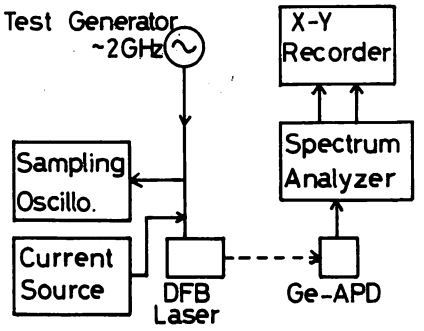

Fig. 1

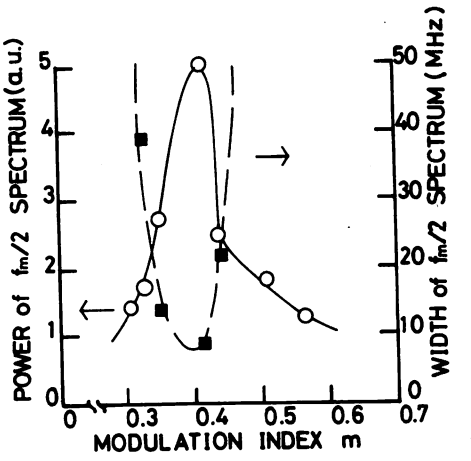

Fig. 2

*Present address:The Institute of Vocational Training, Department of Information Science
1960,Aihara,Sagamihara,Kanagawa,JAPAN

A germanium avalanche photo diode is used to detect laser output. Output signals are supplied to a spectrum analyser to analyse power spectra. High frequency modulation current is superimposed to D.C. bias current for a direct modulation of the laser diode. This modulation current is monitored by a sampling oscilloscope. When the modulation frequency is 1.88 GHz, instability whose frequency is one half of the modulation frequency is induced. An amplitude of this instabilitis increases as the modulation current increases. If the modulation current increases further, this amplitude decreases again. This relation is plotted as open circles in Fig.2. Half line-widths of these instabilities are plotted as full squares in Fig.2. When the modulation frequency is 0.94 GHz, instabilties of this frequency are observed while components of period-two are not observed.

Analogue Computer Simulation

The dynamics of this laser diode are described by the following rate equations for the photon density S and the active carrier density N,

$$\frac{dN}{dt} = \frac{I}{I_{th}} \frac{N_{th}}{\tau_s} - \frac{N}{\tau_s} - A (N - N_o) S \qquad (1)$$

$$\frac{dS}{dt} = A (N - N_o) S - \frac{S}{\tau_p} + \frac{N}{\tau_s} \qquad (2)$$

Here I is the injection current, Ith and Nth are the threshold current and the threshold carrier density, tau s and tau p are the spontaneous electron and photon lifetimes, respectively. A is the gain coefficient, Beta is the fraction of spontaneous emission coupled into a lasing mode. No is the minimum electron density required to obtain a positive gain. The modulation current, normalised by its threshold value, is

$$I = I_b (1 + m \sin 2\pi f_m t) \qquad (3)$$

where, m is the modulation index. The parameters used in the calculation are as follows:

$A = 1 \times 10^{-12}$ m^3/s, $N_o = 1 \times 10^{24}$ m^{-3}, $\beta = 1 \times 10^{-4}$, $\tau_p = 1 \times 10^{-12}$ s,

$\tau_s = 3 \times 10^{-9}$ s, $I_b / I_{th} = 1.4$.

The value of β is selected as an fitting parameter to adjust the threshold modulation index for period-two instabilities at fm /fr = 2 in the experiment and the simulations. Temporal variations of photon densities at fr/fm = 2 are shown in Fig.3. In the small modulation index, oscillations whose frequency is equal to that of the modulation signal are induced(Fig.3-a). Increasing modulation index, these oscillations become spiky(Fig.3-b) and reach period-two instabilities(Fig.3-c). Bifurcation of peak intensities is observed. In the period-two regime, peaks of lower height are not located at the center of two higher peaks. With a further increased the modulation index, these oscillations become chaotic(Fig.3-d). Power spectrum densities of these wave forms are shown in Fig.4. The period-four component is not clear, but its odd order higher harmonics appear.

Wave forms of photon densities at fm/fr = 2.7 are shown in Fig.5. When a modulation index is small, oscillations whose frequency is fm are induced. If a modulation index exceeds some threshold value, the waveform changes rapidly from sinusoidal oscillation to spiky oscillation with period-two. Thus, relaxation oscillation are induced parametrically. In this regime, lower peaks are not clear. Bifurcation of the instability is not observed. Period-four oscillations are induced by increasing the modulation index. With a further increased the modulation index, an output light signal becomes chaotic. Repeating these processes results the instability diagram shown in Fig.6. The abscissa indicates the normalized frequency and the ordinate indicates the modulation index. Routes to chaos are different depending on whether the normalized frequency of the modulation signal is larger than 1.7 or not. An arrow in Fig.6 indicates the range of the experiment. Thus, several times larger modulation index is necessary to realize period two instabilities when fm/fr is less than 1.7. Components of period two at fm/fr = 2 depend on the modulation index as is shown in Fig.7. This shows a similar characteristic as in Fig.2.

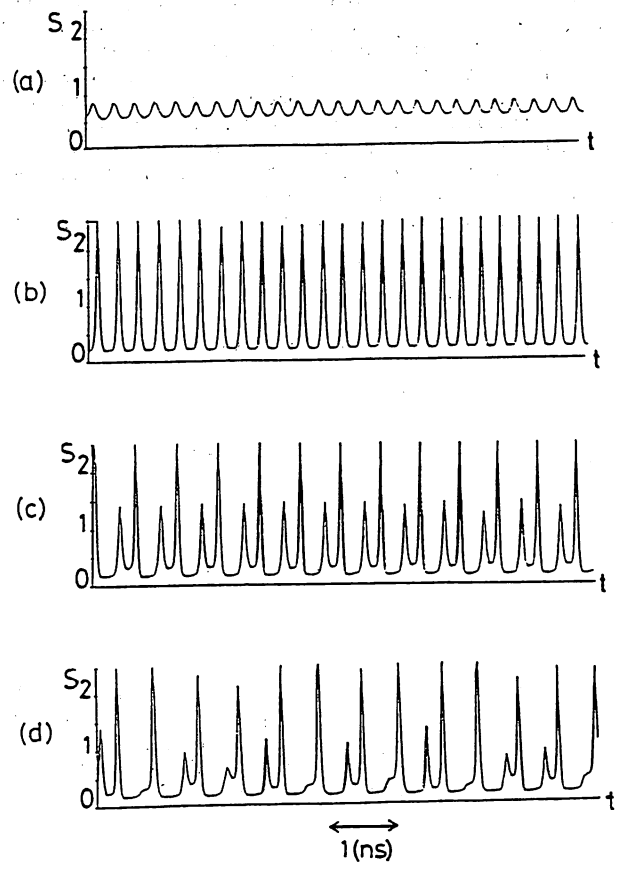

Fig. 3

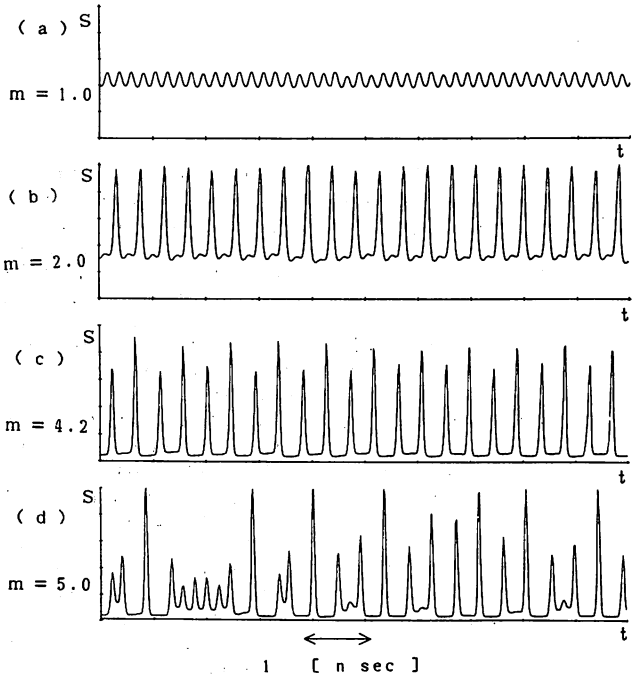

Fig. 4

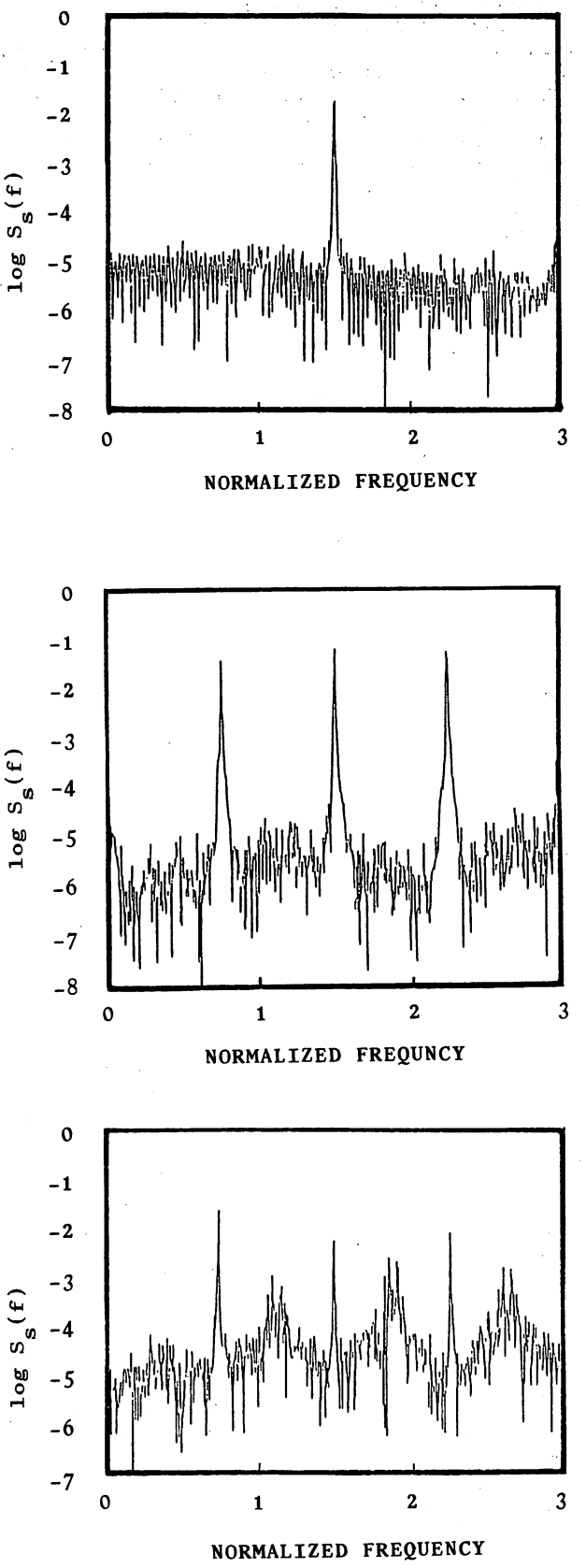

Fig. 5

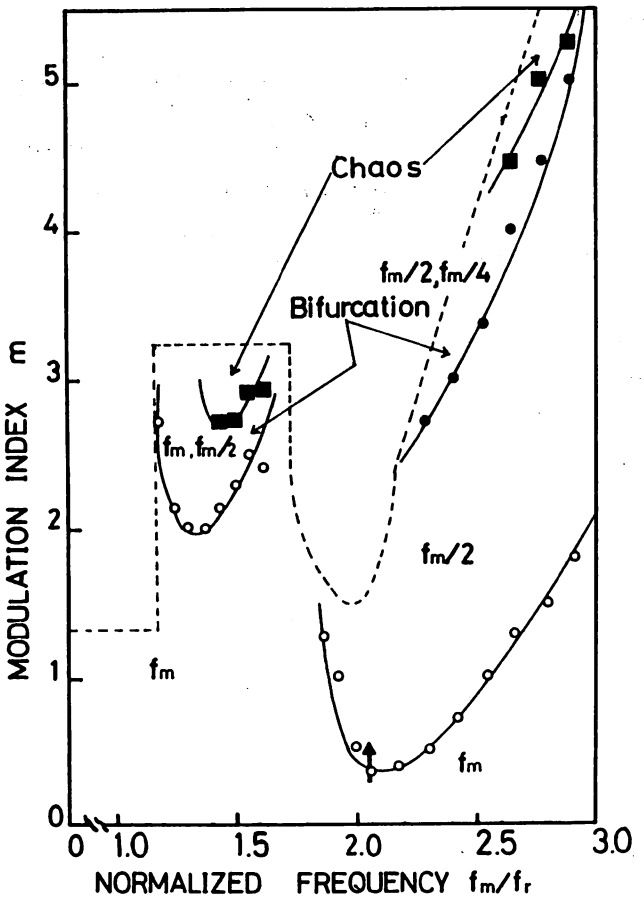

Fig. 6

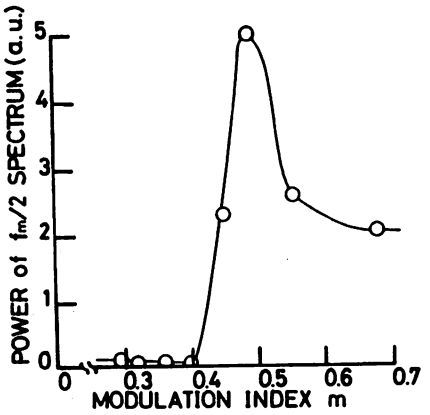

Fig. 7

Acknowledgments

We are deeply appteciate to Dr. C.O.Weiss of P.T.B. in Germany for his cooperation on the experiments and to Dr.H.Kawaguchi of N.T.T.for his helpful sugestions.

References

(1) A.Arimoto,M.Ojima,N.Chinone,and A.Oishi. Technical Digest CLEO, Anaheim California, 19-22, June, 1984
(2) C.H.Lee,T.H.Yoon,and S.Y.Shin, Appl.Phys. Lett. 46,95(1985)
(3) H.Kawaguchi, Appl.Phys.Lett. 45,1264(1984)
(4) Y.C.Chen,H.G.Winful,and J.M.Liu, Appl.Phys.Lett. 47,208(1985)
(5) H.G.Winful,Y.C.Chen,and J.M.Liu, Appl.Phys.Lett. 48,616(1986)
(6) K.Wiesenfeld,and Bruce McNamara, Phys.Rev.Lett. 55,13(1985)
(7) B.Derighetti,M.Ravani,R.Stoop,P.F.Meier,and E.Brun, Phys.Rev.Lett. 55,1746(1985)

Conference on Lasers and Electro-Optics (CLEO'87), April - May 1987, Baltimore, MD, THD3, pp.218 - 219

THD3 Mode stability of a two-wavelength Fabry-Perot/distributed-feedback laser

M. OHTSU, K.-Y. LIOU, AT&T Bell Laboratories, Crawford Hill Laboratory, Holmdel, NJ 07733.

By detuning the Bragg wavelength of a distributed-feedback (DFB) laser away from the peak wavelength of the gain spectrum, simultaneous oscillation of the DFB mode and the Fabry-Perot (F.-P.) mode near the gain peak can be achieved. Such a two-wavelength laser can be used for interferometric sensing or measurement of fiber dispersion. We present calculations of the mode stability for the design of a two-wavelength laser and the observed two-wavelength operation of a F.-P./DFB laser.

Figure 1 shows the longitudinal mode spectrum of a 1.3-μm DFB laser with the DFB mode detuned to $\sim$110 Å shorter than the gain peak. The dual-wavelength spectrum with nearly equal DFB and F.-P. mode powers shown in the figure was due to similar threshold conditions for the DFB and F.-P. modes obtained by temperature control.

In the theory, we use a stochastic approach to calculate the stability for the two-mode condition. Starting with rate equations in density matrix formalism for the carrier density and the powers of the DFB and the F.-P. modes,[1] coupled Langevin equations were derived and then expressed by a multidimensional Fokker-Planck equation. The probabilistic power fluctuations for the DFB and the F.-P. modes were then evaluated by solving the Fokker-Planck equation.

Power fluctuations of the DFB and F.-P. modes arise from the coupling between them, which can be described by a coupling constant

$$\xi = (4/3)/[1 + (2\pi c\tau_{in}\Delta\lambda/\lambda^2)^2],$$

where τ_{in} is the intraband relaxation time, c and λ are the vacuum light speed and wavelength, and $\Delta\lambda$ is the wavelength difference between the DFB and F.-P. modes. Mode stability is also dependent on the pumping level given by $a = C_1(I/I_{th}) - C_2$. The constants $C_1 \simeq 45$ and $C_2 \simeq 40$ have been measured for 0.8- and 1.5-μm lasers at $I > 1.01I_{th}$.[2]

Figure 2 shows the calculated variance σ^2 of the intensity fluctuations, normalized by the average intensity $\langle I(t)\rangle$, at different pumping levels a for the DFB mode. A common critical point at $\xi = 1$ is found for all values of a. Discrete mode hops between the DFB and F.-P. modes due to a strong coupling occur for $\xi > 1$. In the weak coupling regime, $\xi < 1$, and DFB and F.-P. modes oscillate simultaneously. We note that σ^2 decreases drastically with decreasing ξ and that stable two-wavelength operation can be achieved for a sufficiently large pumping level. Figure 2 is valid for all λ and can be used to evaluate τ_{in}.

The temporal intensity fluctuation, $\delta I(t) = I(t) - \langle I(t)\rangle$, was derived from the time-dependent solution of the Fokker-Planck equation. If $(|\delta I(t)|/\langle I(t)\rangle) \leq \epsilon$ is required for the temporal mode stability, the escape probability P_e that $(|\delta I(t)|/\langle I(t)\rangle)$ exceeds ϵ can be calculated. Figure 3 shows calculated P_e for the DFB mode for different ξ and a values. For specified P_e and ϵ values, Fig. 3 gives the coupling constant ξ (or $\Delta\lambda$) and pumping level a that should be designed into the laser to achieve satisfactory system performance.

Summarizing: We developed a theory based on a Fokker-Planck equation to analyze the observed mode behavior of a two-wavelength F.-P./DFB laser. The parametric calculations in the theory provide the mode-stability criteria for the design of stable two-wavelength lasers. **(12 min)**

1. M. Yamada and Y. Suematsu, J. Appl. Phys. **52**, 2653 (1981).
2. M. Ohtsu *et al.*, IEEE J. Quantum Electron. **QE-22**, 535 (1986).

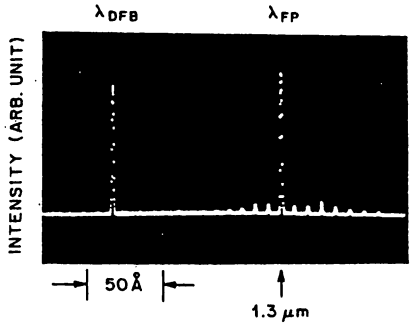

THD3 Fig. 1. Longitudinal-mode spectrum of a Bragg wavelength-detuned DFB laser showing simultaneous oscillation of the DFB and F.-P. modes.

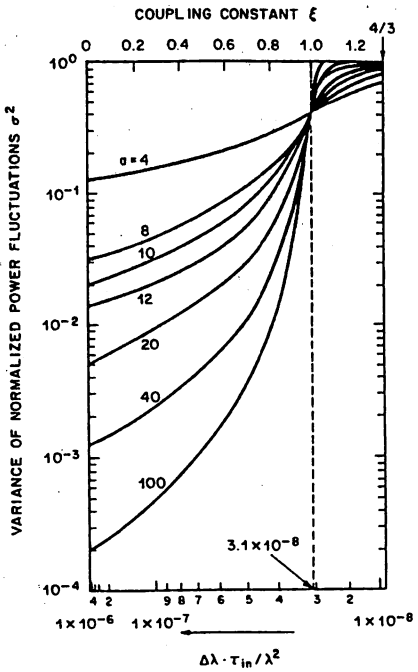

THD3 Fig. 2. Calculated variance σ^2 of normalized intensity fluctuations vs the coupling constant ξ between the DFB and F.-P. modes for different pumping levels a.

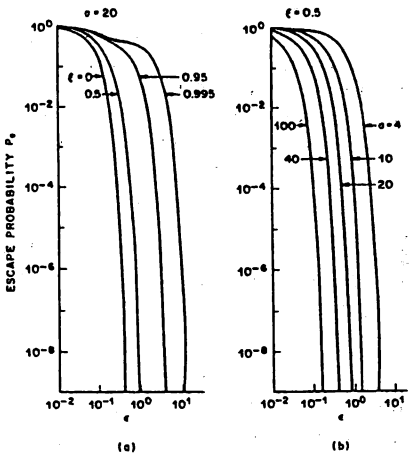

THD3 Fig. 3. Calculated probability P_e that the amplitude of the intensity fluctuation of the DFB mode exceeds a normalized intensity range ϵ.

Experiments on a Semiconductor Laser Pumped Rubidium Atomic Clock

MINORU HASHIMOTO AND MOTOICHI OHTSU

Abstract—**Experiments were carried out to evaluate the performances of a semiconductor laser pumped rubidium (^{87}Rb) atomic clock. Two kinds of Rb gas cells were used and their performances were compared [gas cell *A* (natural rubidium (^{87}Rb/^{85}Rb = $\frac{3}{7}$) and buffer gases) and gas cell *B* (^{87}Rb and buffer gases)]. The highest microwave frequency stabilities were estimated as $3.4 \times 10^{-12}\,\tau^{-1/2}$ and $2.7 \times 10^{-12}\,\tau^{-1/2}$ at the optimal gas cell temperatures of 60°C and 48°C for the gas cells *A* and *B*, respectively (τ: integration time). The light shift, i.e., microwave frequency shift induced by laser light, was measured as −0.50 Hz/MHz and −0.11 Hz/MHz for the gas cells *A* and *B* at their optimal operating conditions given above. As an improved experiment by utilizing high temporal coherence of the laser, a novel double resonance spectral line shape with a drastically narrower linewidth was demonstrated. A technique, similar to FM laser spectroscopy, was employed for this purpose by utilizing laser FM sidebands which are induced by microwave frequency modulation and nonlinear susceptibility of three-level ^{87}Rb atoms. The minimum linewidth obtained was 20 Hz, which can be used as a sensitive frequency discriminator for an improved ^{87}Rb atomic clock.**

I. Introduction

HIGHLY stable microwave frequency oscillators have been required for many applications such as satellite communications, satellite tracking, global positioning system (GPS), and so on. Portable cesium (^{133}Cs) atomic clocks and rubidium (^{87}Rb) atomic clocks have been used for these applications, and improvements of their performances are essential for the progresses of these applications.

For these improvements, optical pumping and optical detection by semiconductor lasers have been proposed for ^{133}Cs atomic clocks [1]. In the case of optical pumping for ^{87}Rb atomic clocks, a replacement of a RF-excited ^{87}Rb lamp by a semiconductor laser has been proposed, and preliminary experiments on laser pumped ^{87}Rb atomic clocks have been reported [2]. However, optimal conditions of optical-microwave double resonance and quantitative evaluations of light shift have not yet been fully documented. Furthermore, an advantageous property of high temporal coherence of lasers has not been utilized.

In the present study, experiments were carried out to improve the performances of ^{87}Rb atomic clocks by using a semiconductor laser. The experimental setup is described in Section II. In Section III, results of the measurements of the signal-to-noise ratio and linewidth of double resonance spectral line are presented to find the optimal conditions for the highest microwave frequency stability. In Section IV, results of quantitative measurements on the light shift, i.e., the microwave frequency shift induced by pumping light, are given. A novel double-resonance spectral lineshape is demonstrated in Section V, which has drastically narrower linewidth obtained by utilizing a high temporal coherence of the laser.

Manuscript received May 26, 1986; revised October 20, 1986. This work was supported in part by a Grant-in-Aid for Scientific Research from the Ministry of Education, Science, and Culture of Japan, and by the Hoso Bunka Foundation.

The authors are with the Graduate School at Nagatsuta, Tokyo Institute of Technology, Midori-ku, Yokohama, Kanagawa 227, Japan.

IEEE Log Number 8613230.

II. Experimental Setup

Fig. 1 shows an experimental setup for a laser pumped ^{87}Rb atomic clock, in which a commercially available ^{87}Rb atomic clock (Fujitsu 5407A) was used. Two kinds of resonance gas cells, which have been used for these ^{87}Rb atomic clocks, were alternately used to compare their properties, i.e., the one with natural rubidium vapor (^{87}Rb/^{85}Rb = $\frac{3}{7}$) and buffer gases (gas cell *A*), and the one with ^{87}Rb vapor and buffer gases (gas cell *B*). The same buffer gases (Ar/N_2 = 1.65 total pressure = 43 torr) were filled in these gas cells. The gas cells were made of cylindrical glass tubes, whose diameter and length were 30 and 35 mm, respectively. An RF-excited ^{87}Rb lamp, a resonance gas cell, and a microwave cavity (TE_{011}) were installed in the resonance part of the clock. The lamp was replaced by a 0.78 μm AlGaAs semiconductor laser (Hitachi HL7802E) in the present study. Optical-microwave double resonance signals were measured by detecting the laser power transmitted through the gas cell by using a solar cell (Sharp SPD110).

The laser light was linearily polarized. Temperature fluctuations of laser was reduced to a value as low as 1 mK at the room temperature by using an alcohol circulating bath and a peltier element. A low noise current supply was used to control the injection current of the laser, whose bandwidth was 1 kHz. The oscillation spectral linewidth of the semiconductor laser was estimated as 40 MHz by observing the spectral linewidth of the beat signal between the independently oscillating two lasers. The laser frequency was stabilized to the center frequency of a linear absorption spectral line in ^{87}Rb, i.e., the ^{87}Rb-D_2 lines, in cell *A* or *B* for the experiments given in Sections III and IV. The resultant laser frequency stability was $4.4 \times 10^{-11}\tau^{-1}$ for 10 ms $\leqq \tau \leqq$ 100 s (τ: integration time), which was as high as the one obtained by using a ^{85}Rb-D_2 line [3]. This stability was high enough for reproduc-

0018-9197/87/0400-0446$01.00

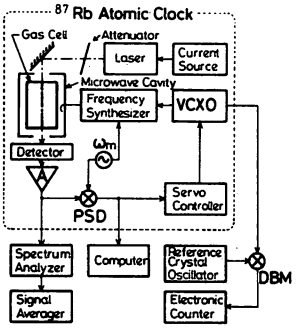

Fig. 1. Experimental setup. PSD: phase sensitive detector. VCXO: voltage controlled crystal oscillator. DBM: double balanced mixer. A: post-detector amplifier. ω_m: angular frequency of a low frequency oscillator used for microwave frequency modulation.

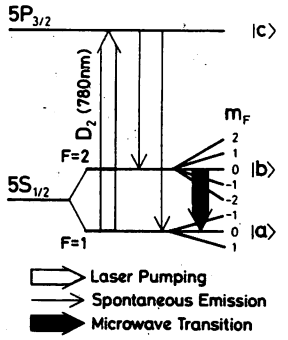

Fig. 2. Energy levels of a ^{87}Rb atom relevant to the present study.

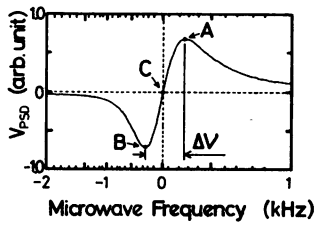

Fig. 3. Derivative of double resonance spectral lineshape $\Delta\nu$: a linewidth defined by a separation between the points A and B. V_{PSD}: output voltage from the phase sensitive detector.

ible measurements of double resonance signals. The laser was used under a free-running condition in Section IV because its frequency must be slowly varied to measure the light shift. However, the frequency stability of this free-running laser was still high enough for reproducible measurements of the light shift because of low fluctuations of temperature and injection current.

In Section III, the signal-to-noise ratio was measured at the output-port of the post-detector amplifier of Fig. 1 by using a spectrum analyzer. A signal averager connected after a spectrum analyzer was used to improve the reproducibility of the signal-to-noise ratio measurements. For precise measurements of the double resonance linewidth, the output signals from the phase sensitive detector were accumulated by a computer to make a smoothing of double resonance spectral lineshape.

For the light shift measurements in Section IV, a divided frequency (5.000000 MHz) of the stabilized output signal from the ^{87}Rb atomic clock was heterodyned with the output frequency (4.999950 MHz) of a highly stable reference crystal oscillator (NDK TS615A) by a double balanced mixer, and the interval of the heterodyned signal was counted by an electronic counter.

III. Temperature Dependences of Double Resonance Signals

The energy levels of ^{87}Rb-D_2 lines are given by Fig. 2. A microwave transition (6.8 GHz) between two hyperfine levels in the ground state, induced by the double-resonance, has been utilized as a frequency reference for ^{87}Rb atomic clocks. Fig. 3 shows the first derivative of such an optical-microwave double resonance spectral line, which was obtained by modulating the microwave frequency (modulation frequency $\omega_m/2\pi$ was 160 Hz) and by tracing the output signal from a phase sensitive detector (PSD). The laser frequency was locked to the center frequency of the optical transition spectral line in ^{87}Rb ($5S_{1/2}$ $F = 1 \rightarrow 5P_{3/2}$). Nonlinearity of the abscissa in this figure was due to the nonlinear voltage-frequency characteristics in the voltage controlled crystal oscillator used. The slope at the center of this dispersive curve can be used as a frequency discriminator for microwave frequency stabilization. The microwave frequency stability depends on the signal-to-noise ratio (SNR) and the linewidth of this derivative signal, i.e., the sensitivity of the frequency discriminator. Therefore, the frequency stability can be expressed as [4]

$$\sigma_y(\tau) = \frac{0.2}{Q(\mathrm{SNR})}\tau^{-1/2} \qquad (1)$$

where $\sigma_y(\tau)$ is the square root of the Allan variance of microwave frequency fluctuations [5], τ is the integration time, and Q is a quality factor of the frequency discriminator which is given by

$$Q = \nu_{M0}/\Delta\nu. \qquad (2)$$

Here, ν_{M0} is the microwave transition frequency (point C in Fig. 3), and $\Delta\nu$ is the linewidth of the derivative shape which is defined as the separation between points A and B of Fig. 3. Since it is essential to find a larger SNR value and a narrower linewidth for higher microwave frequency stability, they were explored in the present study. Fig. 4(a) and (b) shows the temperature dependences of the values of the SNR of cells A and B, respectively, measured at Fourier frequency $\omega_m/2\pi$. As can be seen from these figures, the value of the SNR was increased with increasing the temperature, which is because of the increases of the ^{87}Rb vapor pressure. However, it was decreased by further increases in the temperature. Though the causes of this decrease have not yet been fully investigated, one of the possible causes can be the decrease in population inversion between hyperfine levels of the ground state due to thermal de-excitation. It can be also seen that a saturation effect by higher laser power density decreased the SNR value. Fig. 5(a) and (b) shows the temperature dependences of linewidths of cells A and B,

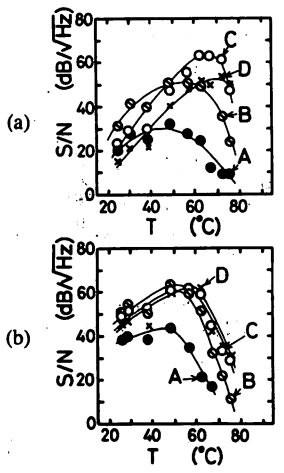

Fig. 4. Temperature dependences of signal-to-noise ratio (SNR) for the gas cells A (a) and B (b) measured at the Fourier frequency $\omega_m/2\pi$ (= 160 Hz). The laser power density was fixed at 14.4 $\mu W/cm^2$ (A, ●), 43.2 $\mu W/cm^2$ (B, ⊘), 288 $\mu W/cm^2$ (C, ○), and 576 $\mu W/cm^2$ (D, ×).

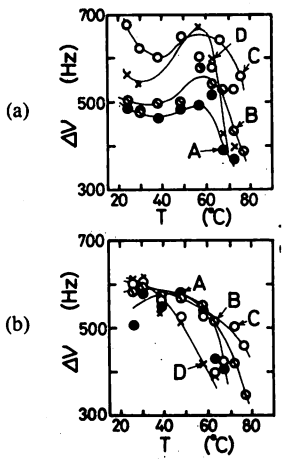

Fig. 5. Temperature dependences of linewidth ($\Delta\nu$) for the gas cells A (a) and B (b). The laser power density was fixed at 14.4 $\mu W/cm^2$ (A, ●), 43.2 $\mu W/cm^2$ (B, ⊘), 288 $\mu W/cm^2$ (C, ○), and 576 $\mu W/cm^2$ (D, ×).

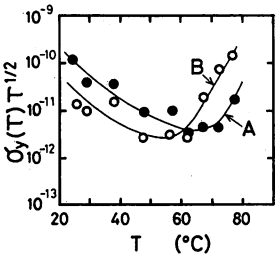

Fig. 6. Temperature dependences of estimated frequency stability for the gas cells A (A, ●) and B (B, ○). $\delta_y(\tau)$: square root of the Allan variance of residual fluctuations in microwave frequency. τ: integration time.

respectively. Substitutions of the measured values of Figs. 4 and 5 into (1) give the estimated frequency stability, which is given by Fig. 6. Two curves in this figure possess the optimal temperatures to realize the highest frequency stability. The highest stabilities were almost equal with each other, and are expressed as

gas cell A:

$$\delta_y(\tau) = 3.4 \times 10^{-12}\tau^{-1/2} \quad \text{at} \quad 60°C, \qquad (3)$$

TABLE I
NUMERICAL VALUES OF OPERATING PARAMETERS TO GIVE THE HIGHEST FREQUENCY STABILITY

Operating Parameters	Numerical Values	
	Cell A	Cell B
Temperature (°C)	60	48
Laser power density ($\mu W/cm^2$)	288	43
Signal-to-noise ratio ($dB/\sqrt{Hz}$)	63	66
Linewidth (Hz)	525	570

gas cell B:

$$\delta_y(\tau) = 2.7 \times 10^{-12}\tau^{-1/2} \quad \text{at} \quad 48°C. \qquad (4)$$

Numerical values of other parameters to give (3) and (4) are all summarized in Table I.

IV. Measurements of Light Shift

The dynamic stark effect by the electric field of pumping light would induce the light shift, i.e., the shift in microwave transition frequency. Since this frequency is used as a frequency reference for ^{87}Rb atomic clocks, the light shift can limit their frequency accuracy as well as frequency stability. Precise evaluations of light shift have been rather difficult in the conventional ^{87}Rb atomic clocks because of the complicated spectral profile of the ^{87}Rb lamp. However, more precise evaluations can be carried out by using semiconductor lasers with their narrower spectral linewidth, which could be useful to improve the frequency accuracy and stability of ^{87}Rb atomic clocks.

Figs. 7 and 8 show the results of light shift measurements of cells A and B, respectively. The measurements were carried out at the temperatures given in (3) and (4). The abscissa and ordinate in each figure represent laser frequency detuning $\Delta\nu_L$ and microwave frequency shift $\Delta\nu_M$, respectively. It is seen that each curve in these figures clearly exhibits a dispersive shape, which is consistent with a result of theoretical predictions [6]. Since all the dispersive curves crossed at a common point, this point was taken as the origin of the axes in each figure. This origin represents the resonance frequency of the microwave transition which is free from the light shift. It means that the laser frequency must be fixed at this point in order to avoid the effect of the light shift to improve the frequency accuracy.

Even if the laser frequency is fixed at this point, the microwave frequency would be fluctuated by the residual laser frequency fluctuations around this point, which can deteriorate microwave frequency stability. The magnitudes of the induced fluctuations in the microwave frequency are proportional to the slope at this point. This slope also depends on the irradiated laser power density, which is shown by Fig. 9. In this figure, the slopes at the laser power densities in Table I are given by

gas cell A:

$$\Delta\nu_M/\Delta\nu_L = -0.50 \text{ Hz/MHz at } 288 \ \mu W/cm^2, \qquad (5)$$

gas cell B:

$$\Delta\nu_M/\Delta\nu_L = -0.11 \text{ Hz/MHz at } 43 \ \mu W/cm^2. \qquad (6)$$

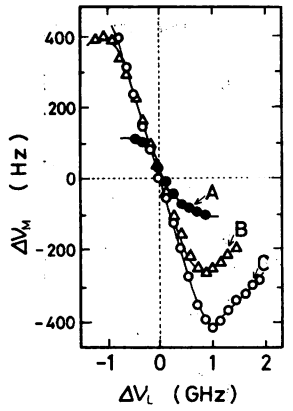

Fig. 7. Light shift $\Delta\nu_M$ induced by laser frequency for the gas cell A at 60°C. $\Delta\mu_L$: the laser frequency detuning. Since all the curves crossed at a common point, this point was taken as the origin of the axes in this figure. The laser power density was fixed at 79.2 $\mu W/cm^2$ (A, ●), 288 $\mu W/cm^2$ (B, Δ), and 562, $\mu W/cm^2$ (C, ○).

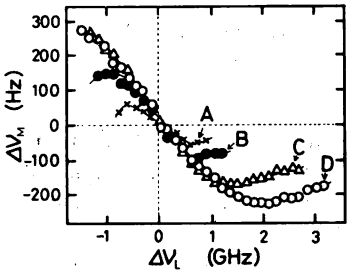

Fig. 8. Light shift $\Delta\nu_M$ induced by laser frequency for the gas cell B at 48°C. $\Delta\nu_L$: the laser frequency detuning. The laser power density was fixed at 43 $\mu W/cm^2$ (A, ×), 79.2 $\mu W/cm^2$ (B, ●), 288 $\mu W/cm^2$ (C, Δ), and 562 $\mu W/cm^2$ (D, ○).

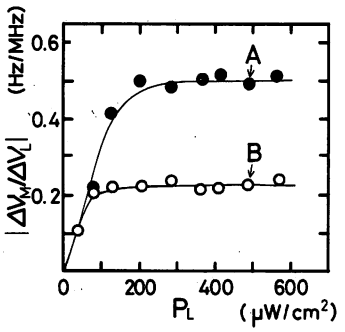

Fig. 9. Slopes of the curves of Figs. 7 (●) and 8 (○) at $\Delta\omega_L = 0$.

From the comparison between these values, it can be concluded that a use of gas cell B is more advantageous to maintain higher microwave frequency stability if the effects of residual laser frequency fluctuations are not neglected.

V. Observation of a Novel Double Resonance Spectral Shape with Narrower Linewidth

Equation (1) indicates that the frequency stability can be improved by using a narrower linewidth of the double-resonance spectral line. Buffer gases have been employed for this purpose, in which a phenomenon of so-called Dicke narrowing has been utilized for the linewidth reduction [7].

However, to our knowledge, any novel linewidth reduction techniques have not been proposed for ^{87}Rb atomic clocks since the proposal of this Dicke narrowing scheme. In this section, a novel technique of linewidth reduction is proposed by utilizing an advantageous property of the laser, i.e., high temporal coherence.

This technique employed the laser FM sidebands induced by microwave frequency modulation and nonlinear susceptibility of three-level ^{87}Rb atoms, which is briefly explained in the following. The three-level model of the atom is employed to analyze the optical-microwave double resonance [8]. As was shown in Fig. 2, two hyperfine levels of the ground state of ($5S_{1/2}$, $F = 1$, $m_F = 0$) and ($5S_{1/2}$, $F = 2$, $m_F = 0$), and an excited state ($5P_{3/2}$) correspond to the relevant three levels, which are expressed as $|a>$, $|b>$, and $|c>$, respectively. The magnetic field of microwave and the electric field of laser are represented as

$$H_M(r, z, t) = \left(H_M J_0(3.832r/R) \sin(k_M z)/2\right) \exp\left[-i\omega_M t\right] + \text{c.c.} \quad (7)$$

$$E_L(z, t) = (E_L/2) \exp\left[-i(\omega_L t - k_L z)\right] + \text{c.c.} \quad (8)$$

where H_M and E_L are amplitudes of the magnetic and electric fields, ω_M and ω_L are angular frequencies, k_M and k_L are wave vectors, J_0 is the Bessel function of the 0th order, R is cavity diameter, z and r are the positions along the cylindrical microwave cavity axis and radius, and c.c. represents a complex conjugate. The transmissivity T of the amplitude of the laser electric field through the gas cell can be derived by solving equations of motion for the density matrix of the three-level model under the perturbations due to external fields given by (7) and (8). The solution can be expressed as $T = \exp[-\delta - i\phi]$, where δ and ϕ are amplitude attenuation and phase shift, respectively. Detailed derivations will be published elsewhere [9], however, the results are summarized in the following.

Though general expressions of δ and ϕ are given by the plasma dispersion function [10], they can be simplified if the drift velocity (v) of ^{87}Rb atoms in buffer gases are sufficiently low, i.e., $|k_L v|$, $|k_M v| \ll 1$, and if the laser frequency is exactly tuned to the optical transition frequency. The simplified expressions are given by

$$\delta = \frac{\omega_{ca} L_g}{2\epsilon_0 c} \chi_{ca} \left[1 + (\gamma''_{ab} - \gamma'_{ab}) \frac{\gamma'_{ab}}{(\omega_{ba} - \omega_M)^2 + \gamma'^2_{ab}}\right] \quad (9)$$

and

$$\phi = \frac{\omega_{ca} L_g}{2\epsilon_0 c} \left[2 + \chi_{ca}(\gamma''_{ca} - \gamma'_{ca}) \frac{(\omega_{ba} - \omega_M)}{(\omega_{ba} - \omega_M)^2 + \gamma'^2_{ab}}\right] \quad (10)$$

where

$$\gamma'_{ab} = \gamma_{ab} + \frac{\gamma_{ca} x_L^2}{\gamma_{cb}\gamma_{ca} + x_M^2} \quad (11)$$

$$\gamma''_{ab} = \gamma_{ab} + \frac{(n_a - n_c)x_L^2 - (n_a - n_b)x_M^2}{(n_a - n_c)\gamma_{cb}} \quad (12)$$

$$\chi_{ca} = \frac{|\mu_{ca}|^2 (n_a - n_c)\gamma_{cb}}{\hbar(\gamma_{cb}\gamma_{ca} + x_M^2).} \quad (13)$$

L_g is the length of the gas cell, c is the speed of light, ϵ_0 is dielectric constant of vacuum, ω_{ca} is angular frequency of the optical transition between the levels $|c>$ and $|a>$, γ_{xy} $(x, y = a, b, c\ x \neq y)$ is a transverse relaxation constant, x_M and x_L are the Rabi angular frequencies of microwave and laser, respectively, μ_{ca} is an electric dipole moment between the levels $|a>$ and $|c>$, and n_x $(x = a, b, c)$ is a population of each level.

Since the phase shift ϕ of (10) depends on the microwave angular frequency ω_M, the phase of the transmitted laser light is modulated by modulating microwave frequency. As a result of such an induced phase modulation, FM sidebands would appear in the electric field of the transmitted laser light. It can be expressed as

$$E_T = (E_L'(t)/2) \exp[-i(\omega_L t - k_L z)] + \text{c.c.} \quad (14)$$

where

$$E_L' = E_L \sum_q T_q(\omega_M + q\omega_m) J_q(M) \exp[iq\omega_m t], \quad (15)$$

ω_m is the modulation angular frequency of the microwave, T_q is the transmissivity at the laser angular frequency $\omega_L + q\omega_m$ $(q = 0, \pm 1, \pm 2, \pm 3, \cdots)$, $J_q(M)$ is the Bessel function of the qth order, and M is the modulation index. The light power detected by a photodetector is given by $I_T(t) = c|E_L'|^2/8\pi$, which is expressed as follows if $|\delta|$, $|\phi| \ll 1$ and the laser FM sidebands up to the third order are retained for calculations

$$I_T(t) = I_0[A + B\cos\omega_m t + C\sin\omega_m t] \quad (16)$$

where

$$I_0 = \frac{c|E_L|^2}{8\pi} \quad (17)$$

$$A = J_3^2(1 - 2\delta_{-3}) + J_2^2(1 - 2\delta_{-2}) + J_1^2(1 - 2\delta_{-1}) + J_0^2(1 - 2\delta_0) + J_1^2(1 - 2\delta_1) + J_2^2(1 - 2\delta_2) + J_3^2(1 - 2\delta_3) \quad (18a)$$

$$B = 2[J_2J_3(\delta_{-3} + \delta_{-2} - \delta_2 - \delta_3) + J_1J_2(\delta_{-2} + \delta_{-1} - \delta_1 - \delta_2) + J_0J_1(\delta_{-1} - \delta_1)] \quad (18b)$$

and

$$C = 2[J_2J_3(\phi_{-3} - \phi_{-2} - \phi_2 + \phi_3) + J_1J_2(\phi_{-2} - \phi_{-1} - \phi_1 + \phi_2) + J_0J_1(\phi_{-1} - 2\phi_0 + \phi_1)]. \quad (18c)$$

δ_q and ϕ_q are the values of attenuation and phase shift at the laser angular frequency $\omega_L + q\omega_m$, respectively. Fig. 10 shows the dependences of A, B, and C of (18) on the microwave angular frequency ω_M. The principal term of A of (18a) is $J_0^2(1 - 2\delta_0)$, in which $(1 - 2\delta_0)$ can be approximated as $\exp(-2\delta_0)$. This quantity represents the laser power attenuation by the ^{87}Rb vapor. The principal terms of B and C of (18b) and (18c) are $J_0J_1(\delta_{-1} - \delta_1)$ and $J_0J_1(\phi_{-1} - 2\phi_0 + \phi_1)$, in which $(\delta_{-1} - \delta_1)$ and $(\phi_{-1} - 2\phi_0 + \phi_1)$ can be approximated as $d\delta/d\omega_M$ and $d^2\phi/d\omega_M^2$, i.e., the first derivative of absorption and the second derivative of dispersion, respectively. The validity of these approximations can be easily confirmed by referring to the profiles of the curves of Fig. 10(a), (b), and (c).

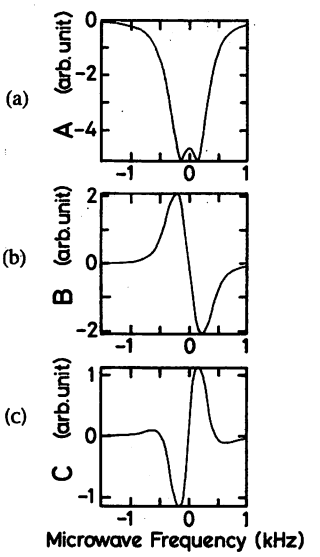

Fig. 10. The dependences of the quantities A, B, and C of (18) on the microwave frequency $\omega_M/2\pi$. Other quantities were fixed at $\omega_m/2\pi$ = 160 Hz, $\gamma_{ab}' = 300\pi$ rad, and $M = 1.8$.

If a reference signal for phase sensitive detection of Fig. 1 is proportional to $\cos(\omega_m t - \theta)$, the output signal V_{PSD} from the phase sensitive detector is expressed as

$$V_{PSD} = V_0[(B/2)\cos\theta + (C/2)\sin\theta]. \quad (19)$$

This equation represents a goal of the present calculations. Since the ratio of the contributions from B and C in this equation is governed by the phase θ, several specific double resonance spectral lineshapes can be obtained by adjusting the value of θ at several values.

Fig. 11(a) shows an example of the experimentally obtained lineshape in gas cell B at 40°C and $\omega_m/2\pi$ = 160 Hz. Similar results were obtained also for gas cell A. Fig. 11(b) shows the simulated result obtained by using (16)–(19), where the values of γ_{ab}', M, and θ were swept so that the lineshape of Fig. 11(b) fits that of Fig. 11(a). This curve was obtained when $\gamma_{ab}' = 140\pi$ rad, $M = 1.8$, and $\theta = 234°$. It is seen from these figures that the lineshape is composed of several fine structures, and the peak-to-peak linewidth at the center of this shape [i.e., the separation between points A and B in Fig. 11(a)] is quite narrower than that of the conventional one (i.e., Fig. 3). Such a narrower linewidth was obtained by utilizing the induced FM sidebands of the laser, and from the discussions given above, it can be recognized that a part of this

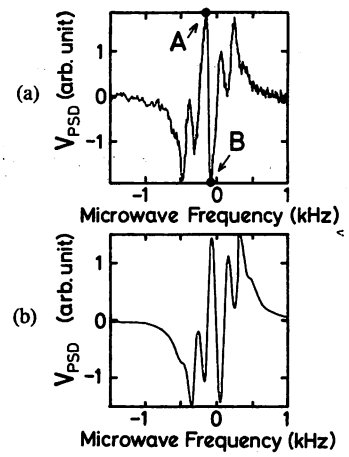

Fig. 11. (a) An example of experimentally obtained lineshape in the cell B at 40°C and $\omega_m/2\pi$ = 160 Hz. (b) Simulated result obtained by using (16)–(19), where the values of γ'_{ab}, M, and θ were swept so that the lineshape of (b) fits that of (a). This fitting was obtained when $\omega_m/2\pi$ = 160 Hz, γ'_{ab} = 140π rad, θ = 234°, and M = 1.8. V_{PSD}: output voltage from the phase sensitive detector.

technique is equivalent to that of the FM laser spectroscopy [11].

Since (19) depends also on several other quantities of ^{87}Rb atoms (e.g., γ'_{ab}, etc), the lineshape of Fig. 11(a) strongly depends not only on θ, but also on the temperature, ω_m, M, x_M^2, and x_L^2. Under a certain temperature, for example, the fine structures of Fig. 11(a) disappeared, and it was reduced the conventional lineshape of Fig. 3 at θ = 0. However, under other operating conditions, the fine structures with a drastically narrow linewidth was appeared, as shown in Fig. 11(a). The minimum linewidth of the gas cell A obtained in the present experiments was 20 Hz at the laser power density of 28.8 μW/cm^2, and that of gas cell B was 56 Hz at 144 μW/cm^2. The linewidth of 20 Hz was $\frac{1}{25}$ times that of the conventional one of Fig. 3. Such a novel lineshape with narrower linewidth can be used as a sensitive frequency discriminator to improve microwave frequency stability. Experiments are now in progress to improve the SNR value of this lineshape in order to use it for this purpose.

V. Summary

Experiments were carried out to evaluate performances of a semiconductor laser pumped ^{87}Rb atomic clock. Two kind of Rb gas cells were used and their performance were compared. The highest microwave frequency stability obtained by using these gas cells were estimated as

Gas cell A (natural Rb and buffer gases):

$$\sigma_y \rightarrow \phi(I) = 3.4 \times 10^{-12}\tau^{-1/2} \text{ at } 60°\text{C}.$$

Gas cell B (^{87}Rb and buffer gases):

$$\sigma_y \rightarrow \phi(\tau) = 2.7 \times 10^{-12}\tau^{-1/2} \text{ at } 48°\text{C}.$$

These values were almost equal with each other. However, the magnitudes of the light shift in these gas cells were quite different with each other, i.e., −0.50 Hz/MHz for gas cell A and −0.11 Hz/MHz for gas cell B, respectively. It can be concluded from these results that a use of the gas cell B is more advantageous to maintain higher microwave frequency stability.

As an improved experiment, a novel double resonance spectral lineshape with a drastically narrower linewidth was demonstrated by utilizing an advantageous property of high temporal coherence of the laser. That is, a technique was employed by utilizing the laser FM sidebands induced by microwave frequency modulation and by nonlinear susceptibility of three-level ^{87}Rb atoms. The minimum linewidth obtained was 20 Hz, which may be used as a highly sensitive frequency discriminator for an improved ^{87}Rb atomic clock.

Acknowledgment

The authors would like to express their gratitude to Messrs. Kasai, Hashi, and Chiba (Fujitsu Co. Ltd.), Prof. Kano (University of Electro—Communication), Dr. Nakayama (Kyoto Institute of Technology), Prof. Oura, Dr. Kuramochi, and Dr. Teramachi (Tokyo Institute of Technology), for their valuable discussions.

References

[1] J. L. Picque, "Hyperfine optical pumping of a cesium atomic beam, and applications," *Metrologia*, vol. 13, pp. 115–119, 1977.
[2] L. Lewis and M. Feldman, "Optical pumping by lasers in atomic frequency standards," in *Proc. 35th Annu. Freq. Control Symp., USAERADCOM*, May 1981, pp. 612–624.
[3] H. Tsuchida, M. Ohtsu, T. Tako, N. Kuramochi, and N. Oura, "Frequency stabilization of AlGaAs semiconductor laser based on the ^{85}Rb-D_2 Line," *Japan. J. Appl. Phys.*, vol. 21, pp. L561–L563, 1982.
[4] J. Vanier and L. G. Bernier, "On the signal-to-noise ratio and short-term stability of passive rubidium frequency standards," *IEEE Trans. Instrum. Meas.*, vol. IM-30, pp. 277–282, 1981.
[5] D. W. Allan, "Statistics of atomic frequency standards," *Proc. IEEE*, vol. 54, pp. 221–230, 1981.
[6] B. S. Mathur, H. Tang, and W. Happer, "Light shifts in the alkali atoms," *Phys. Rev.*, vol. 171, pp. 11–19, 1968.
[7] R. H. Dicke, "The effect of collisions upon the Doppler width of spectral lines," *Phys. Rev.*, vol. 89, pp. 472–473, 1953.
[8] T. W. Hänsch, *Nonlinear Spectroscopy*. Amsterdam, The Netherlands: North-Holland, 1977, pp. 17–86.
[9] M. Hashimoto and M. Ohtsu, submitted to *J. Opt. Soc. Amer. B.*
[10] B. D. Fried and S. D. Conte, *The Plasma Dispersion Function*. New York: Academic, 1961.
[11] G. C. Bjorklund, "Frequency-modulation spectroscopy: A new method for measuring weak absorption and dispersions," *Opt. Lett.*, vol. 5, pp. 15–17, 1980.

Minoru Hashimoto was born in Niigata, Japan, on April 14, 1961. He received the B.S. degree in communication engineering from the University of Electro-Communication, Tokyo, Japan, in 1984, and the M.S. degree in information processing from the Tokyo Institute of Technology, Tokyo, Japan, in 1986.

He is currently working towards the Ph.D. degree in information processing at the Tokyo Institute of Technology, studying the microwave atomic clock.

Mr. Hashimoto is a member of the Japanese Society of Applied Physics.

Motoichi Ohtsu, for a photograph and biography, see this issue, p. 394.

Reprinted from Applied Optics, Vol. 26, Page 464, February 1, 1987

Using a 1.5-μm DFB InGaAsP laser in a passive ring cavity-type fiber gyroscope

Motoichi Ohtsu and Satohiko Araki

It has been demonstrated that a 1.5-μm distributed feedback InGaAsP laser can be used as a coherent light source in a passive ring cavity-type fiber gyroscope. A formula for the detector shot noise-limited sensitivity of detection of rotation was derived for this type of gyroscope. Its value in the present experimental setup was estimated as being $0.8 \cdot \tau^{-1/2}$ degree/hour, where τ represents the integration time of measurements. Experiments showed that the uncertainty of the detection of rotation was 1.5°/h at τ = 100 s, which was governed by the slight reflection of light at the AR-coated fiber edges and residual frequency fluctuations of the laser.

I. Introduction

Fiber gyroscopes have been intensively investigated for use in inertial navigation systems due to their low power consumption and low cost.[1-3] Of these, passive ring cavity-type fiber gyroscopes have attracted attention because of their high sensitivity and small volume. A sensitivity as high as 0.5°/h has been attained using a conventional He–Ne laser as the light source for this type of gyroscope.[4]

On the other hand, AlGaAs and InGaAsP lasers have been fabricated and used for industrial applications, e.g., readout of optical disk memories, optical communications. Improvements in their spectral properties have shown that they can be used for coherent optical measurements and coherent optical communications.[5] One of the authors (M.O.) has demonstrated that the frequency stability of 0.8-μm AlGaAs and 1.5-μm InGaAsP lasers was improved as high as 1.4×10^{-12} (Ref. 6) and 6.7×10^{-11},[7] respectively, from which it can be expected that they can be used as coherent light sources for passive ring cavity-type fiber gyroscopes.

However, in spite of the fact that replacing a conventional gas laser by a semiconductor laser is desirable for further reduction of the volume of the passive ring cavity-type fiber gyroscope, use of a semiconductor laser as a coherent light source has not yet been fully documented.

In this study, a 1.5-μm distributed feedback (DFB) InGaAsP laser was used as the coherent light source for a passive ring cavity-type fiber gyroscope proposed by the authors. The detector shot noise-limited sensitivity was calculated, and uncertainty of the detection of rotation was measured for a fabricated fiber gyroscope.

II. Principle of Operation and Estimation of the Sensitivity Limit

Figure 1 shows the setup of the passive ring cavity-type fiber gyroscope proposed in this study. A part of this setup is similar to that employed in Ref. 4; however, no A/O modulators are required here because the frequency of the semiconductor laser can be directly controlled by modulating injection current, which simplifies the system. For direct modulation of the laser frequency, a low ac current of frequency $\mathbf{f}_m$ was superimposed on the dc injection current. The laser beam was divided by a beam splitter (BS) after passing through a collimator lens and an optical isolator. Two split beams were introduced into the passive ring cavity (a ring Fabry-Perot interferometer) made of a fiber loop and two directional couplers (C_1,C_2), and propagated toward the directions in the cavity which were opposite to each other. Two couplers were the input and output mirrors of the cavity.

When these oppositely propagating beams satisfied the resonance conditions of the ring cavity, they were transmitted through the cavity without suffering attenuation and detected by photodetectors (D_1,D_2). The ac output signals from the detectors with the frequency $\mathbf{f}_m$ were synchronously detected by lock-in amplifiers (LIA_1,LIA_2). Figures 2(a) and (b) show derivatives of the resonance curves, i.e., the frequency dependence of the transmittance of the ring cavity. They were obtained for the two beams when the output

The authors are with Tokyo Institute of Technology, Graduate School at Nagatsuta, 4259 Nagatsuta, Midori-ku, Yokohama, Kanagawa 227, Japan.

Received 12 June 1986.
0003-6935/87/030464-07$02.00/0.

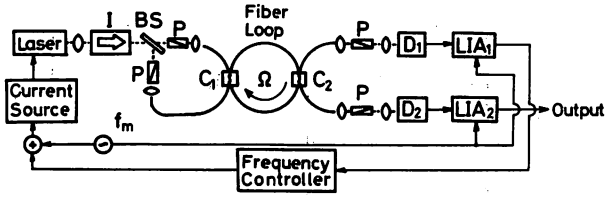

Fig. 1. Experimental setup of the proposed passive ring cavity-type gyroscope: *I*, optical isolator composed of a YIG Faraday rotator and two polarizers; *BS*, beam splitter; *P*, polarizer; C_1,C_2, fiber directional couplers working as input and output mirrors of the ring cavity; D_1,D_2, avalanche photodiodes; LIA_1,LIA_2, lock-in amplifiers.

signals from the lock-in amplifiers are traced on a chart recorder by slowly sweeping the dc injection current of the laser.

If this fiber loop rotates with rotational speed Ω, the Sagnac effect[8] gives the difference between the resonance frequencies ν_{cw} and ν_{ccw} of these resonance curves. The difference can be expressed as

$$\nu_{cw} - \nu_{ccw} = \frac{N}{\lambda}\sqrt{\frac{4A}{\pi}}\,\Omega, \tag{1}$$

where **N** is the number of turns of the fiber loop, λ is the wavelength of the laser, and **A** is the area surrounded by the fiber loop. In this gyroscope, the injection current of the laser was controlled to lock the laser frequency at ν_{ccw} by using the slope of the center part of the curve of Fig. 2(a) as a frequency discriminator. In this locked condition, the output voltage from the lock-in amplifier LIA_2 is proportional to the frequency difference of Eq. (1) as long as the slope of the curve of Fig. 2(b) is approximately a straight line at around ν_{cw}. The value of this voltage can be expressed as

$$V_2 = K\frac{N}{\lambda}\sqrt{\frac{4A}{\pi}}\,\Omega, \tag{2}$$

where **K** is a proportional constant which depends on the sensitivity of the detector D_2, the gain of the lock-in amplifier LIA_2, and the slope of the curve of Fig. 2(b).

Contributions of the shot noise from the detector can be regarded as one of the fundamental noise sources, which gives the sensitivity limit of this gyroscope. This limit is estimated as follows: The profile of the laser oscillation field spectrum is approximated as a Lorentzian for this estimation, which is expressed by

$$P_0(\nu) = \frac{(P_0/\pi)\cdot(\Delta\nu/2)}{(\nu-\nu_0)^2 + (\Delta\nu/2)^2}, \tag{3}$$

where P_0 is a peak power, ν is the instantaneous laser frequency, ν_0 is the center frequency of the spectral profile, and $\Delta\nu$ is its linewidth (FWHM, full width at half-maximum). The laser power incident on detector D_2 can be expressed as[9]

$$P = \int_{-\infty}^{\infty} P_0(\nu)\cdot T_{cw}(\nu)\cdot d\nu, \tag{4}$$

where $T_{cw}(\nu)$ is the transmittance of the ring cavity for the clockwise beam, which can be approximated by[10]

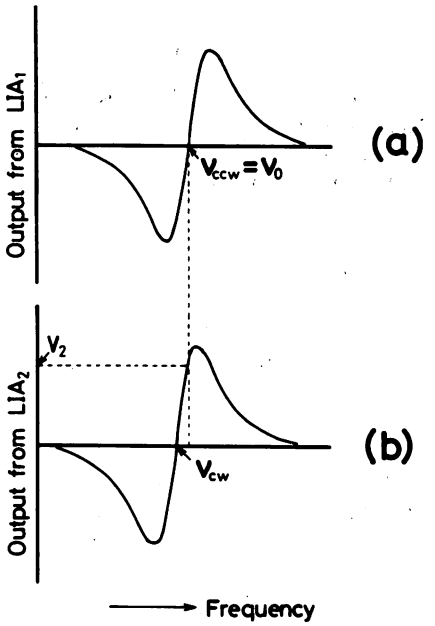

Fig. 2. Derivatives of the resonance curves of the fiber ring cavity for the transmitted laser beams (a) counterclockwise and (b) clockwise: ν_{ccw},ν_{cw}, resonance frequencies of this cavity for the two beams. The laser frequency ν_0 is locked at ν_{ccw}.

$$T_{cw}(\nu) = \frac{T_{cw,p}(\Gamma/2)^2}{(\nu-\nu_{cw})^2 + (\Gamma/2)^2}, \tag{5}$$

where $T_{cw,p}$ is the peak value of T_{cw}, and Γ is the FWHM of the profile of Eq. (5). They are given by

$$T_{cw,p} = \frac{(1-R)^2}{(1-\alpha_t\cdot R)^2}, \tag{6}$$

$$\Gamma = \frac{c}{\pi nL}\cdot\frac{1-\alpha_t R}{\sqrt{\alpha_t R}}, \tag{7}$$

where **R** is the reflectance of the directional couplers, αd_t is the loss of the fiber loop in which the loss due to the reflectance **R** is not included, **c** is the speed of light in vacuum, **n** is the refractive index of the fiber, and **L** is the length of the fiber loop. Substitution of Eqs. (3), (5), (6), and (7) into Eq. (4) gives

$$P = \frac{P_p(w/2)^2}{(\nu-\nu_{cw})^2 + (w/2)^2}, \tag{8}$$

where

$$P_p = P_0\cdot T_{cw,p}\cdot\frac{\Gamma}{\Gamma+\Delta\nu}, \tag{9}$$

$$w = \Gamma + \Delta\nu. \tag{10}$$

Since $\nu_{ccw} - \nu_{cw} = \nu_0 - \nu_{cw}$ under laser frequency locking, the power of Eq. (8) is equal to P_p at $\Omega = 0$. However, a low rotational speed Ω can induce a slight change ΔP in the power of Eq. (8). For phase sensitive detection, it has been pointed out that the value of ΔP can be maximized when the maximum deviation of the modulated laser frequency is equal to $0.59\cdot(w/2)$ and is expressed as[11]

$$P = -0.70 \cdot \frac{P_p(\nu_{ccw} - \nu_{cw})}{w/2} \cdot \quad (11)$$

The signal-to-noise ratio of the rotation detection is given by the ratio between ΔP of this equation and the minimum detectable change in the laser power P_{min} by a photoelectric detector, i.e.,

$$S/N = |\Delta P/P_{min}|, \quad (12)$$

where P_m is given by[12]

$$P_{min} = \sqrt{16P \cdot P_n}. \quad (13)$$

The noise power of the detector P_n due to the shot noise is given by

$$P_n = h\nu/4\eta\tau, \quad (14)$$

where h is Planck's constant, η is the quantum efficiency of the detector, and τ is the integration time of the measurements. Substitution of Eqs. (11) and (13) into Eq. (12) gives

$$S/N = 0.35 \frac{\nu_{ccw} - \nu_{cw}}{w} \sqrt{P_p/P_n}. \quad (15)$$

The minimum detectable frequency difference $(\nu_{ccw} - \nu_{cw})_{min}$ can be derived by S/N = 1, which is expressed as

$$(\nu_{ccw} - \nu_{cw})_{min} = \frac{w}{0.35} \sqrt{P_n/P_p}. \quad (16)$$

Substitution of this equation into Eq. (1) gives the sensitivity limit of the detection of rotation, which is governed by the detector shot noise. Use of Eqs. (6), (7), (9), (10), and (14) gives the following expression for this limit:

$$\Omega_s = 1.27 \cdot \sqrt{2} \cdot \frac{1}{N\sqrt{A}} \sqrt{\frac{h\nu}{\eta\tau}} \frac{1}{\sqrt{P_0}} \frac{1 - \alpha_t R}{1 - R} \left[\frac{c}{\pi n L} \frac{1 - \alpha_t R}{\sqrt{\alpha_t R}} + \Delta\nu \right]^{3/2} \cdot \quad (17)$$

The factor $\sqrt{2}$ was introduced into this equation to represent a contribution from the shot noise from detector D_1 used for frequency locking, which is uncorrelated with that from detector D_2 used for the detection of rotation.

The value of Ω_s of Eq. (17) depends on the performance of the fiber loop and temporal coherence of the laser. This dependence can be extracted from Eq. (17) and is expressed as

$$f(R) = \frac{1 - \alpha_t R}{1 - R} \left[\frac{c}{\pi n L} \frac{1 - \alpha_t R}{\sqrt{\alpha_t R}} + \Delta\nu \right]^{3/2} \cdot \quad (18)$$

Figures 3(a) and (b) show the relationships between $f(R)$ and R for several values of $\Delta\nu$ at $\alpha_t = -0.8$ and -0.1 dB, which indicate that $f(R)$ takes a minimum at a certain value of R. This value of R (represented by R_m) can be analytically expressed only for $\Delta\nu = 0$, which is

$$R_m = -\frac{3}{2}\left(\frac{1}{\alpha_t} - 1\right) + \sqrt{\frac{1}{\alpha_t} + \frac{9}{4}\left(\frac{1}{\alpha_t} - 1\right)^2} \cdot \quad (19)$$

Figure 4 shows a dependence of R_m on α_t numerically calculated for several values of $\Delta\nu$. Figures 3 and 4 represent a specific feature of this type of gyroscope,

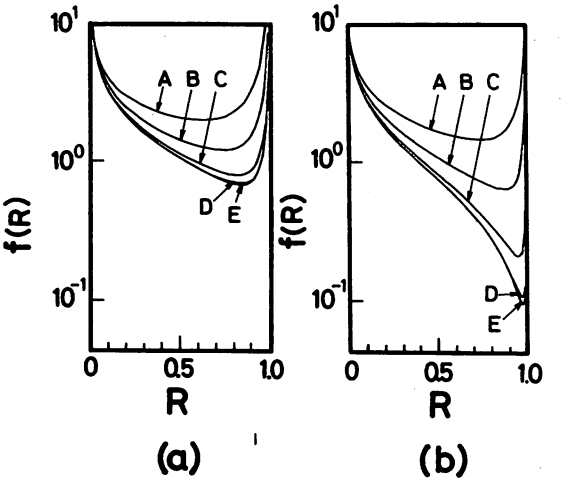

Fig. 3. Relationships between $f(R)$ and R for (a) $\alpha_t = -0.8$ dB and (b) $\alpha_t = -0.1$ dB. The values of laser linewidth $\Delta\nu$ are A, 13 MHz; B, 5 MHz; C, 1 MHz; D, 100 kHz; and E, 0 Hz.

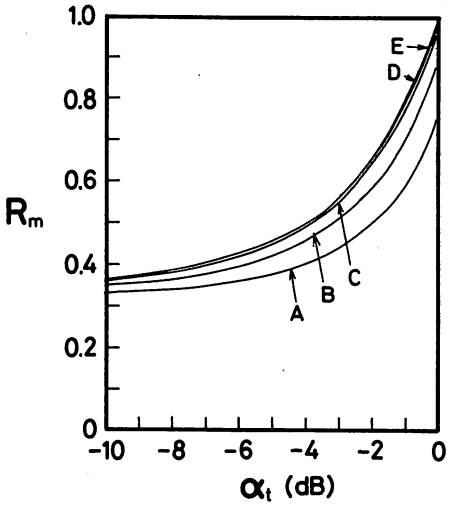

Fig. 4. Relationship between R_m and α_t. The values of laser linewidths $\Delta\nu$ are A, 13 MHz; B, 5 MHz; C, 1 MHz; D, 100 kHz; and E, 0 Hz.

i.e., lower loss α_t and narrower linewidth $\Delta\nu$ would improve the detector shot noise-limited sensitivity Ω_s. Figures 5(a) and (b) show the relationships between Ω_s and the integration time τ, where the value of R was fixed at R_m for each value of α_t and $\Delta\nu$. Other numerical values for Fig. 5 were employed from the experimental conditions in Sec. III, which are

$$n = 1.46, \quad N = 1, \quad A = 0.46\ m^2, \quad \lambda = 1.5\ \mu m,$$

$$\eta = 0.7, \quad \nu_0 = 200\ THz, \quad P_0 = 2\ mW, \quad L = 2.4\ m.$$

Furthermore, for the experimentally obtained values of α_t (= −0.8 dB) and $\Delta\nu$ (= 13 MHz) in this study, the Ω_s of this figure is expressed as

$$\Omega_s = 0.8 \cdot \tau^{-1/2}\ (\text{degree/hour}). \quad (20)$$

Equations (17) and (18) mean that the sensitivity can be improved by reducing the laser linewidth $\Delta\nu$. Figure 5 shows that as narrow a reduction as 100 kHz is

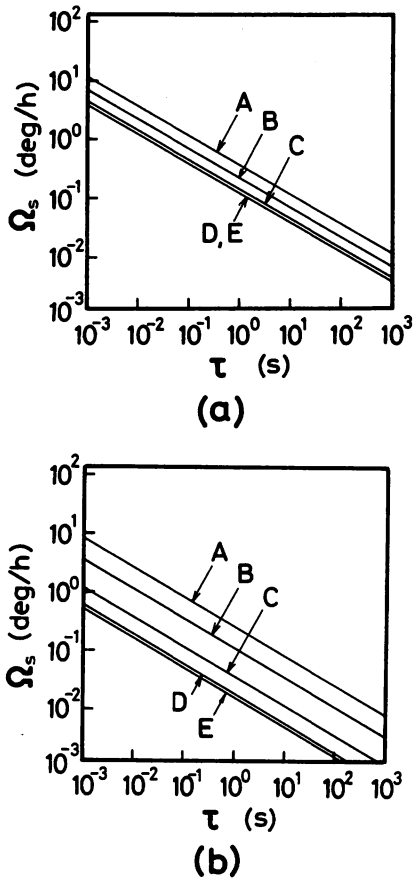

Fig. 5. Relationship between Ω_s and τ for (a) $\alpha_t = -0.8$ dB and (b) $\alpha_t = -0.1$ dB. The values of the laser linewidth $\Delta\nu$ are *A*, 13 MHz; *B*, 5 MHz; *C*, 1 MHz; *D*, 100 kHz; and *E*, 0 Hz.

enough for the present gyroscope because the value of Ω_s for $\Delta\nu \leqq 100$ kHz converges to the value for $\Delta\nu = 0$. Electrical negative feedback[13] can be used as a promising technique to reduce the linewidth for this gyroscope because the locking of the center frequency of the field spectrum can be simultaneously carried out without increasing the cavity volume of the laser. A linewidth as narrow as 330 kHz has already been obtained with this technique, and theoretical estimation has predicted that it can be reduced to as narrow as several hundred hertz.[13]

The contributions of Kerr effect[3] and Rayleigh backscattering[14] in the fiber that should also be taken into account when estimating a more practical limit of sensitivity of this gyroscope, are now being studied.

III. Experimental Setup

A 1.5-μm InGaAsP laser was employed because it is more favorable for the present gyroscope compared with an 0.8-μm AlGaAs laser. This is due to its properties given as follows:

(1) Effect of Rayleigh scattering in the fiber is lower because of a longer wavelength.

(2) Coupling efficiency to the fiber is higher because optical alignment to a larger core diameter single-mode fiber is easier.

(3) Transmission loss of the fiber is lower.

(4) Improved cavity structures, e.g., distributed feedback (DFB)[15] or distributed Bragg reflector (DBR),[16] have been fabricated to achieve a single-longitudinal-mode oscillation for wide ranges of temperature and injection current. The use of this cavity makes it possible to increase the laser power without any discontinuous frequency jump due to mode hopping, which can reduce the laser linewidth and is advantageous for increasing the signal-to-noise ratio of the rotation detection.

(5) Lifetime is estimated as longer than that of AlGaAs lasers.[17]

On the other hand, one of the disadvantages of an InGaAsP laser is its larger temperature dependence of the threshold current (i.e., lower T_0 value),[17] which may deteriorate its coherence due to thermal fluctuations of the frequency.[6] However, this effect was sufficiently lessened in the present experiments by reducing the ambient temperature fluctuations.

A 1.5-μm DFB InGaAsP laser[18] was used in our experiments, and its spectral linewidth was measured by the delayed self-heterodyne technique,[19] which can be expressed as

$$\Delta\nu = 6.5\,(I/I_{th} - 1)^{-1} \quad \text{(MHz)}, \tag{21}$$

where I and I_{th} are the injection current and its threshold value, respectively. The laser was operated at 293 K and $I/I_{th} = 1.5$, which means that $\Delta\nu = 13$ MHz. The normalized frequency deviation of the laser by direct frequency modulation was 1 GHz/mA at $f_m \leqq 50$ kHz, which was measured by a technique using a Michelson interferometer.[20] A low noise current source was used for current injection to the laser, whose current noise was 0.6 nA/$\sqrt{\text{Hz}}$ at 1-kHz Fourier frequency. The frequency controller in Fig. 1 was composed of a proportional amplifier, an integrator, and a differentiator. The response bandwidths of the current source and the frequency controller were 150 kHz. A small copper block was used as a heat sink for the laser, and its temperature fluctuations were reduced to 1×10^{-3} K by using Peltier elements and thermistor bridges for temperature control.

The single-mode fiber used had a core diameter of 5 μm, clad diameter of 124 μm, cutoff wavelength of 1.22 μm, and transmission loss of 0.25 dB/km. A polishing technique was employed to remove a part of the cladding to make the directional couplers (C_1,C_2 in Fig. 1).[21] The resultant loss of each coupler was measured as -0.4 dB, from which it was estimated that the loss of the fiber loop α_t was -0.8 dB. Separation between the cores of two fibers placed in parallel was adjusted by using a piezoelectric transducer to fix the reflectance R of the coupler at 83%. This value of R was chosen from the curves in Fig. 4 at $\alpha_t = -0.8$ dB. However, the laser linewidth $\Delta\nu$ was assumed to be 1 MHz for this choice, which is the value the authors have achieved by electrical negative feedback for this gyroscope and is narrower than that of the actual value (13 MHz). Nevertheless, it can be expected that this difference does not give any trouble in this choice because Fig. 3(a) shows that the value of $f(R)$ at $\alpha_t = -0.8$ dB and $\Delta\nu = 13$ MHz

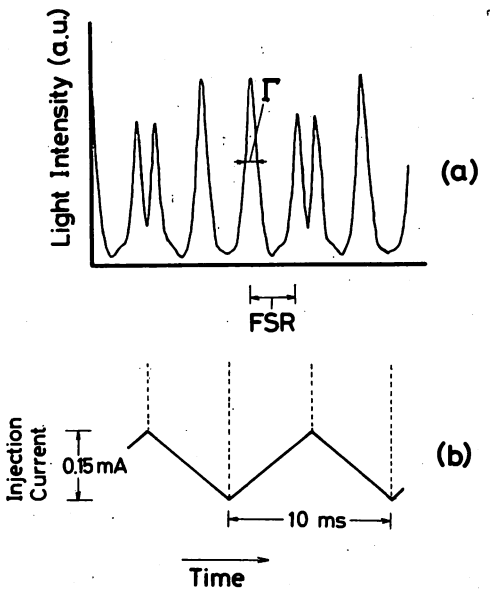

Fig. 6. (a) Resonance curve of the constructed fiber ring cavity for the counterclockwise laser beam: FSR, free spectral range; Γ, FWHM of the resonance curve. (b) A waveform of the injection current of the laser.

is almost independent of **R** within the range of 40% ≦ **R** ≦ 90%. Improved experiments using the laser with a reduced linewidth of 1 MHz are now in progress and will be reported elsewhere.

The finesse determined by this value of **R** was 11. The length of the fiber loop was 2.4 m, which corresponded to a free spectral range of 86 MHz.

Two Ge APDs were used as detectors without applying any bias voltages.

IV. Experimental Results

Figure 6(a) shows resonance curves of the fiber ring cavity for the counterclockwise laser beam, which was observed by applying an injection current with the waveform in Fig. 6(b) to sweep slowly the laser frequency. The FWHM linewidth of this resonance curve was 21 MHz, in which a contribution from the laser linewidth (13 MHz) was included. If this contribution is removed, the resultant linewidth can be estimated as 8 MHz, which is consistent with the value determined by the ratio between the free spectral range and finesse given in Sec. III. The resonance curve for the clockwise beam was almost the same as that in Fig. 6(a). A derivative of the curve in Fig. 6(a), as given by Fig. 2, can be obtained by phase sensitive detection. For this purpose, the laser frequency was directly modulated by an ac current with a modulation frequency f_m of 50 kHz and maximum frequency deviation of 30 MHz. Figure 7(a) shows the resultant derivative of the curve in Fig. 6(a). The technique for slow sweeping of the laser frequency employed was the same as that in Fig. 6(b), which is shown in Fig. 7(b).

The laser frequency was locked at the center of the derivative curve in Fig. 7(a), i.e., the resonance frequency ν_{ccw}. The rotational speed can be detected by measuring the output voltage from the lock-in amplifier LIA_2 for the clockwise laser beam in this condition.

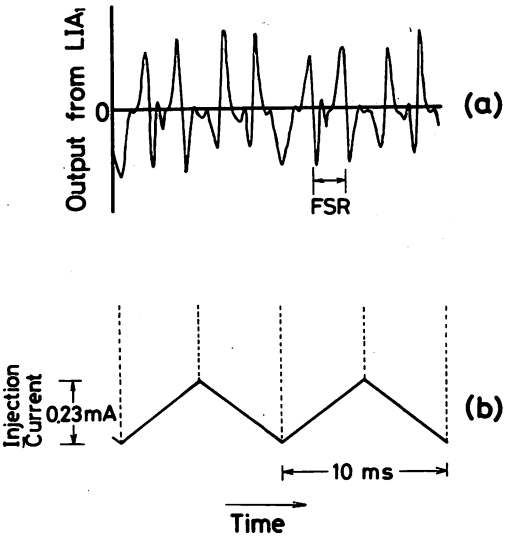

Fig. 7. (a) Derivative of the curve of Fig. 6(a). (b) A waveform of the injection current of the laser.

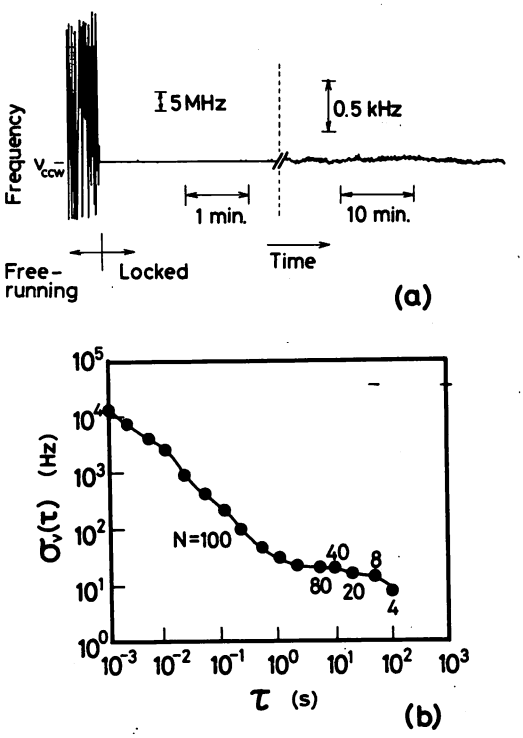

Fig. 8. (a) Waveform of frequency fluctuations of the laser in free-running and locked conditions. (b) Square root of the Allan variance $\sigma_\nu^2(\tau)$ of residual frequency fluctuations of the locked laser: N, number of data; τ, integration time of measurements.

Figure 8(a) represents the laser frequency fluctuations in free-running and locked conditions, where an error signal from the lock-in amplifier LIA_1 was traced on a chart recorder. The square root of the Allan variance $\sigma_\nu^2(\tau)$[22] of the residual fluctuations of the laser frequency was calculated to evaluate quantitatively the frequency stability by using the error signal after A–D conversion. Figure 8(b) shows the result,

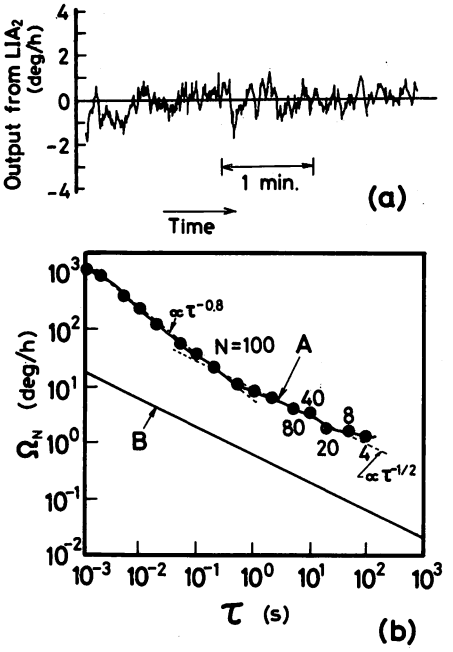

Fig. 9. (a) Waveforms of the output signal from the lock-in amplifier LIA_2 at $\Omega = 0$. (b) Curve A, square root of the Allan variance of the uncertainty of the detection of rotation, which was evaluated by using the output signal from LIA_2 at $\Omega = 0$ and Eq. (2); curve B, value of Eq. (20): N, number of data; τ, integration time of measurements.

and the minimum of $\sigma_\nu(\tau)$ was 10 Hz at $\tau = 100$ s. It was confirmed in Fig. 8 that the laser frequency was tightly locked to the resonance frequency ν_{ccw}. Figure 9(a) shows an output signal from the lock-in amplifier LIA_2 at $\Omega = 0$, which corresponds to the uncertainty of the detection of rotation. Curve A in Fig. 9(b) shows this uncertainty expressed by the square root of the Allan variance, which was calculated using this output signal and Eq. (2). The uncertainty given by this curve can be approximated as

$$\Omega_N = \begin{cases} 6.4 \cdot \tau^{-0.8} & (1\text{ ms} \leqq \tau < 200\text{ ms}), \\ 10 \cdot \tau^{-1/2} & (200\text{ ms} \leqq \tau \leqq 100\text{ s}), \\ & (\text{degree/hour}), \end{cases} \quad (22)$$

which took the minimum of 1.5°/h at $\tau = 100$ s. This value of the uncertainty was limited by residual frequency fluctuations of the laser and the noises contained in the output signal from the lock-in amplifier LIA_2. The principal noise sources found empirically were the effect of the slight reflection of light at the AR-coated fiber edges of the input and output ports. Curve B in this figure represents the detector shot noise-limit of Eq. (20). It is seen that the value of curve A is about 13 times larger than that of curve B. Further reductions of the reflection and residual frequency fluctuations should be carried out to reach the detector shot noise-limited value. Furthermore, evaluations and reductions of other practical noise sources, e.g., Rayleigh backscattering, Kerr effect, should also be carried out for this purpose.

However, it was confirmed by the present experiments that the 1.5-μm DFG InGaAsP laser can be used as a coherent light source for a passive ring Fabry-Perot type gyroscope. Further increases in the sensitivity can be expected by reducing the loss of the fiber loop and laser linewidth.

V. Summary

A passive ring cavity-type fiber gyroscope was proposed and a 1.5-μm DFB InGaAsP laser was employed as its coherent light source. A detector shot noise-limited sensitivity of the detection of rotation was estimated using the numerical value of the constructed gyroscope, which was $0.8 \cdot \tau^{-1/2}$ degree/hour. Experimental results showed that the uncertainty of the detection of rotation was 1.5°/h at $\tau = 100$ s. Reduction of the reflections at the fiber edges and residual fluctuations of laser frequency were required for this uncertainty value to reach the theoretically estimated limit. Improvement of the theoretically estimated limit can also be expected by reducing the loss of the fiber loop and laser linewidth.

The authors would like to express their gratitude to H. Osanai, F. Suzuki, and T. Sioda of Fujikura, Ltd. for the discussion on fibers and to T. Yamamoto and S. Akiba of KDD Research and Development Laboratories for discussions on 1.5-μm InGaAsP lasers.

References

1. R. A. Bergh, H. C. Lefevre, and H. J. Shaw, "Overview of Fiber-Optic Gyroscopes," IEEE/OSA J. Lightwave Technol. **LT-2**, 91 (1984).
2. J. L. Davis and S. Ezekiel, "Techniques for Shot-Noise Limited Inertial Rotation Measurement Using a Multiturn Fiber Sagnac Interferometer," Proc. Soc. Photo-Opt. Instrum. Eng. **157**, 131 (1978).
3. R. A. Bergh, B. Culshaw, C. C. Cutler, H. C. Lefevre, and H. J. Shaw, "Source Statistics and the Kerr Effect in Fiber-Optic Gyroscopes," Opt. Lett. **7**, 563 (1982).
4. R. E. Meyer, S. Ezekiel, D. W. Stowe, and V. J. Tekippe, "Passive Fiber-Optic Ring Resonator for Rotation Sensing," Opt. Lett. **8**, 644 (1983).
5. T. Okoshi, "Recent Progress in Heterodyne/Coherent Optical-Fiber Communications," IEEE/OSA J. Lightwave Technol. **LT-2**, 341 (1984).
6. M. Ohtsu, H. Fukada, T. Tako, and H. Tsuchida, "Estimation of the Ultimate Frequency Stability of Semiconductor Lasers," Jpn. J. Appl. Phys. **22**, 1157 (1983).
7. M. Ohtsu, H. Kotani, and H. Tagawa, "Spectral Measurements of NH_3 and H_2O for Pollutant Gas Monitoring by 1.5 μm InGaAsP/InP Lasers," Jpn. J. Appl. Phys. **22**, 1553 (1983).
8. E. J. Post, "Sagnac Effect," Rev. Mod. Phys. **39**, 475 (1967).
9. S. Tai, K. Kyuma, and T. Nakayama, "Novel Measuring Method for Spectral Linewidth of Laser Diodes Using Fiber-Optic Ring Resonator," Electron. Lett. **21**, 91 (1985).
10. S. J. Pechowski, T. G. Giallorenzi, and S. K. Sheem "A Sensitive Fiber-Optic Fabry-Perot Interferometer," IEEE J. Quantum Electron. **QE-17**, 2168 (1981).
11. K. Shimoda, "Ultimate Stability of Methane-Stabilized Lasers," Jpn. J. Appl. Phys. **12**, 1222 (1973).
12. K. Shimoda, "Limits of Sensitivity of Laser Spectrometers," Appl. Phys. **1**, 77 (1973).
13. M. Ohtsu and S. Kotajima, "Linewidth Reduction of a Semiconductor Laser by Electrical Feedback," IEEE J. Quantum Electron. **QE-21**, 1905 (1985).

14. C. C. Cutler, S. A. Newton, and H. J. Shaw, "Limitation of Rotation Sensing by Scattering," Opt. Lett. **5**, 488 (1980).
15. K. Utaka, S. Akiba, K. Sakai, and Y. Matsushima, "Room-Temperature CW Operation of Distributed Feedback Buried-Heterostructure InGaAsP/InP Laser Emitting at 1.57 μm," Electron. Lett. **17**, 961 (1981).
16. F. Koyama, S. Arai, T. Tanbun-Ek, K. Kishino, and S. Suematsu, "Low Threshold Current GaInAsP/InP Integrated Twin Guide Lasers with Distributed Bragg Reflector Emitting at 1.55 μm," in *Technical Digest, Topical Meeting on Integrated and Guided-Wave Optics* (Optical Society of America, Washington, DC, 1982), paper WB5.
17. M. Yano, H. Nishi, and M. Takusagawa, "Temperature Characteristics of Threshold Current in InGaAsP/InP Double Heterostructure Lasers," J. Appl. Phys. **51**, 4022 (1980).
18. S. Akiba, K. Utaka, K. Sakai, and Y. Matsushima, "Distributed Feedback InGaAsP/InP Lasers with Window Region Emitting at 1.5 μm Range," IEEE J. Quantum Electron. **QE-19**, 1052 (1983).
19. T. Okoshi, K. Kikuchi, and A. Nakayama, "Novel Method for High Resolution Measurement of Laser Output Spectrum," Electron. Lett. **16**, 630 (1980).
20. H. Tsuchida, T. Tako, and M. Ohtsu, "A Novel Technique for Measuring the Frequency Deviation of Semiconductor Laser Under Direct Modulation," Jpn. J. Appl. Phys. **22**, L19 (1983).
21. M. J. F. Digonnet and H. J. Show, "Analysis of a Tunable Single Mode Optical Fiber Coupler," IEEE J. Quantum Electron. **QE-18**, 746 (1982).
22. D. Allan, "Statistics of Atomic Frequency Standards," Proc. IEEE **54**, 221 (1966).

XIV International Quantum Electronics Conference (IQEC'86), June 1986, San Francisco, CA, THFF2, pp.164 - 165

THFF2 Semiconductor laser-pumped rubidium atomic clocks and attainment of 20-Hz double-resonance linewidth

MINORU HASHIMOTO, MOTOICHI OHTSU, Tokyo Institute of Technology, Graduate School of Nagatsuta, 4259 Nagatsuta, Midori-ku, Yokohama, Kanagawa 227, Japan.

Rubidium (^{87}Rb) atomic clocks have been widely used as highly stable microwave oscillators for communication, astronomy, ranging, and so on. They have utilized an optical-microwave double-resonance spectral line in ^{87}Rb as a frequency reference for microwave-frequency stabilization.

Use of semiconductor lasers, a potential optical pumping source, has been proposed recently to improve the clock performances.[1] This proposal has attracted not only industrial interest but also purely scientific interest based on quantum electronics. Preliminary experiments and calculations have been carried out.[2,3] However, systematic experimental studies have not yet been done because of the insufficient reliability of semiconductor lasers.

We have pointed out that our highly stabilized semiconductor lasers are reliable enough for this purpose and tried several experiments.[4] This presentation reports further progress.

Figure 1 shows microwave frequency shifts (light-induced frequency shifts) induced by laser-frequency variations. Dispersive line shapes can be clearly seen which have been theoretically predicted. They have not yet been measured for conventional ^{87}Rb clocks because of the temporal incoherence of pumping source, i.e., a ^{87}Rb isotope lamp.

Figure 2 shows the short-term stability of microwave frequency of a laser-pumped ^{87}Rb clock. Even though the servo-control parameters have not yet been optimized, the stability of $9.4 \times 10^{-12}\ \tau^{-1/2}$ was obtained when the temperature of ^{87}Rb vapor was 48°C, which was as high as that of carefully designed conventional ^{87}Rb clocks. The attainment of such high stability was attributed to high-power density and the temporal coherence of the laser.

For the higher stability of microwave frequency, reduction of the double-resonance linewidth is essential. Although this linewidth has been reduced to ~500 Hz (curve *B* of Fig. 3) by employing buffer gases, significant progress in this reduction has not been reported for 30 years.

In this study, a novel FM sideband technique was introduced for this reduction: ^{87}Rb vapor was used not only as a sample but also as a phase modulator for the laser light wave. This can be achieved due to the nonlinear susceptibility of three-level ^{87}Rb atoms when the incident microwave frequency is modulated. By using resultant FM sidebands of the laser and synchronous detection, higher-order derivative shapes of absorptive and dispersive parts in a double-resonance spectral line were measured. Part of this technique is similar to that of FM laser spectroscopy.[5] The upper trace in Fig. 3 shows the result. For this measurement, the coherently interacting time between the laser and atoms was increased by decreasing the vapor temperature to 36°C. A sharp and narrow linewidth spectral shape can be seen at the center of the curve. The minimum of the width obtained was 20 Hz, which was ~1/25 that of conventional ones, from which great progress in linewidth reduction can be confirmed. The microwave-frequency stability of $1.8 \times 10^{-11}\ \tau^{-1/2}$ was obtained by using this ultranarrow spectral line as a frequency reference. This is as high as that of carefully designed conventional clocks, and higher stability can be expected by improving the SNR value of spectral measurements.

(Invited paper, 25 min)

1. J. L. Picque, Metrologia 13, 115 (1977).
2. L. L. Lewis and M. Feldman, in *Proceedings, Thirty-fifth Annual Frequency Control Symposium*, Fort Monmouth, NJ (May 1981), p. 612.
3. J. C. Camparo and R. P. Frueholz, in *Seventeenth Annual Precise Time and Time Interval (PTTI) Applications and Planning Meeting*, Washington, DC (Dec. 1985), paper 15.
4. M. Ohtsu, M. Hashimoto, and H. Ozawa, *Proceedings, Thirty-ninth Annual Frequency Control Symposium* (May 1985), p. 43.
5. G. C. Bjorklund, Opt. Lett. 5, 15 (1980).

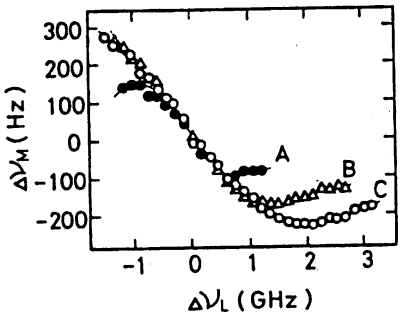

THFF2 Fig. 1. Microwave frequency shift $\Delta\nu_M$ induced by laser-frequency variation $\Delta\nu_L$. Laser power densities were (A) 79.2, (B) 288, and (C) 562 $\mu W/cm^2$, respectively.

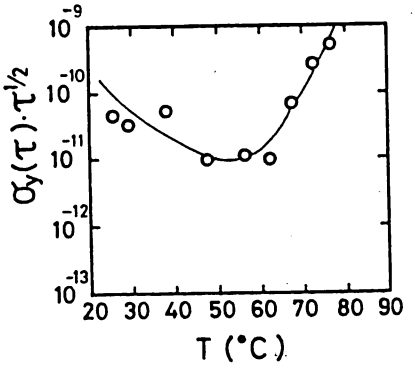

THFF2 Fig. 2. Relationship between short-term stability σ of microwave frequency and ^{87}Rb cell temperature. τ represents integration time. Laser power density was 43.2 $\mu W/cm^2$.

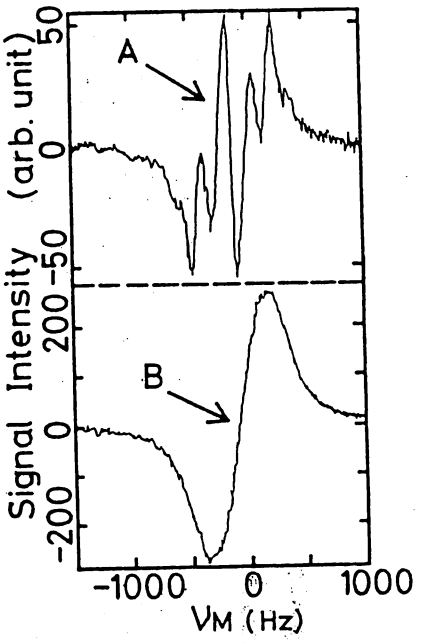

THFF2 Fig. 3. (A) Laser-pumped double-resonance spectral shape measured by a novel detection scheme of laser FM sidebands. ^{87}Rb cell temperature was 36°C. (B) Laser-pumped double-resonance spectral shape measured by a conventional detection scheme. ^{87}Rb cell temperature was 48°C.

A Workshop on Fundamental Measurements on Optically Prepared Atoms, September 1986, Gaithersburg, MD, D5

ULTRAHIGH SENSITIVE FREQUENCY DISCRIMINATION IN DIODE LASER PUMPED ^{87}Rb ATOMIC CLOCKS

Motoichi Ohtsu, Minoru Hashimoto, and Hiroyuki Furuta

Graduate School at Nagatsuta
Tokyo Institute of Technology
4259 Nagatsuta, Midori-ku, Yokohama, Kanagawa 227, JAPAN

A novel double resonance spectral shape with the linewidth as narrow as 20 Hz is demonstrated by utilizing FM sidebands of a coherent diode laser, which were induced by microwave frequency modulation. A part of this technique is equivalent to the FM laser spectroscopy. Theoretical analysis shows that further reductions of the linewidth can be expected by optimal choice of modulation parameters, which gives an increase of sensitivity of microwave frequency discrimination of about 100 times that of a conventional ^{87}Rb atomic clocks. Effects of the laser linewidth on this spectral lineshape are also investigated.

Furthermore, a novel ^{87}Rb atomic beam clock is proposed to get optically prepared but freely propagating atomic beams in order to utilizing more actively the advantageous property of the present detection scheme. Quite higher frequency stability and accuracy can be expected by this novel clock.

Proceedings of the 41st Annual Frequency Control Symposium, June 1987, Philadelphia, PA, Session B3, Paper number 3

ULTRA-SENSITIVE FREQUENCY DISCRIMINATION In A DIODE LASER PUMPED ^{87}Rb ATOMIC CLOCK

M. Hashimoto, M. Ohtsu*, and H. Furuta

Department of Imformation Processing
Graduate School at Nagatsuta
4259 Nagatsuta, Midori-ku, Yokohama, Kanagawa 227, Japan

*Presently, AT&T Bell Laboratories
Room HOH R237, Holmdel, New Jersey 07733, USA

<ABSTRACT>

We proposed a novel FM sideband technique to reduce drastically the double resonance linewidth in a Rb atomic clock pumped by a stabilized diode laser. This could be achived by the use of the nonlinear susceptibility of three-level Rb atoms when the incident microwave signal is modulated. By using resultant FM sidebands of the laser and synchronous detection, high-order derivative shapes of absorptive and dispersive parts of double-resonance spectral line were measured. The linewidth as narrow as 20 Hz was obtained, which was 1/18 times that of the rf-excited ^{87}Rb atomic clock. Optimum values of modulation parameters were found by the computer simulation. Futhermore, contributions of the laser frequency detuning to the light shifts were also estimated to attain the microwave frequency accuracy as high as 10^{-12}.

I. Introduction

Highly stable microwave frequency oscillators have been required for many applications such as satellite communications , satellite tracking, global positioning system (GPS), and so on. Portable Cesium (^{133}Cs) atomic clocks and Rubidium (^{87}Rb) atomic clocks have been used for these applications, and improvements of their performances are indispensable for the progresses of these applications.

For these improvements , the optical pumping and the optical detection by diode lasers have been proposed for ^{133}Cs atomic clocks[1]. In the case of the optical pumping for ^{87}Rb atomic clocks, the replacement of a rf - excited ^{87}Rb lamp by a diode laser has been proposed , and preliminary experiments on laser pumped ^{87}Rb atomic clocks have been reported[2]. The authors already showed that a quantitative evaluation of light shift and a novel double resonance lineshape with a drastically narrower linewidth can be obtained by utilizing an advantageous property of a high temporal coherence of the laser[3]. This can be achived by the use of FM laser sidebands induced by the nonlinear susceptibility of three-level ^{87}Rb atoms and the microwave frequency modulation. However, to the author's knowledge, this effect has not been known yet and is employed as an advanced technique for improved ^{87}Rb atomic clocks. Therefore, extremely high stability of microwave frequency can be obtained by using this technique at optimal conditions.

In this paper, a theoretical analysis for this technique and an evaluation of microwave frequency stability for a diode laser pumped ^{87}Rb atomic clock are carried out. In section II, the observation of some novel double-resonance lineshapes with narrower linewidth are demonstrated. In section III, the theoretical analysis for double-resonance by means of the equations of motion of density matrix elements are given. In section IV, optimal conditions for the highest microwave frequency stability are found by the computer simulation. Finally, in section V, both contributions of the laser frequency detuning to the light shifts and effects of laser linewidth on microwave frequency stability are investigated.

II. Observation of Double Resonance Spectral Shapes with Narrower Linewidth

Figure 1 shows an experimental setup for a laser pumped ^{87}Rb atomic clock, in which a commercially available ^{87}Rb atomic clock (Fujitsu, 5407A) was used. The rubidium gas cell with natural rubidium vapor (^{87}Rb/^{85}Rb = 3/7) and buffer gases was installed in the microwave cavity. Figure 2 (a) and (b) show examples of novel optical-microwave double resonance spectrum. The vertical axes of these figures are the output voltage of the phase sensitive detector (P.S.D.) in Fig.1. At first glance, the lineshapes of Fig.2 (a) and (b) seem to be quite different. These

difference, however, only stems from the difference of the modulation index (M), the modulation frequency ($\omega_m/2\pi$), and the phase defference (θ) between the output signal from the post-detector amplifier and the reference signal for P.S.D. Other conditions, for instance, the laser power density and the rubidium gas cell temperature, were equal.

It is worth to mention that the peak-to-peak linewidths at the center of these figures, i.e., the separation between points A and B in Fig.2 (a) and (b), are much narrower than those of rf-excited ^{87}Rb atomic clocks. In the case of Fig.2 (a) and (b), the linewidths were 75 Hz and 110 Hz, respectively. In contrast with them, the linewidth of rf-excited ^{87}Rb atomic clock was 360 Hz as shown in Fig.3. Furthermore, the slope at the center of these lineshapes were too steep, and depended upon the modulation parameters such as M , $\omega_m/2\pi$, and θ . The slope is related to the microwave frequency stability given by[4]

$$\sigma_y(\tau) = \frac{0.2}{Q(S/N)}\,\tau^{-1/2} , \qquad (1)$$

where $\sigma_y(\tau)$ is the square root of the Allan variance of microwave frequency fluctuations[5], τ is the integration time, S/N is the signal-to-noise ratio of the signal from post-detector amplifier, and Q is the quality factor of the frequency discriminator which is given by

$$Q = \nu_{Rb}/\Delta\nu \quad . \qquad (2)$$

In eq.(2), ν_{Rb} is the microwave transition frequency , and $\Delta\nu$ is the linewidth of the derivative shape which is defined as the separation between the points A and B of Fig.2. Eq.(1) also can be expressed by the use of $S_1(=S/\Delta\nu)$, as

$$\sigma_y(\tau) = \frac{0.2\ N}{\nu_{Rb}}\,\frac{1}{S_1}\,\tau^{-1/2} \quad . \qquad (3)$$

Since microwave frequency stability $\sigma_y(\tau)$ is inversely proportional to S_1, large S_1 value improves the microwave stability. Thus, to find optimal conditions for larger slope is useful to improve the microwave frequency stability for a laser pumped ^{87}Rb atomic clock.

III. Analysis of Optical-Microwave Double Resonance

The three - level model of an atom is employed to analyze the optical - microwave double resonance[6]. As showed in Fig.4, two hyperfine levels of the ground state of $(5S_{1/2}, F=1, m_F=0)$ and $(5S_{1/2}, F=2, m_F=0)$, and an excited state $(5P_{3/2})$ correspond to the relevant three levels, which are expressed as $|a\rangle$, $|b\rangle$, and $|c\rangle$, respectively. The magnetic field of microwave and the electric field of a laser are represented as

$$H_M(r,z,t) = (H_{M0}J_0(3.832r/R)\sin(k_Mz)/2)\cdot \exp[-i\omega_M t] + C.C. \ , \qquad (4)$$

$$E_L(z,t) = (E_L/2)\exp[-i(\omega_L t - k_L z)] + C.C. \ , \qquad (5)$$

where H_M and E_L are the amplitudes of the magnetic and the electric field, ω_M and ω_L are angular frequencies, k_M and k_L are wave vectors, respectively, J_0 is the Bessel function of the 0-th order, R is the cavity diameter, z and r are the positions along the cylindrical microwave cavity axis and the radius, respectively, and C.C. represents a complex conjugate. The transmissivity T of the amplitude of the laser electric field through the gas cell can be derived by solving the equations of motion for the density matrix of the three - level model under the perturbations due to external fields given by eqs.(4) and (5). The solution can be expressed as $T = \exp[-\delta - i\phi]$, where δ and ϕ are the amplitude attenuation and the phase shift, respectively. The δ and ϕ can be described by using nonlinear complex susceptibility $\chi_e^{(3)} (= \chi_e'^{(3)} - i\chi_e''^{(3)})$

$$\delta = \frac{\chi_e''^{(3)}\,\omega\,L_g}{2c} \qquad (6)$$

and

$$\phi = \left[1 + \frac{1}{2}\chi_e'^{(3)}\right]\frac{\omega\,L_g}{c} \qquad (7)$$

where, c is the speed of light, L_g is the length of ^{87}Rb gas cell. The macroscopic polarization (P) of ^{87}Rb gas can be described as

$$P = \varepsilon_0\,\chi_e^{(3)}E_L = Tr(\mu_e\,\rho) \ , \qquad (8)$$

where, ε_0 is dielectric constant of vacuum, μ_e is the electric dipolemoment operator, and ρ is the ensemble-averaged density matrix.

On the other hand, the atomic density matrix obeys the Schrödinger equation

$$\frac{\partial \rho}{\partial t} = \frac{1}{i\hbar}[H, \rho] + \frac{\partial \rho_{exec}}{\partial t} + \frac{\partial \rho_{relax}}{\partial t} \quad (9)$$

where, t is the time, $\hbar$ is Plank's constant, H is the Hamiltonian including the atomic interactions with the laser light field and the microwave field, ρ_{exec} and ρ_{relax} represent the atomic excitation and relaxation processes in a phenomenological ay. The Doppler effect on account of the atomic motion is not taken into account, because the drift velocity (v) of ^{87}Rb atoms in buffer gases is sufficiently low, i.e., $|k_L v|$, $|k_M v| \ll 1$ [7]. The Schrödinger equation (9) of three-level density matrix can be solved by taking account third-order perturbations arisen by external fields. The results, of which details of this derivation will be published[8], from eq.(4)-(9) are

$$\delta = \int_{-\infty}^{+\infty} \frac{\omega_{ca} L_g |\mu_{e(ca)}|^2}{2c\varepsilon_0 \hbar} \frac{\xi_{ca}^{(3)} \gamma_{ab}' - \zeta_{ca}^{(3)}(\omega_{ba}' - \omega_M)}{(\omega_{ba}' - \omega_M)^2 + \gamma_{ab}'^2} \rho(\omega_L) d\omega_L \quad , \quad (10)$$

and

$$\phi = \int_{-\infty}^{+\infty} \frac{\omega_{ca} L_g}{2c} \left[2 + \frac{|\mu_{e(ca)}|^2}{\varepsilon_0 \hbar} \frac{\xi_{ca}^{(3)}(\omega_{ba}' - \omega_M) + \zeta_{ca}^{(3)} \gamma_{ab}'}{(\omega_{ba}' - \omega_M)^2 + \gamma_{ab}'^2} \right] \rho(\omega_L) d\omega_L \quad , \quad (11)$$

where

$$\omega_{ba}' = \omega_{ba} - \frac{\gamma_{ab}(\gamma_{cb} + \gamma_{ca}) + x_L^2}{\gamma_{cb}\gamma_{ca} + x_M^2 - \Delta\omega_L^2} \Delta\omega_L \quad , \quad (12)$$

$$\gamma_{ab}' = \gamma_{ab} + \frac{\gamma_{ca} x_L^2 + (\gamma_{cb} + \gamma_{ca})(\omega_{ba} - \omega_M)\Delta\omega_L}{\gamma_{cb}\gamma_{ca} + x_M^2 - \Delta\omega_L^2} \quad , \quad (13)$$

$$\xi_{ca}^{(3)} = \frac{[(n_a - n_c) - (\gamma_a^{-1} + \gamma_c^{-1}) w_L + \gamma_a^{-1} w_M][\gamma_{cb}\gamma_{ab} + x_L^2 + (\omega_{ba} - \omega_M)\Delta\omega_L] - [(n_a - n_b) + (\gamma_a^{-1} + \gamma_b^{-1}) w_M - \gamma_a^{-1} w_L] x_M^2}{\gamma_{cb}\gamma_{ca} + x_M^2 - \Delta\omega_L^2} \quad , \quad (14)$$

and

$$\zeta_{ca}^{(3)} = \frac{[(n_a - n_c) - (\gamma_a^{-1} + \gamma_b^{-1}) w_L + \gamma_a^{-1} w_M][\gamma_{cb}(\omega_{ba} - \omega_M) - \gamma_{ab}\Delta\omega_L]}{\gamma_{cb}\gamma_{ca} + x_M^2 - \Delta\omega_L^2} \quad , \quad (15)$$

ω_{xy} is the angular frequency of the optical transition between the levels $|x\rangle$ and $|y\rangle$, γ_{xy} (x,y = a,b,c $x \neq y$) is a transverse relaxation constant , γ_x (x = a,b,c) is a longitudinal relaxation constant, x_M and x_L are the Rabi angular frequencies of microwave and laser, respectively, $\mu_{e(ca)}$ is the electric dipole moment between levels $|a\rangle$ and $|c\rangle$, n_x (x = a,b,c) is the population of each level , $\Delta\omega_L (= \omega_{ca} - \omega_L)$ is the laser angular frequency detuning, w_M and w_L are products of the population and the transition probability of microwave and laser, respectively, and $\rho(\omega_L)$ is an energy density of the laser field which is given by

$$\rho(\omega_L) = \frac{1}{\pi} \frac{\Delta\omega_l/2}{(\omega_0 - \omega_L)^2 + (\Delta\omega_l/2)^2} \quad . \quad (16)$$

Here, ω_0 is a center angular frequency of the laser, and $\Delta\omega_l$ is a FWHM of the laser.

The second term of the right side of eq.(12) represents light shift, i.e., the microwave frequency shift induced by laser frequency detuning. The second term $\gamma_{ca}x_L^2$ and the third term $(\gamma_{cb}+\gamma_{ca})(\omega_{ba}-\omega_M)\Delta\omega_L$ of right side of eq.(13) represent a power broadening and an inhomogeneous broadening induced by light shift, respectively.

IV. Optimal Conditions for the Highest Microwave Frequency Stability

In order to obtain a frequency discrimination pattern, the microwave signal applied to microwave cavity was modulated as given by

$$\omega_M(t) = \omega_M[\,1 + M\sin\omega_m t\,] \quad . \tag{16}$$

Since the phase shift of eq.(11) depends on the microwave angular frequency ω_M, the phase of the transmitted laser light is modulated by means of modulation of microwave signal. As a result of such an induced phase modulation , FM sidebands would appear in the electric field of the transmitted laser light. It can be expressed as

$$E_T = (E_L'(t)/2)\exp[-i(\omega_L t - k_L z)] + C.C. \quad , \tag{17}$$

where

$$E_L' = E_L \sum_q T_q(\omega_M + q\omega_m)J_q(M)\exp[iq\omega_m t] \quad , \tag{18}$$

T_q is the transmissivity at the laser angular frequency $\omega_L + q\,\omega_m$ ($q = 0, \pm1, \pm2, \pm3$, the q-th order. The light power detected by a photodetector is given by $I_T(t) = c|E_L'|^2/8\pi$. If $|\delta|, |\phi| << 1$ and the laser FM sidebands up to the third order are retained for calculations. $I_T(t)$ can be written

$$\begin{aligned} I_T(t) = I_0[&A + B\cos\omega_m t + C\sin\omega_m t \\ &+ D\cos 2\omega_m t + E\sin 2\omega_m t \\ &+ F\cos 3\omega_m t + G\sin 3\omega_m t] \quad , \end{aligned} \tag{19}$$

where

$$I_0 = \frac{c|E_L|^2}{8\pi} \quad , \tag{20}$$

$$\begin{aligned} A = {} & J_3^2(1-2\delta_{-3}) + J_2^2(1-2\delta_{-2}) \\ & + J_1^2(1-2\delta_{-1}) + J_0^2(1-2\delta_0) + J_1^2(1-2\delta_1) \\ & + J_2^2(1-2\delta_2) + J_3^2(1-2\delta_3) \quad , \end{aligned} \tag{21a}$$

$$\begin{aligned} B = {} & 2[J_2J_3(\delta_{-3}+\delta_{-2}-\delta_2-\delta_3) \\ & + J_1J_2(\delta_{-2}+\delta_{-1}-\delta_1-\delta_2) \\ & + J_0J_1(\delta_{-1}-\delta_1)] \quad , \end{aligned} \tag{21b}$$

$$\begin{aligned} C = {} & 2[J_2J_3(\phi_{-3}-\phi_{-2}-\phi_2+\phi_3) \\ & + J_1J_2(\phi_{-2}-\phi_{-1}-\phi_1+\phi_2) \\ & + J_0J_1(\phi_{-1}-2\phi_0+\phi_1)] \quad , \end{aligned} \tag{21c}$$

$$\begin{aligned} D = {} & 2[J_1J_3(\delta_{-3}+\delta_{-1}+\delta_1+\delta_3) \\ & + J_0J_2(\delta_{-2}+2\delta_0+\delta_2) \\ & - J_1^2(\delta_{-1}+\delta_1) \quad , \end{aligned} \tag{21d}$$

$$\begin{aligned} E = {} & 2[-J_1J_3(\phi_{-3}-\phi_{-1}+\phi_1-\phi_3) \\ & - J_0J_2(\phi_{-2}-\phi_2) \\ & + J_1^2(\phi_{-1}-\phi_1) \quad , \end{aligned} \tag{21e}$$

$$\begin{aligned} F = {} & 2[-J_1J_2(\delta_{-2}-\delta_{-1}+\delta_1-\delta_2) \\ & + J_0J_3(\delta_{-3}-\delta_3) \quad , \end{aligned} \tag{21f}$$

and

$$\begin{aligned} G = {} & 2[-J_1J_2(\phi_{-2}-\phi_{-1}+\phi_1-\phi_2) \\ & + J_0J_3(\phi_{-3}-2\phi_0+\phi_3) \quad , \end{aligned} \tag{21g}$$

δ_q and ϕ_q are values of the attenuation and the phase shift at the laser angular frequency $\omega_L + q\,\omega_m$, respectively. The principal term of A of (21a) is $J_0^2(1-2\delta_0)$, in which $(1-2\delta_0)$ can be approximated as $\exp(-2\delta_0)$. This term represents the attenuation of the laser power on account of ^{87}Rb vapor. The principal terms of B and C of (21b) and (21c) are $J_0J_1(\delta_{-1}-\delta_1)$ and $J_0J_1(\phi_{-1}-2\phi_0+\phi_1)$, in which $(\delta_{-1}-\delta_1)$ and $(\phi_{-1}-2\phi_0+\phi_1)$ can be approximated as $d\delta/d\omega_M$ and $d^2\phi/d\omega_M^2$, i.e., the first derivative of the absorption and the second derivative of the dispersion, respectively. Figure 5 shows the dependences of A, B, C, D, E, F, and G of eq.(21) on the microwave frequency. The measured spectral profile of A, B, and C are shown in Fig.6.

As the profiles of B and C cross the abscissa at the center frequency, they can be used as a frequency discriminator. If a reference signal for the phase sensitive detection of Fig.1 is proportional to $\cos(\omega_m t - \theta)$, the output signal V_{PSD} from the phase sensitive detector is expressed as

$$V_{PSD} = V_0[(B/2)\cos\theta + (C/2)\sin\theta] \quad . \tag{22}$$

Since the ratio of contributions from B and C in eq.(22) is governed by the phase θ , several specific double resonance spectral lineshapes can be obtained by adjusting the value of θ at several values. Figure 7 (a) and (b) show the simulated result obtained by using eq.(22), where the values of γ_{ab}', M, and θ were swept so that the lineshape of Fig.7 fits that of Fig.2. The conditions of the present experimental result of Fig.2 (a) were given below

$$\begin{aligned} &M = 1.8\,\omega_m/\gamma_{ab}' = 2.3 \quad \theta = 234^\circ \\ &S_1 = 4.3 * 10^{-5} \quad (1/Hz) \end{aligned} \tag{23}$$

where, S_1 is the slope which is defined as a frequency discrimination sensitivity in eq.(3). It is seen from these figures that the lineshape is composed of several fine structures, and the peak-to-peak linewidth at the center of this shape is much narrower than that of the rf-excited ^{87}Rb atomic clock (,i.e., Fig.3). Such a narrower linewidth was obtained by utilizing the induced FM sidebands of the laser, and from the discussion given above, it can be recognized that a part of this technique is equivalent to that of the FM laser spectroscopy[9]. The minimum linewidth obtained in the present experiment was 20 Hz at the laser power density of 28.8 $\mu W/cm^2$. The linewidth of 20 Hz is 1/18 times that of the rf-excited ^{87}Rb atomic clock of Fig.3.

Values of parameters given in eq.(23) have not been optimized yet to get the steepest slope. Figure 8 shows the results of the dependence of the slope on these parameters calculated to find the optimal value of parameters. Figure 9 shows the dependence of this maximum value on the normalized modulation frequency and the modulation index. From Fig.8 and Fig.9, the optimal conditions for the highest microwave frequency stability are found as follows

$$M = 1.2\ \omega_m/\gamma_{ab}' = 1.0 \quad \theta = 120^{\circ}$$
$$S_{1(MAX)} = 1.3 * 10^{-4}\ (1/Hz) \quad . \qquad (24)$$

It is seen that the maximum slope is 3 times larger than that of the present experimental results of eq.(23), which means that value of the slope can be expected by optimizing the operating parameters in Fig.2 (a).

It is rather difficult to utilize the second order harmonics D and E in frequency discriminators because they do not cross the absissa at the center frequency. The third order harmonics F and G, however, can be utilized in it. If the reference signal is $\cos(3\ \omega_m t - \theta)$, the output signal is

$$V_{PSD} = V_0[(F/2)\cos\theta + (G/2)\sin\theta] \quad . \qquad (25)$$

Figure 10 shows the dependence of the slope of F and G of eq.(23) on the modulation and phase sensitive detection parameters. Figure 11 shows the dependence of this maximum value on the normalized modulation frequency and modulation index. From Fig.10 and Fig.11, the optimal conditions for the heighest microwave frequency stability are found by the computer simulation as follows

$$M = 3.6\ \omega_m/\gamma_{ab}' = 0.5 \quad \theta = 270^{\circ}$$
$$S_{1(MAX)} = 6.1 * 10^{-5} \quad (1/Hz) \quad . \qquad (26)$$

It was confirmed that the maximum slope was only a half that of the fundamental components of eq.(24). It is worth to mention, however, that the use of the phase sensitive detection at higher Fourier frequency is more favorable to reduce the effects of noise as long as the system is governed by flicker noise.

V. Light Shift

The dynamic stark effect by the electric field of pumping light would induce the light shift,i.e., the shift in microwave transition frequency. Since this frequency is used as a frequency reference for ^{87}Rb atomic clocks, the light shift can limit their frequency accuracy as well as frequency stability. Precise evaluations of the light shift have been rather difficult in the conventional ^{87}Rb atomic clocks because of the complicated spectral profile of the ^{87}Rb lamp. However , more precise evaluations can be carried out by using diode lasers with their narrower spectral linewidth, which could be useful to improve the frequency accuracy and the stability of the ^{87}Rb atomic clocks.

Figure 12 shows the relations between the microwave frequency shift ($\Delta\nu_{Rb}$) of the center of the spectrum and the laser frequency detuning ($\Delta\nu_L$) from the center frequency of an optical transition spectral line. It is seen that two curves in this figure exhibit clearly dispersive shapes, which is consistent with theoretical predictions[10]. At the first glance, it can be recongnized that the microwave frequency shift is increased with increasing the laser power density. The origin point of this figure represents the resonance frequency of the microwave transition which is free from the light shift. It means that the laser frequency must be tuned at this point, so that the affection of the light shift can be avoided, for the improvement of the frequency accuracy. For example, in the case of the curve B of Fig.12, laser frequency detuning should be less than 57 kHz to get the microwave frequency accuracy better than 10^{-12}.

Especially, at the laser power density as high as 2880 $\mu W/cm^2$, the discrimination patterns suffered light shift were observed for the study of the spectral lineshape. Figure 13 (a) shows examples of the frequency discrimination pattern correspond to several different detunings of the laser frequency. From this figure, it is apparent that frequency discrimination patterns are extreamly transformed according as laser frequency detunings are far from zero. Good coincidencses of the measured resuts of

Fig.13 (a) and the calculated results of Fig.13.(b) were obtained. The transformations of the amplitude attenuation and the phase shift correspond to the frequency discrimination pattern as a function of laser frequency detuning are also shown in Fig.14. From these figures, it can be concluded that the dynamic stark effect would not cause only energy-level shifts but also transformations of double resonance spectral lineshape. Similar results have been obtained by Camparo et al, but somewhat different model was employed for their analysis[11].

The effects of laser linewidth on microwave frequency stability were theoretically investigated by using eq.(16), by which the amplitude attenuation and the phase shift are calculated by the convolution with the laser oscillation spectral shape. As a result of it, it is seen from Fig.15 that the slope is increased with reducing the linewidth. However, from the fact that the linewidth of the laser used here is as broad as 40 MHz, it can be recognized that any remarkable increase of the slope can not be obtained even if the linewidth is reduced.

VI. Summary

The theoretical analysis for a novel FM sideband technique was carried out to improve the microwave frequency stability of the laser pumped ^{87}Rb atomic clocks. By using this technique, novel double resonance spectral lineshapes with ultra-narrower linewidths were obtained. The minimum linewidth obtained was 20 Hz, which was 1/18 times that of the rf-excited ^{87}Rb atomic clock.

The optimal conditions for the attainment of the best microwave frequency stability are found as follows;

$M = 1.2 \quad \omega_m/\gamma_{ab}' = 1.0 \quad \theta = 120^{\circ}$.

provided that the frequency discrimination pattern is composed of fundamental components.

The laser frequency detuning should be less than 57 kHz to attain the microwave frequency accuracy better than 10^{-12}.

Acknowledgements

The authors would like to express their gratitudes to Messrs. Kasai, Hashi, and Chiba (Fujitsu Co. Ltd.), Prof. Kano (University of Electro-Communication), Dr. Nakayama (Kyoto Institute of Technology), Prof. Oura, Drs. Kuramochi, and Teramachi (Institute of Vocational Training), for their valuable discussions. This work was partially supported by a Grant-in-Aid for Scientific Reseach from the Ministry of Education, Science and Culture of Japan, and by the Hoso Bunka Foundation.

REFERENCES

[1] J.L.Picque,"Hyperfine Optical Pumping of a Cesium Atomic Beam, and Applications", Metrologia vol.13, pp.115-119, 1977

[2] L.Lewis and M.Feldman, "Optical Pumping by Lasers in Atomic Frequency Standards", Proc. 35th Ann. Freq. Control Symposium, USAERADCOM pp.612-624, May 1981

[3] H.Hashimoto and M. Ohtsu, "Experiments on a Semiconductor Laser Pumped Rubidium Atomic Clock", IEEE J. Quantum Electron., vol. QE-23, pp.446 - 451, 1987

[4] J.Vanier, "On the Signal-to-Noise Ratio and Short-Term Stability of Passive Rubidium Frequency Standards", IEEE Trans. Instrum. and Meas., vol.IM-30, pp.277-282, 1981

[5] D.W.Allan, "Statistics of atomic frequency standards ", Proc. IEEE, vol.54,pp.221-230, 1981

[6] T.W.Hänsch, "Nonlinear Spectroscopy", North-Holland Publishing Company, pp.17-86, 1977

[7] R.H.Dicke, "The Effect of Collisions upon the Doppler Width of Spectral Lines", Phys.Rev., vol.89, pp.472-473, 1953

[8] M.Hashimoto and M.Ohtsu, Submitted to J.Opt.Soc.Am.B.

[9] G.C.Bjorklund, "Frequency-modulation spectroscopy: a new method for measuring weak absorption and dispersions", Opt. Lett., Vol.5, No.1, pp.15-17, January 1980

[10] B.S.Mathur, H.Tang, and W.Happer, "Light Shifts in the Alkali Atoms", Phys.Rev., vol.171, pp.11-19, 1968

[11] J.C.Camparo, R.P.Frueholz, and C.H.Volk, "Inhomogeneous light shift in alkali-metal atoms", Phys.Rev., Vol.27, pp.1914-1925, April 1983

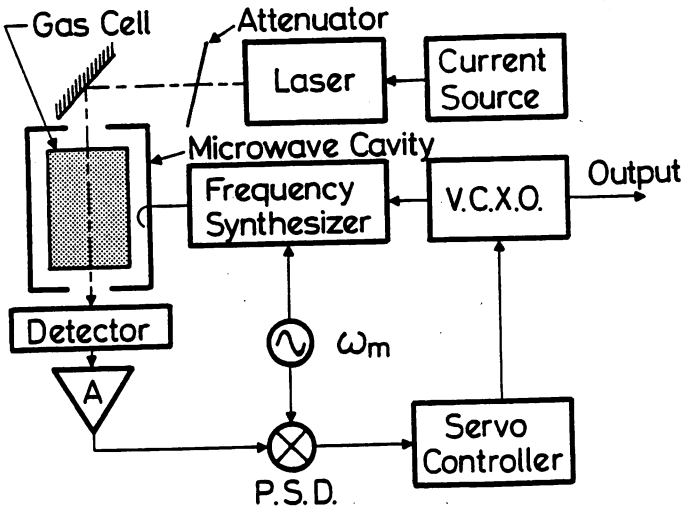

Fig.1 Experimental setup.
P.S.D. : Phase sensitive detector.
V.C.X.O. : Voltage controlled crystal oscillator.
A : Post - detector amplifier.
ω_m : Angular frequency of a low frequency oscillator for microwave frequency modulation.

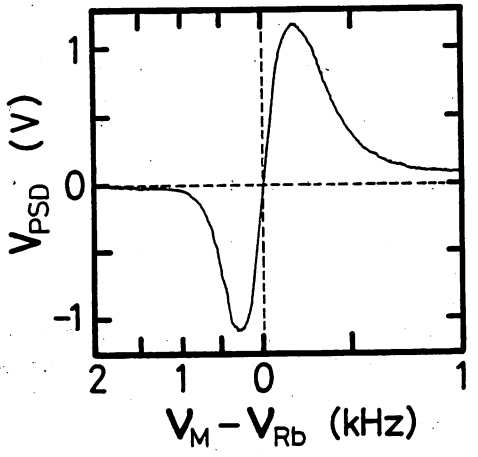

Fig.3 An example of experimentally obtained lineshape in rf-excited ^{87}Rb atomic clock. The modulation frequency was fixed at 160 Hz.

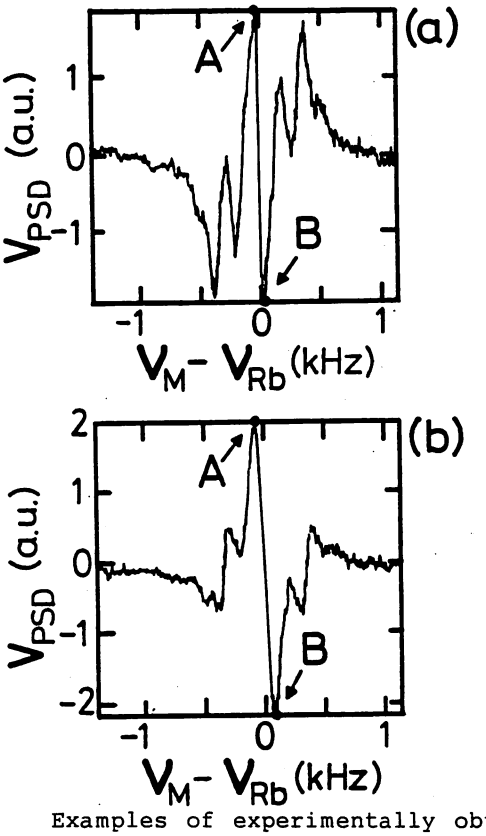

Fig.2 Examples of experimentally obtained lineshape in diode laser pumped ^{87}Rb atomic clock. The modulation frequency ($\omega_m/2\pi$) was fixed at 160 Hz (a) and 200 Hz (b). The laser power density was fixed at 14.4 $\mu W/cm^2$. Other conditions were not explict.
V_{PSD} : Output voltage from the phase sensitive detector.
ν_M : Microwave frequency. ($=\omega_M/2\pi$)
ν_{Rb} : Microwave resonance frequency. ($=\omega_{ba}/2\pi$)

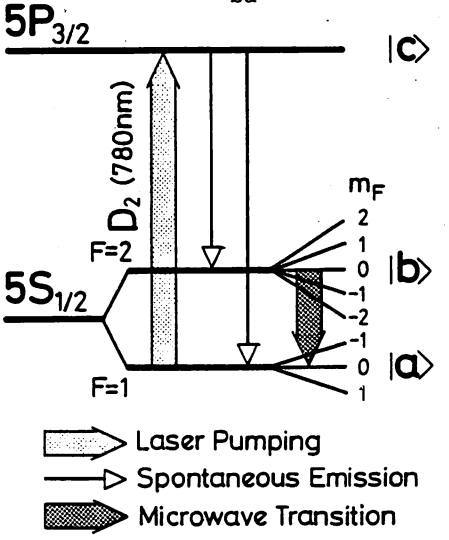

Fig.4 Energy levels of a ^{87}Rb atom relevant to the present study

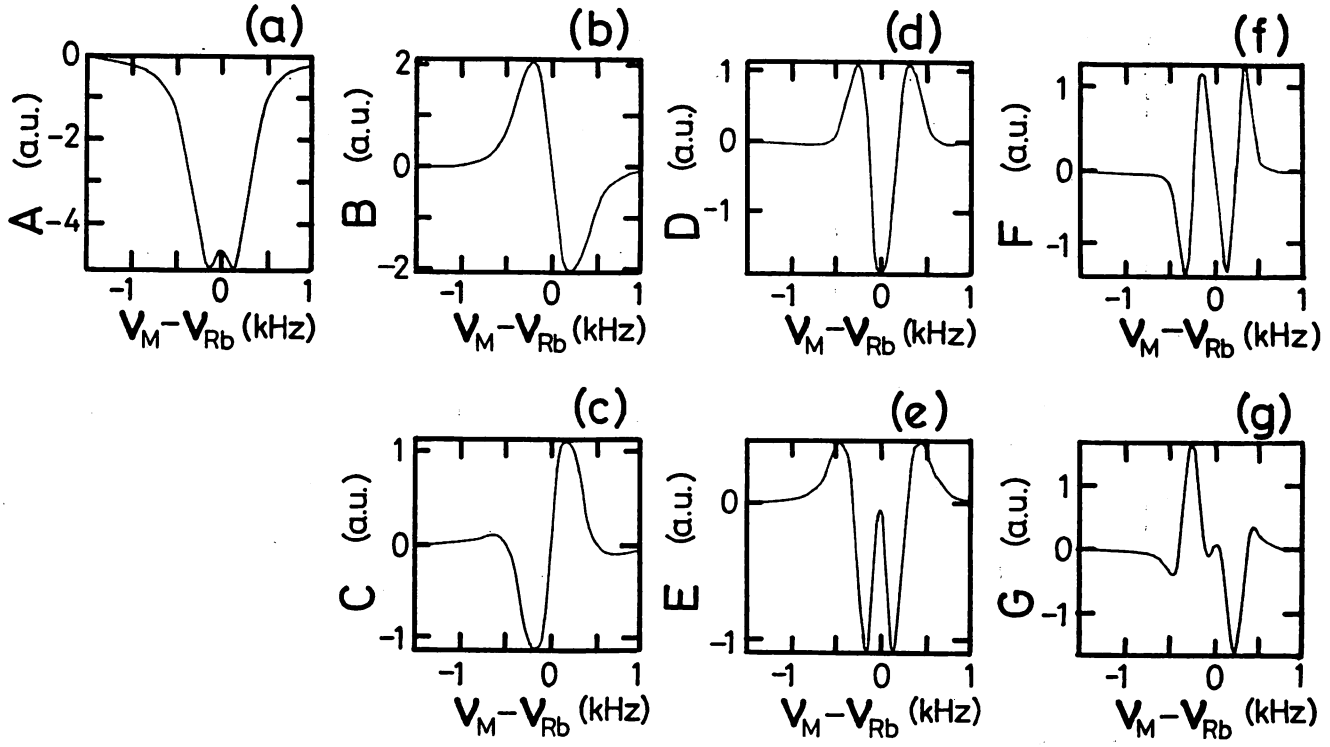

Fig.5 The dependences of the quantities A, B, C, D, E, F, and G of eq.(21) on the microwave frequency $\omega_M/2\pi$. Other quantities were fixed at $\omega_m/2\pi$=160 Hz, $\gamma_{ab}'/2\pi$= 150 Hz, and M=1.8.

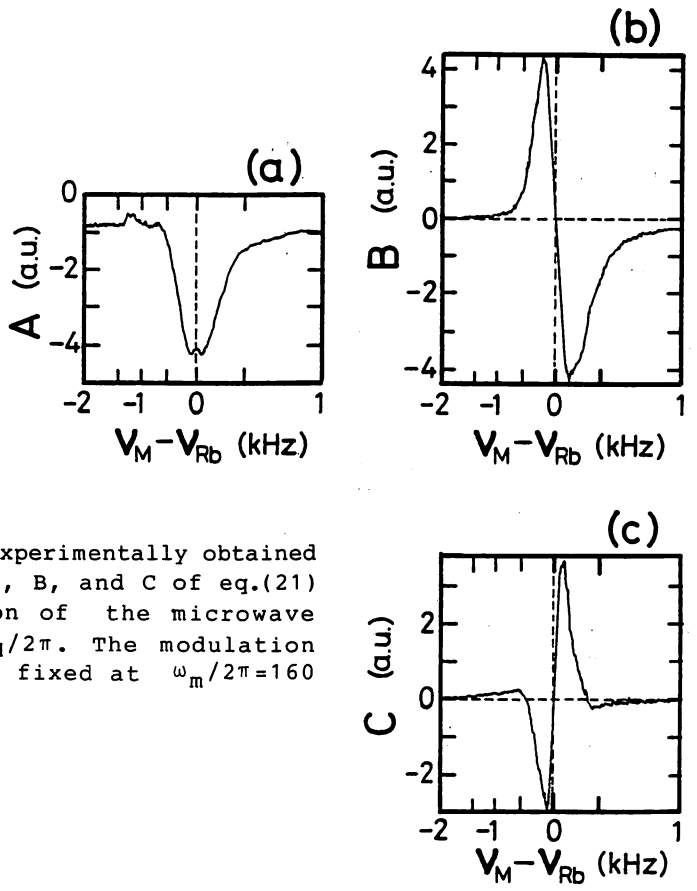

Fig.6 Exmaples of experimentally obtained quantities A, B, and C of eq.(21) as a function of the microwave frequency $\omega_M/2\pi$. The modulation frequncy was fixed at $\omega_m/2\pi$=160 Hz.

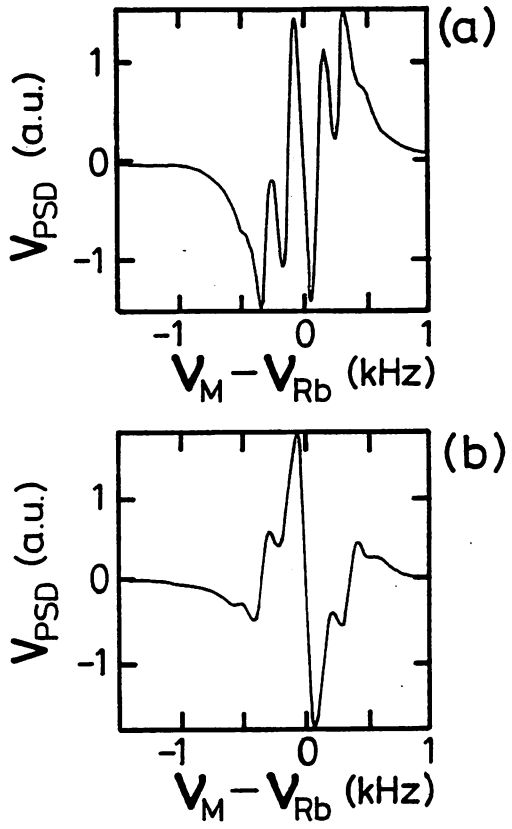

Fig.7 Simulated result obtained by using eq.(19)-(22), where the values of γ_{ab}', M, and θ were swept so that the lineshape of Fig.7(a) and (b) fit that of Fig.2(a) and (b), respectively.
(a)This fitting was obtained when $\omega_m/\gamma_{ab}' = 2.3$, $\theta = 234^o$, and M=1.8.
(b)This fitting was obtained when $\omega_m/\gamma_{ab}' = 2.9$, $\theta = 270^o$, and M=1.6.

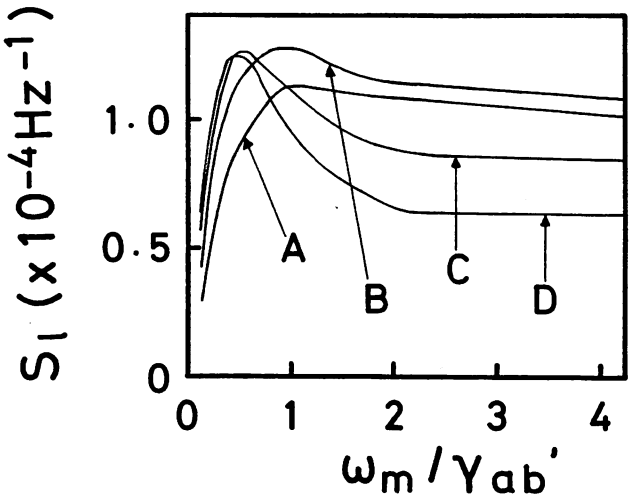

Fig.9 The dependence of the maximum slope of fundamental components on normalized frequency and modulation index. The phase differences were fixed at optimum value.

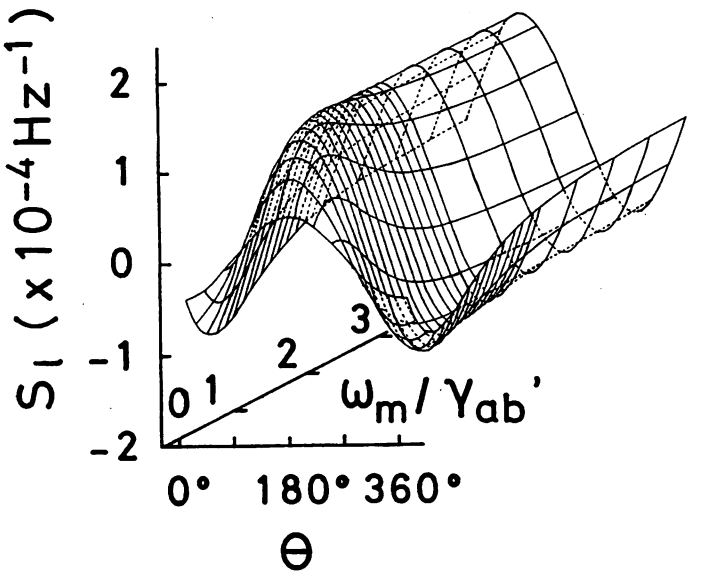

Fig.8 The dependence of the slope of fundamental components on the normalized frequency and phase difference. The modulation index was fixed at M = 1.2.

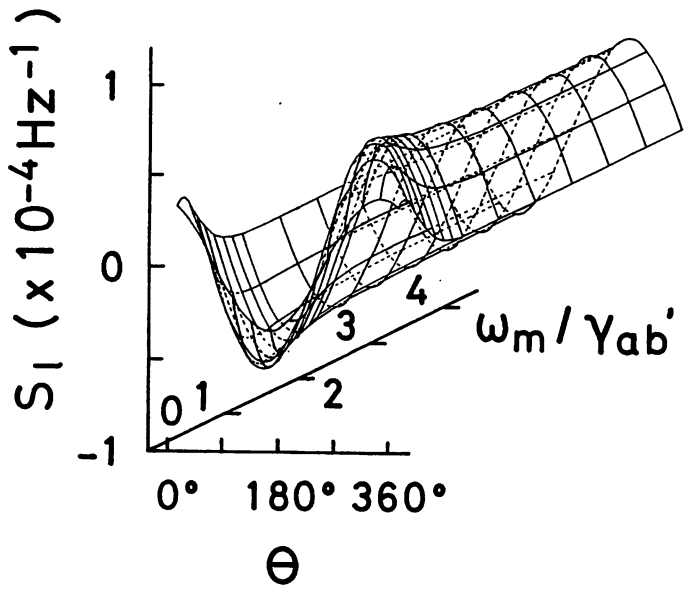

Fig.10 The dependence of the slope of third-harmonics components on the normalized frequency and phase difference. The modulation index was fixed at M = 3.6.

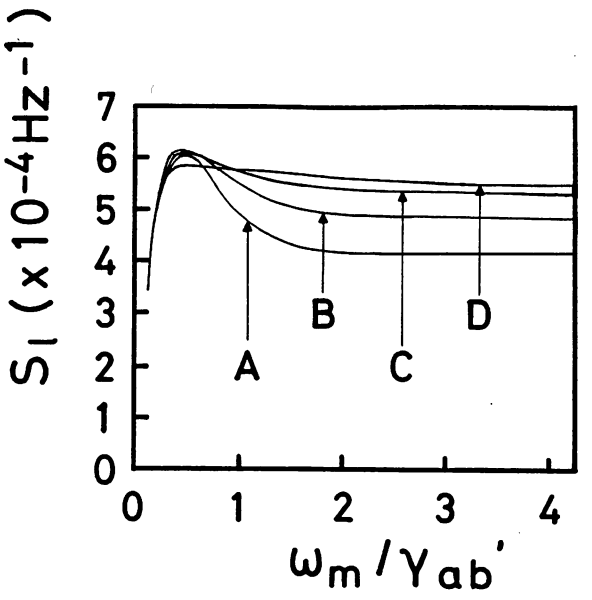

Fig.11 The dependence of the maximum slope of third-harmonics components on normalized frequency and modulation index. The phase differences were fixed at optimum value.

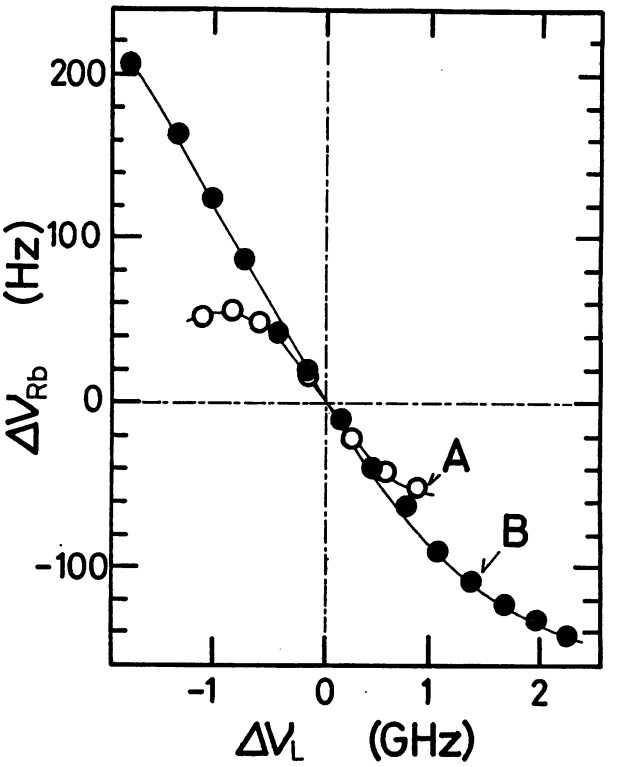

Fig.12 Light shift $\Delta\nu_{Rb}$ induced by laser frequency for the gas cell at 48°C. Since all the curves crossed at a common point, this point was taken as the origin of the axes in this figure. The laser power density was fixed at 57.6 μWcm^2(A,o) and 2880 $\mu W/cm^2$(B,●).
$\Delta\nu_L$: The laser frequency detuning. ($=\Delta\omega_L/2\pi=(\omega_{ca}-\omega_L)/2\pi$)
$\Delta\nu_{Rb}$: The microwave resonance frequency shift. ($=(\omega_{ba}'-\omega_{ba})/2\pi$)

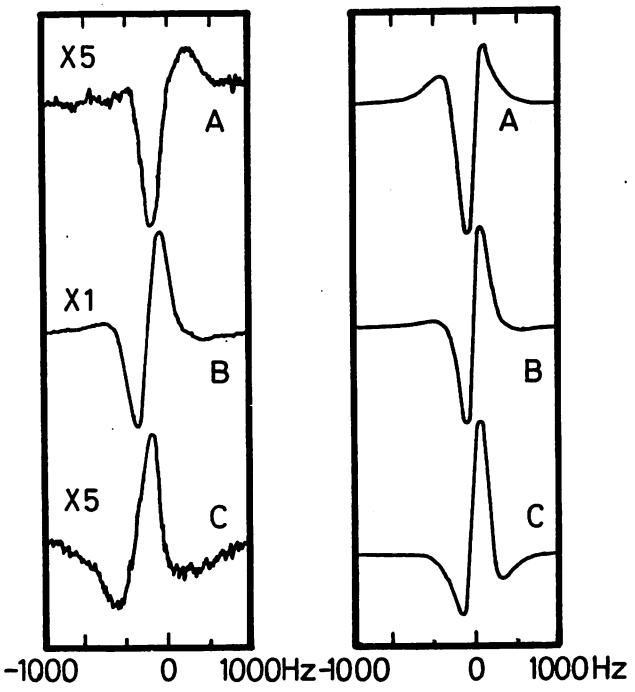

Fig.13 The frequency discrimination pattern suffered light shift on the microwave frequency. (a)The measured results. (b)The calculated results. The laser frequency detuning was fixed at 2070 MHz (A), 0 MHz (B), and -1800 MHz (C). The laser power density was fixed at 2880 $\mu W/cm^2$.

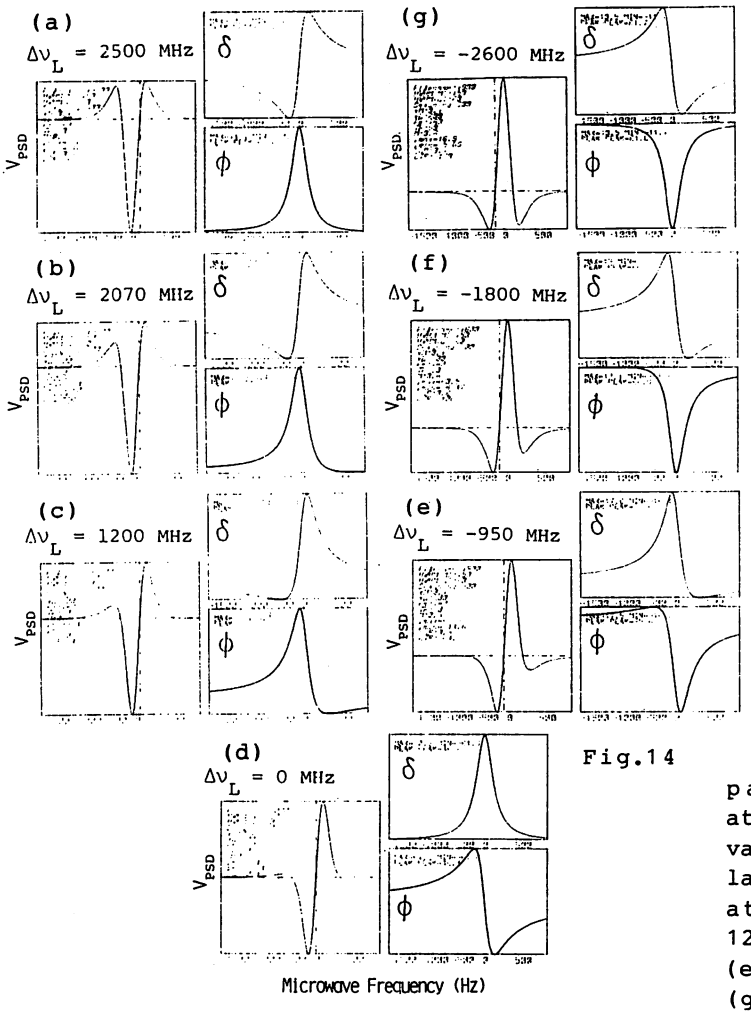

Fig.14 The frequency discrimination patterns, the amplitude attenuation, and the phase shift at various microwave frequencies. The laser frequency detuning was fixed at 2500 MHz (a), 2070 MHz (b), 1200 MHz (c), 0 MHz (d), -950 MHz (e), -1800 MHz (f), and -2600 MHz (g).

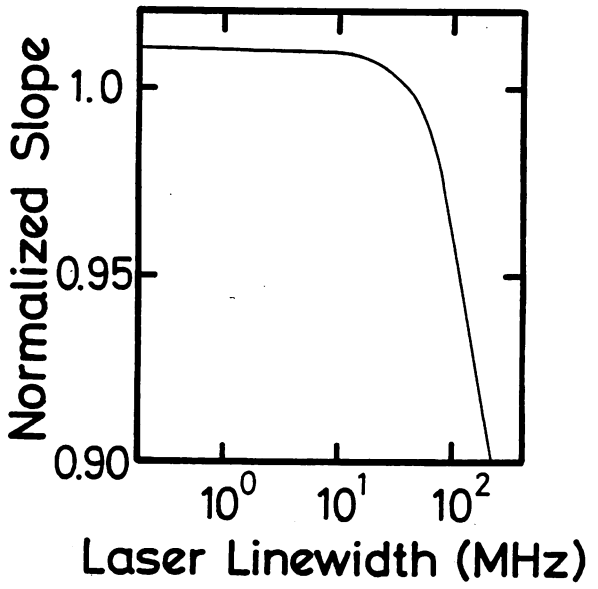

Fig.15 The normalized slope on laser linewidth.